From the Institute of Neuro and Bioinformatics
of the University of Lübeck
Director: Prof. Dr. rer. nat. Thomas Martinetz

Neural mass models of the sleeping brain

Dissertation

for Fulfillment of Requirements

for the Doctoral Degree

of the University of Lübeck

from the Department of Computer Sciences

Submitted by

Michael Schellenberger Costa

from Leipzig

June 2016

First referee: Priv.-Doz. Dr. rer. nat. habil. Jens Christian Claussen
Second referee: Prof. Dr. rer. nat. Andreas Rößler
Chairman: Prof. Dr. rer. nat. Christian Hübner
Date of oral examination: 28.10.2016
Approved for printing, Lübeck 31.10.2016

Acknowledgements

Like any great endeavor we undertake in our life, a thesis is ultimately defined by a series of smaller and larger events. If one is lucky as I was, the most significant of those consist of meetings with extraordinary people.

First and foremost, I would like to thank Jens Christian Claussen for the opportunity to pursue this journey. His enthusiasm about my work and science in general has been infectious. There was never a day where his door was closed for new ideas or just long talks.

The same gratitude goes towards Thomas Martinetz, whose tremendous support throughout the years kept the ship going. Whenever I was in danger of drifting afar, he brought me back on track and helped me focus on the important tasks ahead.

What is a journey without companions? Words cannot describe what I owe to my partners in crime Arne Weigenand and Hong-Viet V. Ngo. We went through the best and the worst of it together and neither of it would have been possible alone.

Life on the road is never easy, but all the wonderful colleagues at the INB made work much more enjoyable than it had any right to be.

In the end this thesis is only the final part of a longer journey. Whatever route I took my family was there to support me. The person I am today is the result of this support and the opportunities they made possible.

But all of this would be meaningless without Melanie and Erik. You are the loves of my life and my every reason to get up in the morning.

Abstract

In contrast to wide belief, the brain is highly active during sleep. Over the course of the night, it cycles between the different stages of sleep. While rapid eye movement (REM) sleep depicts EEG activity that is comparable to that of wakefulness, this changes drastically with the emergence of K-complexes, slow oscillations, and thalamic sleep spindles during non-REM (NREM) sleep. The transition between the different sleep stages and wakefulness is regulated by circadian and ultradian rhythms, which emerge from an intricate interplay between multiple neuronal populations in the brainstem, forebrain and hypothalamus and the resulting varying levels of neuromodulators. Over the last years intracellular recordings and detailed neuron models have helped tremendously to elucidate the mechanisms responsible for the generation of the sleep EEG and how they are affected by neuromodulators.

However, detailed neuron models are highly complex and computationally demanding, which renders the analysis of both model and data cumbersome. Furthermore, it is still poorly understood how these findings translate from the individual neuron to the population activity responsible for the generation of the EEG and its temporal dynamics. Here, mean field approximations such as the neural mass framework of the involved neuronal populations have been highly successful in the reproduction of EEG activity during wakefulness and provided a better understanding of the underlying brain dynamics.

Unfortunately, some mechanisms involved in the generation of the observed sleep phenomena, such as firing rate adaptation and bursting, violate fundamental assumptions of neural mass models. The purpose of this work is the extension of neural mass models with physiologically inspired mechanisms to circumvent these limitations. This approach enables the reproduction of realistic sleep EEG activity including K-complexes, slow oscillations and thalamic sleep spindles, while also allowing to analyze the underlying dynamics in detail.

The first model presented here is devoted to the generation of K-complexes and slow oscillations during sleep stages N2 and N3 respectively. Based on previous detailed model a cortical neural mass is extended by an activity dependent firing rate adaptation. The dynamical repertoire of the model is characterized via a bifurcation analysis, allowing insights into the generating mechanisms of the related sleep phenomena, questioning the current opinion that K-complexes are isolates Slow Oscillations.

In the second model the generation of thalamic sleep spindles is investigated. Similar to the previous approach, intrinsic currents are adopted from detailed studies and included into a neural mass model of the thalamus. A bifurcation analysis reveals the different dynamical modes of the model, leading to the different observed oscillatory modes. In the combined thalamocortical model the effect of external acoustic stimula-

tion is then investigated and validated with experimental data from a stimulation study in humans.

Finally, the third model builds upon the neural mass model of the sleeping cortex and investigates the effect of a generic sleep regulatory network on the dynamics of the cortex and the corresponding transition between wakefulness and the different sleep stages. It is shown that modulation of the bifurcation parameters of the model through varying levels of neuromodulators is sufficient to generate the essential features of human EEG over a full day.

In sum, the modeling studies presented in this work demonstrate that with simple extensions neural mass models are capable of reproducing the EEG activity observed in humans during sleep and wakefulness. The individual models have been published in high impact scientific journals and at the time of writing constitute the state-of-the-art regarding the generation of the sleep EEG. The mathematical analysis of the models reveals their dynamical repertoire, challenging the previous concept of a bistable cortex during slow wave sleep. Utilizing physiologically motivated mechanisms has the further advantage that these extensions can directly be related to neuromodulatory levels in the brain, enabling the validation of arbitrary sleep regulatory networks by means of the EEG.

Zusammenfassung

Entgegen der landläufigen Meinung zeigt das Gehirn während des Schlafes einen hohen Grad an Aktivität. Im Verlauf einer Nacht wechselt es dabei zyklisch zwischen den verschiedenen Schlafstadien. Im Elektroenzephalogramm zeigt der sogenannte rapid eye movement (REM) Schlaf Aktivität, die vergleichbar mit der des Wachzustandes ist. Dies ändert sich allerdings drastisch mit dem Auftreten von K-Komplexen, Slow Oscillations und thalamischen Schlafspindeln während des non-REM (NREM) Schlafes. Der Übergang zwischen den verschiedenen Schlafstadien und dem Wachzustand wird durch das Zusammenspiel von neuronalen Netzwerken im Hirnstamm, dem Zwischenhirn und des Hypothalamus reguliert, die für die Ausschüttung von Neuromodulatoren verantwortlich sind. Im Verlauf der letzten Jahre haben physiologische Studien und detaillierte Neuronenmodelle dazu beigetragen, die dem Schlaf-EEG zugrunde liegenden Mechanismen und deren Manipulation durch Neuromodulatoren zu verstehen.

Aufgrund ihrer hohen Komplexität benötigen detaillierte Neuronenmodelle allerdings einen sehr hohen Ressourceneinsatz und sind dementsprechend schwer zu analysieren. Darüber hinaus ist es unklar, inwieweit sich die Ergebnisse von Studien an Einzelneuronen auf eine ganzen Neuronenpopulation übertragen lassen, deren Aktivität die Grundlage für das EEG bildet. In diesem Zusammenhang haben mean field Näherungen wie neural mass Modelle große Erfolge in der Modellierung des Wach-EEGs gefeiert und stark zum Verständnis der zugrunde liegenden Gehirndynamik beigetragen.

Unglücklicherweise führen einige der Schlafdynamik zugrunde liegenden Mechanismen, wie Feuerraten-Adaption und Bursting modes, dazu, dass grundlegenden Annahmen der neural mass Modelle niht erfüllt werden. Das Ziel dieser Promotion ist die Erweiterung bestehender neural mass Modelle durch physiologisch inspirierte Mechanismen, um diese Nachteilen zu überwinden. Der Ansatz ermöglicht nicht nur die detaillierte Analyse der Gehirndynamik, sondern auch die Modellierung des Schlaf-EEGs einschließlich von K-Komplexen, Slow Oscillations und thalamischen Schlafspindeln.

Das erste Modell befasst sich mit der Entstehung von K-Komplexen und Slow Oscillations während der Schlafphasen N2 und N3. Aufbauend auf früheren detaillierten Neuronenmodellen wurde ein neural mass Modell des Neokortex mit einer aktivitätsabhängigen Feuerraten Adaption erweitert. Mit Hilfe einer Bifurkationsanalyse wurde die Dynamik des Modells charakterisiert. Dies lies Schlussfolgerungen auf die Entstehung der jeweiligen Phänomene zu und widerspricht der bisherigen Theorie, dass K-Komplexe isolierte Slow Oscillations darstellen.

Das zweite Modell untersucht die Generation thalamischer Schlafspindeln während des Tiefschlafes. In Anlehnung an das kortikale Modell wurden Ionenströme von detaillierten physiologischen Modellen adaptiert und in ein neural mass Modell des Thalamus

eingefügt. Eine Bifurkationsanalyse lieferte wiederum Erkenntnisse über die verschiedenen dynamischen Modi des Modells, die zu den beobachteten Oszillationen im Thalamus führen. Im Anschluss wurde im kombinierten thalamokortischen Modell der Einfluss externer akustischer Stimulation untersucht und anhand von EEG-Daten aus einer Humanstudie validiert.

Abschließend behandelt das dritte Modell den Einfluss eines generischen Schlafregulations-Netzwerkes auf die kortikale Dynamik und den damit einhergehenden Übergang zwischen den verschiedenen Schlafstadien beziehungsweise des Wachzustandes. Es wird gezeigt, dass die Modulation der Bifurkationsparameter des kortikalen Modells durch Neuromodulatoren ausreicht um das menschliche EEG im verlauf eines vollen Tages nachzubilden.

Zusammenfassend haben die hier entwickelten Modelle gezeigt, dass neural mass Modelle durch einfache Erweiterungen in die Lage versetzt werden menschliche EEG Aktivität, sowohl im Schlaf als auch während des Wachzustandes, abzubilden. Die einzelnen Modelle wurden in angesehenen Fachzeitschriften veröffentlicht und repräsentieren zum jetzigen Zeitpunkt den state-of-the-art in der Modellierung des Schlaf-EEGs. Die mathematische Analyse der Modelle zeigt eine Dynamik auf, die die bisherige Lehrmeinung eines bistabilen Kortex in Frage stellt. Durch die Verwendung physiologisch motivierter Mechanismen können die beobachteten Phänomene direkt mit der Aktivität von Neuromodulatoren in Zusammenhang gebracht werden. Dies ermöglicht es unter anderem beliebige Schlafregulatorische Modelle durch die so generierte EEG Aktivität zu validieren.

Contents

List of Figures

List of Tables

Publications and Funding

Journal Publications

[Weigenand and Schellenberger Costa et al., 2014] Weigenand A., Schellenberger Costa, M., Ngo H.-V. V., Claussen J. C., and Martinetz T. (2014). Characterization of K-Complexes and Slow Wave Activity in a Neural Mass Model. *PLoS Computational Biology*, 10(11):e1003923.

[Schellenberger Costa et al., 2016] Schellenberger Costa, M., Born J., Claussen J. C., and Martinetz T. (2016). Modeling the effect of sleep regulation on a neural mass model. *Journal of Computational Neuroscience*, pages 1–14.

[Schellenberger Costa and Weigenand et al., 2016] Schellenberger Costa M., Weigenand A., Ngo H.-V. V., Marshall L., Born J., Martinetz T., and Claussen J. C. A thalamocortical neural mass model of the EEG during NREM sleep and its response to auditory stimulation. In Print at *PLoS Computational Biology*.

Conference Presentations

Schellenberger Costa M., Martinetz T., and Claussen J. C. Introducing Ca^{2+}-dependent plasticity into a cortical active/silent state model. *DPG Frühjahrstagung*, 2012, Berlin

Schellenberger Costa M., Krioneriti1 D., Claussen J. C., Marshall L., and Martinetz T. Modelling the effects of slow wave sleep on synaptic plasticity. *Bernstein Conference*, 2012, München

Schellenberger Costa M., Martinetz T., and Claussen J. C. A biophysical model of the effects of slow wave sleep on synaptic plasticity. *Dynamics of Memory*, 2012, Barcelona

Schellenberger Costa M., Martinetz T., and Claussen J. C. Bifurcation analysis of a thalamocortical mean field model. *DPG Frühjahrstagung*, 2013, Regensburg

Schellenberger Costa M., Weigenand A., Martinetz T., and Claussen J. C. A neural mass model of the thalamo-cortical system during sleep. *Bernstein Conference*, 2013, Tübignen

Schellenberger Costa M., Weigenand A., Martinetz T., and Claussen J. C. A population model of the thalamo-cortical system during deep sleep. *Annual Computational Neuroscience Meeting*, 2013, Paris

Weigenand A., Schellenberger Costa M., Ngo H.-V. V., Marshall L., Martinetz T., and Claussen J. C. Dynamics of the thalamo-cortical system driven by pulsed sensory stimulation. *Annual Computational Neuroscience Meeting*, 2013, Paris

Schellenberger Costa M., Weigenand A., Ngo H.-V. V., Claussen J. C., and Martinetz T. Modeling the sleeping thalamo-cortical system. *Summer School Memory and Consciousness*, 2014, Tübingen

Schellenberger Costa M., Born J., Marshall L., Claussen J. C., and Martinetz T. Modulating cortical dynamics with a sleep regulatory network. *Collaborative Research in Computational Neuroscience - Main Meeting*, 2015, Seattle

Weigenand A., Schellenberger Costa M., Ngo H.-V. V., Marshall L., Born J., Claussen J. C., and Martinetz T. Closed-loop and phase-independent auditory stimulation during NREM sleep in a thalamocortical neural mass model. *Collaborative Research in Computational Neuroscience - Main Meeting*, 2015, Seattle

Weigenand A., Schellenberger Costa M., Ngo H.-V. V., Mölle M., Marshall L., Claussen J. C., and Martinetz T. A thalamocortical neural mass model of evoked potentials during NREM sleep. *COSYNE*, 2016, Salt Lake City

Funding

EU-Flagschiff Human Brain Project

Deutsche Forschungsgemeinschaft TransRegio-SFB 654 Schlaf und Plastizität

BMBF Deutschland - USA Zusammenarbeit in Computational Neuroscience

BMBF Bernstein Netzwerk Computational Neuroscience

Chapter 1

Introduction

The following section gives a short overview over sleep and its related EEG phenomena. Afterwards, the cortical and thalamic architecture, that is responsible for the generation of the sleep EEG and builds the foundations of the models described here is discussed. In the final two sections the different synapse types are introduced, together with an overview over the effect of neuromodulation on the brain.

1.1 Sleep

Sleep is a naturally occurring transient behavioral state, that is characterized by reduced mobility, a loss of consciousness, and a reduced responsiveness to external stimuli [Aserinsky and Kleitman, 1953]. It can be observed in a wide variety of organisms, including mammals, birds, reptiles [Cirelli and Tononi, 2008] and to a certain extend even insects [Huber et al., 2004b, Raizen et al., 2008].

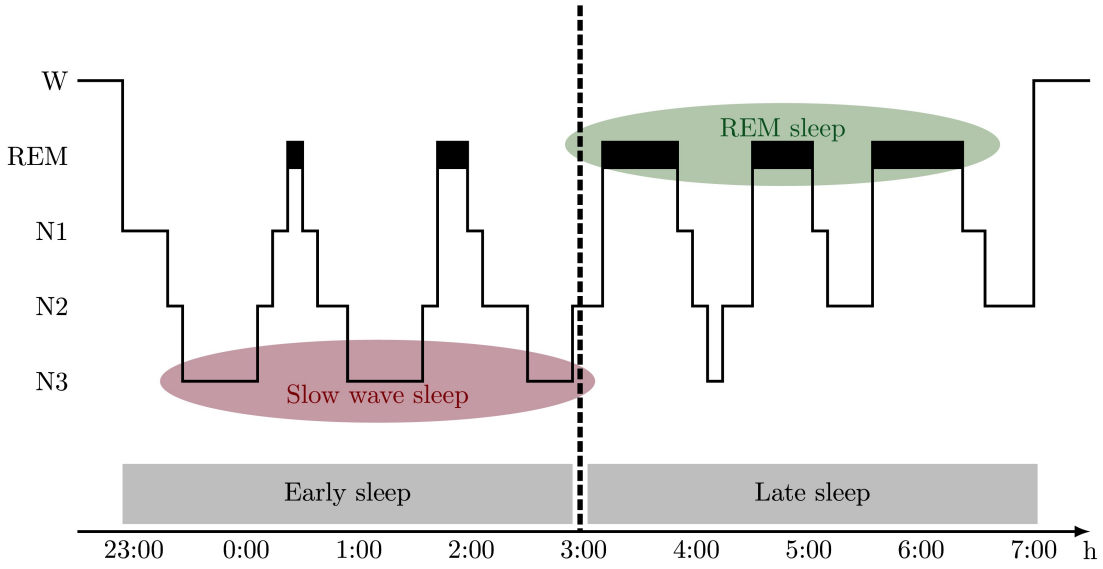

Figure 1.1: Typical human sleep profile This picture depicts a typical hypnogram during a night. The early night is dominated by NREM sleep, that is further subdivided into sleep stages N1-N3, whereas REM sleep prevails during the second half (late sleep). During NREM sleep, cholinergic activity is at a minimum, while REM sleep shows similar or even higher levels than wakefulness. Aminergic activity is high during waking, intermediate during SWS, and minimal during REM sleep. Modified from [Rasch and Born, 2013].

Generally, sleep is divided into two main sleep stages, rapid-eye-movement (REM)

sleep and non-REM (NREM) sleep, which is further subdivided into sleep stages N1-N3, that are dominated by low-frequency high-amplitude oscillations in the electroencephalogram (EEG). Sleep stage N2, that covers about 50-60% of human sleep is hallmarked by the occurrence of sleep spindles and K-complexes (KCs), whereas deeper N3 sleep is dominated by slow wave activity (SWA) [Kales and Rechtschaffen, 1968, Iber et al., 2007]. In contrast, REM sleep exhibits low amplitude activity of higher frequency, which resembles the EEG found during wakefulness. Over the course of the night the brain alternates between these stages in cycles of about 60-90 minutes. These cycles start with lighter NREM sleep stages N1/N2, that then transition into N3 and finally REM sleep. Initially there is a predominance of NREM sleep in the early part of the night, whereas REM sleep dominates the second half of the night (See Fig. 1.1).

The severe drawbacks of sleep with respect to environmental hazards together with its prevalence suggests an crucial functional role of sleep, which has long been debated [Foster, 1901, Siegel, 2005]. Areas with a connection to sleep include saving of energy during night time [Webb, 1988, Berger and Phillips, 1995], regeneration of body tissue/functions [Oswald, 1980, Siegel, 2009], regulation of immune responses [Lange et al., 2010, Besedovsky et al., 2012], but also developmental processes in infants [Denenberg and Thoman, 1981, Mirmiran et al., 1983, Marks et al., 1995, Mirmiran, 1995].

However, one of the most prominent role of sleep lies in its contribution to memory consolidation [Jenkins and Dallenbach, 1924, Buzsáki, 1998, Huber et al., 2004a, Diekelmann and Born, 2010, Rasch and Born, 2013]. Over the recent years, there has been a lot of effort to elucidate the contribution of sleep to memory consolidation. It has become apparent, that the different sleep stages cover certain aspects of memory consolidation [Maquet, 2001, Smith, 2001, Gais and Born, 2004]. REM sleep has been hypothesized to be involved in the processing of emotional [Nishida et al., 2009, Groch et al., 2013] and procedural memory [Smith, 1995, Smith, 2001] but its role in the consolidation of declarative memory is highly debated [Fishbein and Gutwein, 1977, Tilley and Empson, 1978, Stickgold and Walker, 2007, Siegel, 2009].

On the other hand, many studies indicate a functional role of slow wave sleep (SWS) in the formation of declarative memory [Walker and Stickgold, 2004, Diekelmann and Born, 2010, Rasch and Born, 2013]. The synchronization of fast spindle activity to the depolarized up state [Mölle et al., 2002] appears to be critical for the consolidation as it provides a window of opportunity conditions for plastic changes [Gais et al., 2002, Rosanova and Ulrich, 2005, Mölle et al., 2009, Mölle et al., 2011, Cox et al., 2012]. Furthermore, it has been shown that memory consolidation can be improved by transcranial electric and auditory stimulation [Marshall et al., 2006, Ngo et al., 2013b, Ngo et al., 2015] and vice versa sleep deprivation results in an impairment of memory consolidation [Landsness et al., 2009, van der Werf et al., 2009].

1.2 Cortical architecture

The neocortex is a highly complex, hierarchically organized structure, which exhibits a layered structure [Gray, 1918, DeFelipe et al., 2002] and an extensive connectome. Each of the six layers contains different types of neurons. Pyramidal neurons, which are located in layers III and V represent the main source of excitation [Braitenberg

and Schüz, 1991, Braitenberg and Schüz, 2013]. Pyramidal cells are the only neuron type, which develops long range axonal connections, that spread both within the cortex as well as into other brain structures, e.g. thalamus or hippocampus. These parallel long range axonal connections are the main contributors for the generation of the EEG [Buzsáki, 2006, Buzsáki and Wang, 2012]. A second type of excitatory neurons are spiny stellate cells in the internal granular layer IV, that receive thalamic input [Miller et al., 2001, Miller, 2003, da Costa and Martin, 2011, Sun et al., 2016] and form excitatory feedback loops with the pyramidal cells. However, they do not form long range axonal connections.

In contrast GABAergic interneurons are distributed over all layers, developing vast local connections [DeFelipe et al., 2002, Banks et al., 2000, Braitenberg and Schüz, 2013]. In addition to balancing excitation in the cortex, they are known facilitate synchronization between neuronal populations [Cobb et al., 1995, Louvel et al., 2001, Szabadics et al., 2001]. Furthermore, fast GABAergic interneurons are key pacemaker for the generation of fast gamma band oscillations in the cortex [Kisvárday et al., 1993, Sik et al., 1995, Wang and Buzsáki, 1996, White et al., 1998, Tiesinga and José, 2000, Mann et al., 2005, Traub et al., 2005, Bartos et al., 2007]. Similarly to spiny stellate cells GABAergic interneurons only develop local connections within their close proximity.

1.3 Cortical slow oscillations/K-complexes

In the healthy organism KCs and slow oscillations (SOs) emerge at the transition from light into deep sleep and increase in intensity as NREM sleep deepens. In the human electroencephalogram (EEG) SOs are defined as waves with a frequency of 0.5-2 Hz and a peak-to-peak amplitude $> 75\mu$V [Steriade, 1993, Achermann and Borbély, 1997, Steriade, 2003], representing the largest endogenous events in the EEG (See Fig. 1.2).

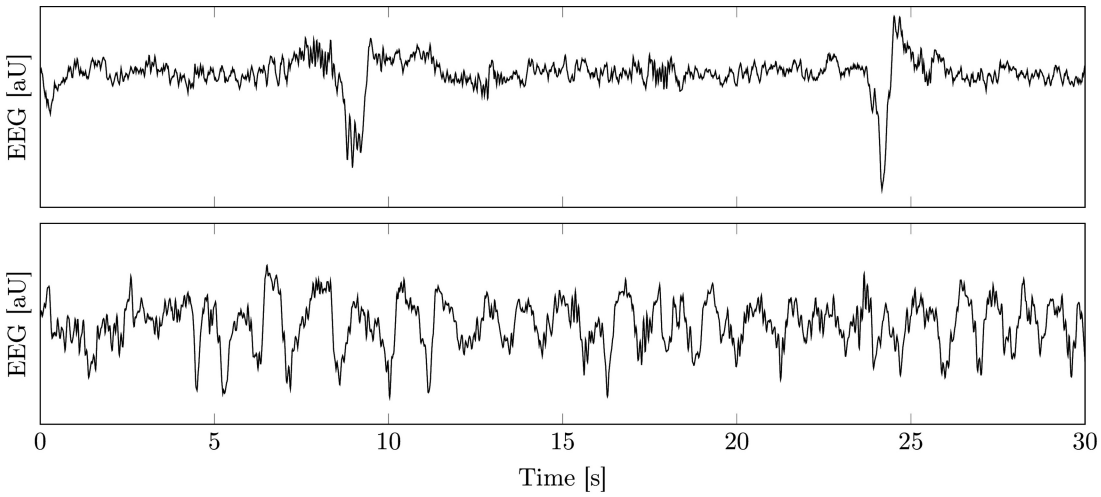

Figure 1.2: Example time series of SOs and KCs This figure depicts typical z-scored EEG signals found during human NREM sleep. The upper panel shows K-Complexes during sleep stage N2. On the other hand the lower panel illustrates slow oscillations during sleep stage N3.

The K-complex and the SO are of intracortical origin [Amzica and Steriade, 1997b, Amzica and Steriade, 1997a, Sanchez-Vives and McCormick, 2000, Timofeev et al., 2000]. Underlying them is a widespread, almost synchronous alternation of neocortical networks

between phases of depolarization (active or up state) and hyperpolarization (silent or down state) [Steriade and Amzica, 1998, Massimini et al., 2004, Peyrache et al., 2012], that behaves like a traveling wave [Sanchez-Vives and McCormick, 2000, Steriade, 2003]. Previously KCs during light NREM sleep (N2) were identified to be an isolated down state [Cash et al., 2009]. However, as shown in Chapter 3 this might be challenged by the findings on the dynamical properties of the sleeping cortex.

Modeling and experimental studies indicate a role for both, synaptic mechanisms and intrinsic currents, in the generation of SOs [Bazhenov et al., 2002, Compte et al., 2003, Holcman and Tsodyks, 2006, Benita et al., 2012], with the active state being generated by excitatory and inhibitory postsynaptic potentials and a voltage-dependent persistent Na+ current I_{NaP} [Steriade et al., 1993a]. The silent state then appears due to removal of synaptic inputs (disfaciliation), and also adaptation processes within the cortical neurons through activity dependent potassium currents [Contreras and Steriade, 1996, Timofeev et al., 2001b, Massimini and Amzica, 2001].

However, thalamo-cortical inputs may trigger onset of cortical active states [El Boustani et al., 2007, Lemieux et al., 2014] increasing synchrony, whereas the reason for the large-scale synchrony of the silent state is yet unknown [Volgushev et al., 2006]. Furthermore, neocortical SOs impact activity in the hippocampus. Sharp wave-ripple events of the hippocampus become suppressed during silent states and show a rebound during development of the active state [Isomura et al., 2006, Mölle et al., 2009]. Recently, it was shown that cells in the prefrontal cortex fire consistently within 100 ms after hippocampal cells in naturally sleeping animals, and that in association with strong hippocampal bursts short-latency prefrontal responses are augmented by increased spindle band activity [Wierzynski et al., 2010].

1.4 Thalamic architecture

The thalamus is a complex brain structure which is located near the very center of the brain and consists of 15 nuclei, whose main function is the processing and gating of sensory information to the neocortex [Jones, 1985, Guillery and Sherman, 2002]. Therefore, the thalamic relay cells which constitute the main cell type within the thalamic nuclei form long range afferents into different areas of the neocortex, with most of the sensory systems targeting one distinct nuclei [Jones, 2001]. In contrast to the pyramidal neurons in the cortical layer V they generally do not form local connections within the population.

As discussed above in Section 1.2 the axons of thalamic relay cells target mainly spiny stellate cells in the cortical layer IV. Their input is then feed to the pyramidal neurons in layer V, which in turn project it back into the thalamus, closing the thalamo-cortical loop.

The thalamic reticular nucleus (TRN) encapsulates the other thalamic nuclei providing inhibition through GABAergic reticular cells and plays an important part in the information processing [Jones, 2002]. It receives input both from layer VI of the neocortex as well as from the dorsal thalamic nuclei [Jones, 1975], with those originating from the cortex being far more numerous [Liu and Jones, 1999]. As GABAergic neurons spread locally, the TRN does not project back into the neocortex.

1.5 Thalamic spindle oscillations

Sleep spindle oscillations consist of waxing-and-waning field potentials of 9-15 Hz which last between one and three seconds and recur every 5-15 sec. They have been recorded from the cat thalamus after in vivo decortication [Morison and Bassett, 1945, Steriade and Deschênes, 1984, Contreras and Steriade, 1996, Timofeev and Steriade, 1996] suggesting a thalamic origin for spindle oscillation. Their generation is heavily linked to low threshold spikes (LTSs), that occur through deinactivation of T-type calcium currents [Steriade et al., 1985, Steriade and Llinás, 1988, Steriade et al., 1990, von Krosigk et al., 1993].

LTSs by the inhibitory thalamic reticular (RE) neurons in the TRN cause an hyperpolarization of the thalamic relay nuclei, that in turn deinactivates the T-type calcium currents in the thalamic relay (TC) cells. In the thalamic relay nuclei the ongoing spindle oscillation is then terminated by the ensuing depolarization through calcium dependent I_{h} currents [McCormick and Pape, 1990, Bal and McCormick, 1996, Lüthi and McCormick, 1999], whereas synaptic input from the thalamic relay nuclei terminates them in the TRN [Timofeev et al., 2001a].

It has been shown, that the TRN alone is capable of generating self-sustained rhythmic activity via LTSs [Steriade et al., 1987, Bazhenov et al., 1999] and that this activity is necessary for spindle oscillations in the thalamic relay nulei [Steriade et al., 1985]. However, the interaction between the thalamic reticular and thalamic relay cells is necessary for the projection of spindle oscillations into the cortex [Steriade and Llinás, 1988].

It was first proposed that the waning phase of spindle occurs as a result of Ca^{2+} induced cAMP up-regulation of an hyperpolarization activated cation current, I_{h}, in the TC cells [Bal and McCormick, 1996, Budde et al., 1997, Lüthi and McCormick, 1998], that modulates the amplitude of the spindle oscillations. More recently, combined experimental and modeling studies suggest that the neocortex may play a critical role in initiation and termination of spindles [Timofeev et al., 2001b, Bonjean et al., 2011]. Furthermore, it has been shown that patterns of spindle oscillations in the cortex depend on the TC projections, which is reflected in the different synchronization properties of EEG vs MEG recordings during sleep spindles in humans [Bonjean et al., 2012].

Recent studies demonstrated that cortically recorded spindle oscillations are not homogeneous, but can be split into at least two types: fast spindles (12-15 Hz) and slow spindles (9-12 Hz). In humans, the fast spindles can be recorded over centroparietal region, whereas slow spindles are predominantly localized over frontal cortical areas [Andrillon et al., 2011, Mölle et al., 2011]. Furthermore, the mechanisms generating these two types of spindles appear to be different [Timofeev and Chauvette, 2013], as slow spindles are usually either independent of ongoing slow oscillatory activity or they start at the transition from the active to the silent states [Andrillon et al., 2011, Mölle et al., 2011].

1.6 Synapses

There are four main types of chemical synaptic channels, glutamatergic, GABAergic, cholinergic, and adrenergic that are expressed in different regions of the body. The

first one are ionotropic glutamate receptors, which are subdivided into AMPA, NMDA, and Kainate channels and are the main contributors of excitatory neurotransmission between neurons [Dingledine et al., 1999, Madden, 2002]. These channels all activate to the release of glutamate into the synaptic cleft, however each on a different time scale with AMPA being the fastest and NMDA the slowest. In addition to pure synaptic transmission AMPA channels are known to be involved in synaptic plasticity through receptor trafficking [Shi et al., 2001, Malinow and Malenka, 2002, Sheng and Hyoung Lee, 2003, Montgomery and Madison, 2004, Gu and Stornetta, 2007, Castellani et al., 2009]. Similarly NMDA channels are closely related to spike time dependent plasticity acting as coincidence detectors [Maren and Baudry, 1995, Shouval et al., 2002b, Urakubo et al., 2008, Hunt and Castillo, 2012]. This enables them to intricately gating of calcium spikes [Castellani et al., 2001, Shouval et al., 2002a, Kampa et al., 2004, Evans et al., 2012]. On the other hand Kainate receptors are known to modulate inhibitory transmissions in the hippocampus [Rodriguez-Moreno et al., 1997, Rodriguez-Moreno and Lerma, 1998, Frerking et al., 1999, Min et al., 1999, Ali et al., 2001].

The second type of GABAergic receptors are associated with inhibitory neurotransmission leading to a hyperpolarization of the postsynaptic target neuron. There are two subdivisions the GABAA and GABAB type, with the former depicting the fast and the latter slow timescales [Kohl and Paulsen, 2010]. GABAergic neurons are generally associated with synchronization of neural oscillations [Cobb et al., 1995, Louvel et al., 2001, Szabadics et al., 2001] and generation of fast brain rhythms including gamma band oscillations [Kisvárday et al., 1993, Sik et al., 1995, Wang and Buzsáki, 1996, White et al., 1998, Tiesinga and José, 2000, Mann et al., 2005, Traub et al., 2005], sharp wave ripples [Maier et al., 2003, Vladimirov et al., 2013] and other high frequency oscillations [Miles et al., 1996, Traub et al., 2004, Bartos et al., 2007, Jefferys et al., 2012].

However, they are also strongly involved in neuromodulation by activating potassium channels [Dutar and Nicoll, 1988, Gage, 1992, Do et al., 2013]. Furthermore, GABAergic interneurons in the thalamic reticular nuclei have been shown to be crucial for the generation of thalamic spindles through rebound bursts [McCormick and Bal, 1997, Timofeev et al., 2000, Bazhenov et al., 2002, Destexhe and Sejnowski, 2003].

In contrast to the former two types of chemical synapses, the other two cholinergic, and adrenergic synapses are not directly involved in the generation of action potentials in neurons. Rather than directly affecting neuronal activity they modulate it by altering certain properties of the cells. It has been shown, that firing rate adaptation of cortical neurons is affected by acetylcholine [Madison et al., 1987, Barkai and Hasselmo, 1994, Hasselmo and Barkai, 1995, Liljenström and Hasselmo, 1995] mainly through blockage of potassium channels [McCormick, 1989, McCormick and Huguenard, 1992]. Similarly, different transmitters of adrenergic synapses alter firing rate adaptation, e.g. serotonin [Colino and Halliwell, 1987, Davies et al., 1987] and noradrenaline [Madison and Nicoll, 1982, Madison and Nicoll, 1986]. On the other hand neural gain is increased by acetylcholine [Barkai and Hasselmo, 1994, Disney et al., 2007, Gulledge et al., 2009, Soma and Shimegi, 2012], serotonin [Zhang and Arsenault, 2005], and noradrenalin [McCormick, 1989, Timmons et al., 2004].

Beside chemical synapses, neurons are known to interact through gap junctions, which are direct electrical channels between the individual neurons. As they do not involve

transmitter release but are directly voltage gated, gap junctions act on faster timescales than chemical synapses [Munro and Börgers, 2010, Perez Velazquez and Carlen, 2000]. They are widely believed to be involved in the generation of high frequency oscillations especially in the hippocampus [Skinner et al., 1999, Traub et al., 1999, Traub and Bibbig, 2000, Stacey et al., 2009, Vladimirov et al., 2013] and enhance synchrony within neural populations [Carlen et al., 2000, Tamás et al., 2000, Szabadics et al., 2001]. However, while there are neural mass models that include gap junctions [Steyn-Ross et al., 2005, Steyn-Ross et al., 2007], they are only considered for the interaction between different columns.

As cholinergic, and adrenergic synapses are not directly involved in the generation of the EEG but its modulation, they will not be considered until the transition between the different sleep stages is investigated in Chapter 5. Furthermore, during sleep the EEG is dominated by slow oscillatory activity in the delta and spindle band. These oscillations are generated by intrinsic mechanisms rather than synaptic interactions. Therefore, one restrict oneself to two one more or less generic synapse type for excitation (AMPA) and inhibition (GABA) each. For the generation of wake EEG with all its different frequency bands this simplification might not be valid.

1.7 Neuromodulation

Over the course of the day, the brain undergoes drastic changes in its activity. The transition between wakefulness and the sleep stages and therewith the corresponding levels of neuromodulators [Lydic and Baghdoyan, 2015], is coordinated by the activity of neuronal populations distributed in different brain areas, primarily the forebrain, brainstem and hypothalamus [Moruzzi, 1972, Saper et al., 2005]. Depending on the participating neuromodulators and brain structures and due to their specific temporal dynamic there is a differentiation between a wake-NREM switch and REM-NREM cycling, respectively [Booth and Diniz Behn, 2014]. The wake-NREM switch has been successfully described by the two-process model, which is based on a homeostatic sleep drive [Borbély, 1982, Daan et al., 1984] or more specifically mutual inhibition between wake-promoting (locus coeruleus (LC), dorsal raphe nucleus (DR)) and sleep-promoting populations (ventrolateral preoptic nucleus (VLPO)) [Saper et al., 2001, Diniz Behn and Booth, 2010]. The activity of those populations is closely related to the levels of the neurotransmitter noradrenalin and serotonin. Additionally, the sleep wake transition is heavily influenced by the circadian rhythm, which is mainly acting through the suprachiasmatic nucleus (SCN) [Kronauer, 1982, Liu and Gillette, 1996, Fleshner et al., 2011].

The NREM-REM cycling has originally been assumed to be driven by reciprocal interaction between cholinergic REM promoting and aminergic wake promoting REM-off populations [McCarley and Hobson, 1975, Luppi et al., 2006, Datta and MacLean, 2007]. However, recent research indicates an involvement of GABAergic populations in the regulation of REM sleep [Lu et al., 2006, Fuller et al., 2007, Brown et al., 2008, Vanini et al., 2012], that also involve mutual inhibition. Additionally, the NREM-REM rhythm is affected by orexinergic neurons located in the perifornical area [Peyron et al., 1998].

Cortical acetylcholine levels are lowest during slow wave sleep and highest during wake and REM sleep, whereas serotonin and norepinephrine levels are highest during

wake, intermediate during SWS and lowest during REM sleep [Weitzman et al., 1971, Aston-Jones and Bloom, 1981, Marrosu et al., 1995, Born et al., 1997, Léna et al., 2005]. Application of acetylcholine blocks potassium currents [McCormick, 1989, McCormick and Huguenard, 1992], such as I_{KNa}, whereas they are activated by GABA. Furthermore, the neural gain is modulated by acetylcholine [Disney et al., 2007, Gulledge et al., 2009, Soma and Shimegi, 2012], serotonin [Zhang and Arsenault, 2005], and norepinephrine [McCormick, 1989, Timmons et al., 2004], with those levels changing in specific patterns throughout the sleep-wake cycle [Léna et al., 2005].

Chapter 2

Methods

This chapter contains an introduction to the methods and modeling approaches employed throughout this work. The first section briefly captures the seminal work of Hodgkin and Huxley. The conductance based modeling approach that they developed will be the basis of the extended neural mass models employed in this work. The second section introduces firing rate based models as a simplification of the conductance based approach that enable the analysis of the brain dynamics on the population level. The third section focuses on neural mass models as a special case of spatially lumped firing rate models. There, the general modeling framework that is utilized in this work is introduced in detail. In the following fourth section, the limitations of firing rate models with respect to certain properties of neurons are discussed. A possible solution employing an hybrid approach, that respects nonlinear properties of neurons arising from intrinsic currents, is discussed in the fifth section. The following two sections give a short introduction into bifurcation theory and stochastic differential equations and their application to neuroscience. Finally, the last section covers computational methods and the documentation of the simulation routines.

2.1 Conductance based models

Conductance based models date back to the seminal work of Hodgkin and Huxley on the squid giant axon [Hodgkin and Huxley, 1952b, Hodgkin and Huxley, 1952a], in which they describe the generation of action potentials. It is generally assumed to be the foundation of theoretical neuroscience. As depicted in Fig. 2.1, the membrane of a neuron is modeled as a capacitor, that is charged by the ionic currents flowing through specific ion channels, with the membrane voltage V_m defined as the difference in the electric potential between the extracellular and intracellular space.

The evolution of the membrane voltage V_m is then given by charging the membrane capacitor through the ion currents.

$$C_m \dot{V}_m = I_{\mathrm{L}} + I_{\mathrm{Na}} + I_{\mathrm{K}} + I_{ext}. \tag{2.1}$$

These currents I_j are driven by the Nernst potentials E_j that arise from the different concentrations of ion types j in the intracellular and extracellular space. The conductance $\bar{g}_j$ of channel type j is dependent on the fraction of open channels of that type. In the simplest case, these channels are voltage sensitive, but can also be subject to ion

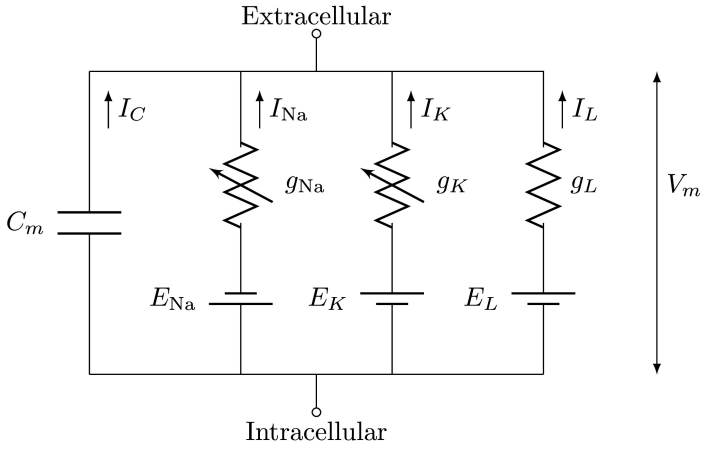

Figure 2.1: Circuit diagram of a simple neuronal cell membrane. Ionic currents driven by varying ion concentrations in the intracellular and extracellular fluid charge the membrane capacitor, leading to a change in the membrane voltage V_m. The conductances $\bar{g}_{\mathrm{Na}}$ and $\bar{g}_{\mathrm{K}}$ depend on the fraction of open voltage gated ion channels. A generic leak current I_{L} captures the passive properties of the membrane (Adopted from [Hodgkin, 1957]).

concentrations and other messengers. Their dynamics can be described by gating functions α_j and β_j. In the case of the classical Hodgkin-Huxley model there is an activation variable n_{K} for the fast potassium current, as well as an activation variable m_{Na} and an inactivation variable h_{Na} for the sodium current.

$$\begin{aligned} \dot{n}_{\mathrm{K}} &= \alpha_n(V_m)(1 - n_{\mathrm{K}}) - \beta_n(V_m)n_{\mathrm{K}}, \\ \dot{m}_{\mathrm{Na}} &= \alpha_m(V_m)(1 - m_{\mathrm{Na}}) - \beta_m(V_m)m_{\mathrm{Na}}, \\ \dot{h}_{\mathrm{Na}} &= \alpha_h(V_m)(1 - h_{\mathrm{Na}}) - \beta_h(V_m)h_{\mathrm{Na}}. \end{aligned} \tag{2.2}$$

The current I_j is then given as the product between the maximal conductance $\bar{g}_j$, the gating variables to a power of k and the voltage difference between the Nernst equilibrium E_j and the membrane voltage V_m.

$$\begin{aligned} I_{\mathrm{K}} &= \bar{g}_{\mathrm{K}} n_{\mathrm{K}}^4 (V_m - E_{\mathrm{K}}), \\ I_{\mathrm{Na}} &= \bar{g}_{\mathrm{Na}} m_{\mathrm{Na}}^3 h_{\mathrm{Na}} (V_m - E_{\mathrm{Na}}). \end{aligned} \tag{2.3}$$

With their simple model, Hodgkin and Huxley were the first to simulate the generation of action potentials in neuronal cells. More recent models integrate additional currents [Wang, 1998], describe different neuron types [McCormick and Pape, 1990, Destexhe et al., 1994a, Llinás and Steriade, 2006] and also consider the sophisticated morphology of neurons, that is modeled by compartmentalizing the neuron into multiple circuits, that are then linked together [Traub et al., 1991, Traub et al., 2012].

2.2 Firing rate models

While detailed conductance based models are capable of generating output that closely resembles that of individual cells as well as neuronal networks, they have one main drawback, that is their complexity. Even small networks of a few thousand neurons exceed the capacity of modern personal computers and require access to supercomputing centers, severely limiting their applicability. There are situations, where this level of

detail is required, e.g. synaptic plasticity requires an after hyperpolarization of the dendrite through a back propagating action potential [Shouval et al., 2010, Carlson and Giordano, 2011, Graupner and Brunel, 2012], however in most cases it is unnecessary.

There are generally two distinct simplification approaches. On one hand, the individual neuron model can be simplified. This includes lower dimensional reductions, that preserve the general dynamical properties, e.g. the three dimensional Hindmarsh-Rose model [Hindmarsh and Rose, 1984] or the two dimensional Morris-Leclar [Morris and Lecar, 1981] and FitzHugh-Nagumo [Fitzhugh, 1961] models. The most common reduction is comprised by the integrate and fire neuron, that introduces a threshold at which a spike, usually modeled by a delta function, is inserted followed by a reset of the membrane voltage to a predefined value [Brunel et al., 2007, Izhikevich et al., 2004]. More recently map based approaches [Rulkov et al., 2004, Bazhenov et al., 2005, Lazar et al., 2009] have been developed, that utilize discrete difference equations rather than ordinary differential equations, greatly reducing the computational load.

On the other hand, the exact time course of every individual neuron might not be relevant for the model. Especially the interaction between larger brain structures depends on the overall firing rate of the neural population rather than activity of an individual neuron [Buzsáki, 2006, Buzsáki and Lopes da Silva, 2012]. Additionally, many physiological measurements such as the EEG, functional magnet resonance imaging (fMRI) or local field potentials represent averaged quantities that are accumulated from a large neuronal population rather than an individual neuron.

Here, rate models have show great success describing the activity of large neuronal populations. There are different related approaches, that data back to the early work of [Wilson and Cowan, 1973], [Amari, 1974], [Lopes da Silva et al., 1974], and [Nunez, 1974]. Instead of the membrane voltage of the individual neurons, they capture the mean firing rate of a whole neural population, that is related to its averaged membrane voltage.

2.3 Neural mass models

Neural mass models represent one of the different formulations of rate models. They are a subtype of neural field models [Deco et al., 2008], that assume a spatial homogeneity within the neuronal population, thus neglecting spatial extensions. Below the formalism of neural mass models, that dates back to the work of [Lopes da Silva et al., 1974], [Nunez, 1974], and more recently [Liley et al., 1999] is introduced. The main variable is the average membrane voltage V_m, which is transformed into a firing rate via a sigmoidal mapping [Jansen et al., 1993, Robinson et al., 1997]

$$Q_k(V_k) = \frac{Q_k^{\max}}{1 + \exp\left(-C(V_k - \theta_k)/\sigma_k\right)}. \tag{2.4}$$

Here $Q^{\max}$ accounts for the maximal firing rate of the respective population, while θ describes the firing rate threshold of the population and σ the slope or steepness of the transition. $C = \pi/\sqrt{3}$ acts as a scaling factor that relates the slope of the sigmoid function to the standard deviation of its derivative.

Spikes travel along the axonal fibers to the dendrites of the target population. For a

fixed axonal length, this can be described by a damped wave equation [Robinson et al., 1997]

$$\ddot{\phi}_k = \nu^2 \left(Q_k(V_k) - \phi_k + v^2 \bigtriangledown^2 \phi_k \right) - 2\nu\dot{\phi}_k, \tag{2.5}$$

that is related to the corresponding cable equation. Here v describes the mean axonal conduction speed and ν the product of v and the mean inverse length of the axons [Steyn-Ross et al., 2005]. However, as neural mass models average over spatial extensions the spatial derivate can be omitted and the time evolution of the incoming spike rate ϕ_k simplifies to

$$\ddot{\phi}_k = \nu^2 \left(Q_k(V_k) - \phi_k \right) - 2\nu\dot{\phi}_k, \tag{2.6}$$

Note that this is equivalent to the convolution of the firing rate with an alpha function α_ν representing the average axonal conduction delay

$$\phi_k = \alpha_\nu(t) \otimes Q_k, \qquad \alpha_\nu(t) = \nu^2 t \exp(-\nu t).$$

For local connections within a neural population $\nu \gg 1$ holds true and the alpha function approaches the δ-distribution. In that case ϕ_k can be replaced by the instantaneous firing rate $Q_k(V_k)$.

As second order differential equations are generally difficult to handle, they are usually split into two first oder differential equations by introduction of an additional variable

$$\begin{aligned} \dot{\phi}_k &= y_k, \\ \dot{y}_k &= \nu^2 \left(Q_k(V_k) - \phi_k \right) - 2\nu y_k. \end{aligned} \tag{2.7}$$

At the dendrites incoming spikes elicit transmitter release into the synaptic cleft. The fraction of open synaptic channels s_{lk}, can be described by a convolution with an alpha function α_l, that represents the average response to a single spike [Tuckwell, 1988].

$$s_{lk} = \sum_{k' \text{ to } k} \alpha_l(t) \otimes N_{kk'} \phi_{k'}, \qquad \alpha_l(t) = \gamma_l^2 t \exp(-\gamma_l t).$$

The sum is over all spikes from sources k' that emerge at the synapses type l of population k, scaled by $N_{kk'}$ that accounts for the mean number of synaptic connections originating from presynaptic population k' to postsynaptic population k. The inverse rise time γ_l determines the shape of the response. Similarly to (2.6) the convolution integral can be transformed into a second order differential equation:

$$\ddot{s}_{lk} = \gamma_l^2 \left(\sum_{k' \text{ to } k} N_{kk'} \phi_{k'} - s_{lk} \right) - 2\gamma_l \dot{s}_{lk}. \tag{2.8}$$

Please note, that the alpha function is often written differently as

$$\alpha_l = \Gamma_l \gamma_l \exp(-\gamma_l t). \tag{2.9}$$

There, Γ_l covers the amplitude of the synaptic response, which allows for a better fit of the synaptic response to experimental measurements. However, while this suggests a more physiological description this notation has two disadvantages. First, it breaks the symmetry of Eq. (2.8) and second it can be shown, that only the full product of

$\Gamma_l \gamma_l N_{kk'} Q_{k'}$ determines the amplitude of the overall synaptic response, resulting in an over-parametrization of the model. Therefore, the formulation of Eq. (2.6) has been chosen, absorbing the scaling of the synaptic response function into the connectivities.

The majority of neural mass models determines the EEG signal by directly summing up the synaptic inputs s_{lk} [Jansen et al., 1993, David and Friston, 2003, Moran et al., 2007, Ursino et al., 2010, Bhattacharya et al., 2011]. This is based on the assumption that there is an equilibrium state, the system is always close to [Wilson and Cowan, 1973, Robinson et al., 1997], resulting in a linear approximation of the neuronal response to synaptic input, that treats inputs independently from the state of the system. However, for larger oscillations and events like evoked potentials or slow oscillations, this assumption is invalid.

A generalization was presented by [Liley et al., 1999, Liley et al., 2002] with the introduction of a weighting function Ψ, that scales the inputs with respect to the state the population is in. A comparison with the detailed Hodgkin-Huxley type models presented in Section 2.1 reveals that the scaling function is indeed a normalized formulation of the driving term $(V_k - E_l)$ utilized in Eq. (2.3). Consequently, the Liley model can be rewritten with respect to physiological conventions from the conductance based models, leading to a formulation that exemplifies its similarity with the conductance based models Hodgkin-Huxley and provides a close link to physiology. The evolution of the mean membrane voltage of population k then follows

$$\tau_k \dot{V}_k = -(V_k - E_{\mathrm{L}}^k) - \sum_l g_l s_{lk} (V_k - E_l). \tag{2.10}$$

Here, g depicts the weight and E the Nernst potentials of the respective channel. Note that in contrast to the Hodgkin-Huxley model, g does not carry the unit of a conductance. To better discriminate between the two we denote the physical contuctances with $\bar{g}$. The spike generating currents I_{K} and I_{Na} from Eq. (2.1) have been replaced by the firing rate function Eq. (2.4), reducing the computational load significantly.

2.4 Limitations

The fundamental assumption of the neural mass models presented in Section 2.3 is the mapping between firing rate and the average membrane voltage of the neural population given in Eq. (2.4). While this assumption is valid for most cases, there are notable exceptions, with spike-frequency adaptation (SFA) and bursting modes being the most prominent ones [Fuhrmann et al., 2002, Contreras et al., 1992].

SFA occurs due to a slow negative feedback, that reduces the excitability of the neuron. Physiologically there are three distinct mechanisms that cause SFA [Benda and Herz, 2003]. The first is the partial inactivation of the spike generating sodium channels thus reducing spiking activity [Fleidervish et al., 1996]. The other mechanisms are based on the activation of slow hyperpolarizing currents either due to the increase in membrane voltage (M-type currents) [Brown and Adams, 1980, Pospischil et al., 2008] or through the change in certain ion concentrations (A-type currents) [Madison and Nicoll, 1984, Compte et al., 2003].

Next to tonic firing, bursting is one of the fundamental firing modes observed in

vivo. During a burst, a neuron generates a short series of spikes, that is followed by a prolonged period of quiescence. That behavior is usually achieved by the interaction between a fast spiking and a slow adaptive current, that modulates the spiking, and is associated with synchronization of neural populations and the generation of motor patterns. A special case are thalamic relay neurons, where the fast spiking is generated through deinactivation of T-type calcium currents, that are then inactivated by the generated activity [Huguenard and McCormick, 1992, Destexhe et al., 1996b], but also have a slow anomalous rectifier current, that modulates the amplitude [Destexhe et al., 1996a].

While slow adaptive currents are intrinsic mechanisms that depend on the activity of the respective individual neuron, they greatly affect population dynamics, which is exemplified by slow oscillatory activity in the cortex or spindle activity in the thalamus.

2.5 Hybrid models

A possible approach to overcome the limitations of neural mass models depicted above is the so called hybrid approach. There, one combines the neural masses with the respective adaptation mechanisms. This is enabled by the slow timescale those processes usually act upon, so that one can assume a certain level of homogeneity across the population.

The first hybrid model that investigated the effect of firing rate adaptation on a neural mass model was developed by [Ardekani et al., 2005, Molaee-Ardekani et al., 2007] to study anesthesia. They included different potassium channels, that were dependent on the firing rate of the excitatory population. A high firing rate would increase the gating variable of the respective adaptation current, leading to negative feedback via the ensuring hyperpolarization of the population. Importantly, while the adaptation currents were taken from a detailed Hodgkin-Huxley model, their activation was solely dependent on the firing rate of the population which is the natural variable of neutral mass models.

Similarly burst-like activity can be achieved by the inclusion of additional mechanisms. This was illustrated in a previous neural mass model of spindle activity [Żygierewicz, 2000, Żygierewicz et al., 2001], that featured both bursting through T-type calcium currents as well as firing rate adaptation through activity dependent potassium currents. Finally, in [Langdon, 2012] the authors arrive at a Hodgkin-Huxley-type extension of their population model of thalamic burst activity, which has been derived from integrate-and-fire-or-burst neurons.

2.6 Bifurcation analysis

Bifurcation theory describes the qualitative changes in the dynamics of a given dynamical system as model parameters are varied. These changes are directly related to the topological structure of the underlying phase space. As bifurcation theory is a braod topic of ongoing research, this section can only be a brief introduction. For more detailed discussions on dynamical systems and bifurcation theory please see [Kuznetsov, 1998] and [Izhikevich, 2007, Ermentrout and Terman, 2010] for direct applications to neuroscience.

A bifurcation is defined as the point where the system transitions from one dynamic mode into another one under the change of one or more parameters. This is closely related to the equilibria of the dynamical system and the qualitative change of its eigenvalues at those equilibria. An equilibrium point P is defined as $\dot{f}(P) = 0$ with f denoting the ODEs describing the dynamical system. It is considered stable when there is a surrounding $U(P)$ of P so that the system stays within $U(P)$ for all $t \in [0, \infty]$. It can be shown that an equilibrium is only stable, when all eigenvalues have a negative real part [Lyapunov, 1892, Kuznetsov, 1998].The definition of stability also includes trajectories that stay in the vicinity of P. If there exists a closed trajectory, it is called a limit cycle. This is the case if the imaginary part of the eigenvalues is nonzero.

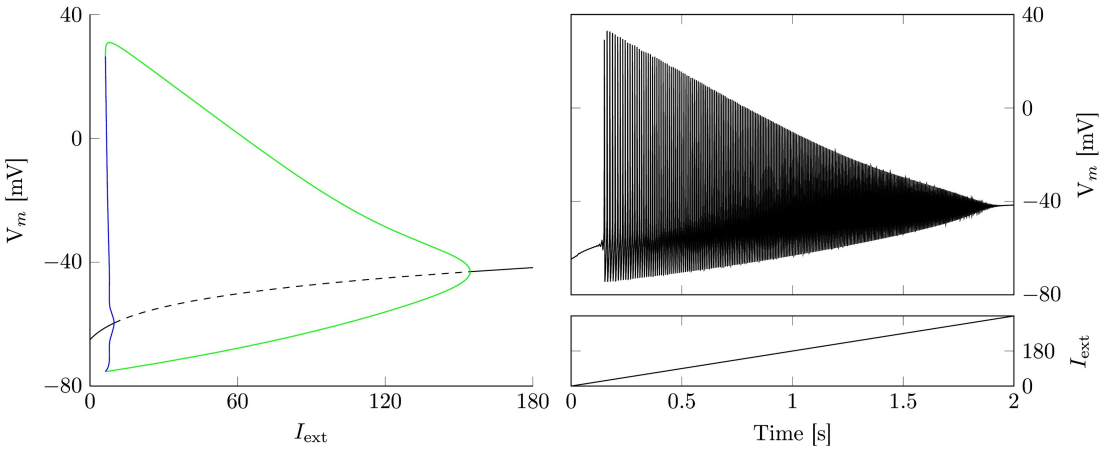

Figure 2.2: Bifurcation analysis of the Hodgkin-Huxley Model This figure illustrates the bifurcation structure of the Hodgkin-Huxley model discussed in Section 2.1 with respect to the input current I_{ext}. The left panel shows the bifurcation analysis with the two Hopf bifurcations leading to the existence of a limit cycle. The amplitude of the limit cycles is depicted in green, whereas the blue line marks the unstable limit cycles, that separate the attractors of the stable states. The upper right panel depicts the outcome of a simulation of the Hodgkin-Huxley neuron given the input current in the lower right panel.

The transition between a stable equilibrium point and a limit cycle is marked by the famous Hopf bifurcation [Hopf, 1942]. It is responsible for the tonic excitation often seen in neurons. In Fig. 2.2 the bifurcation analysis of the Hodgkin-Huxley neuron with respect to the input current is shown. It depicts two Hopf bifurcations between which the neuron generates continuous spiking. The amplitude of those oscillations is given by the green line in the left panel of Fig. 2.2. A comparison with a numerical simulation of the Hodgkin-Huxley neuron in the upper right panel illustrates the match between the bifurcation analysis and the behavior of the model. Other important bifurcations include the saddle-node bifurcation, where two equilibria coalesce and vanish, or the cusp bifurcation that marks the emergence of two saddle-nodes.

2.7 Stochastic differential equations

Every naturally occurring process is subject to some form of random fluctuations. Depending on the strength of those fluctuations and the type of ongoing process, these fluctuations might have a great effect on the systems behavior [Adomian, 1990, Gardiner, 2004, Miller et al., 2005, Sauer, 2012]. Early work on developing a mathematically rigorous theory of stochastic differential equations (SDEs) dates back to Itô [Itô, 1944, Itô,

1951, Itô, 1984] and Stratonovich [Stratonovich, 1966, Stratonovich, 1967], which has since been heavily investigated.

Stochasticity plays a crucial role for dynamical systems as it enriches the dynamical repertoire of a model compared to the deterministic case, where the system is fully defined by its parameters and the resulting bifurcation structure. Due to stochastic input it is possible that the system may be pushed beyond a bifurcation leading to new behavior.

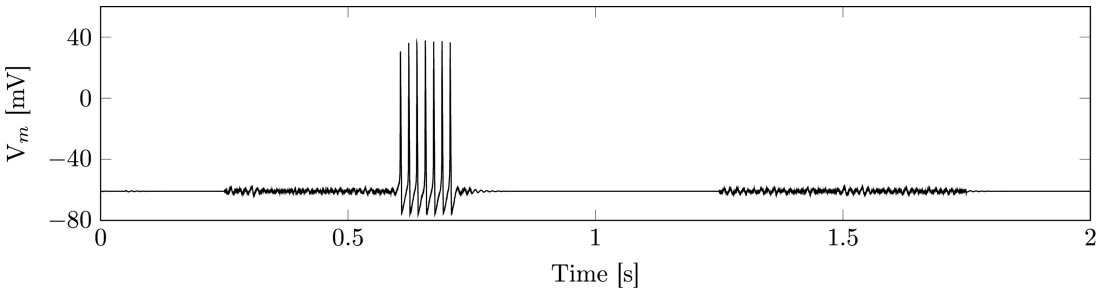

Figure 2.3: Stochasticity in the Hodgkin-Huxley Model. While the neuron is in a stable equilibrium state, stochastic input is able to push it into the attractor of the coexisting limit cycle. Afterwards the stochastic input leads to the transition back to the stable equilibrium.

This is illustrated in Fig. 2.3. There, the Hodgkin-Huxley neuron from Section 2.1 is at $I_{\text{ext}} = 6.5$ where the stable limit cycle from the subcritical Hopf bifurcation coexists with the stable equilibrium. The neuron receives stochastic input during the intervals $t \in [0.25s, 0.75s]$ and $t \in [1.25s, 1.75s]$ resulting in occasional switching between the stable states. As shown later in Chapter 3 this might play a crucial role for the cortical dynamics during NREM sleep.

Table 2.1: Generic Butcher tableau of the SRK method

$c^{(0)}$	$A^{(0)}$	$B^{(0)}$	$c^{(1)}$
	α^T	${\beta^{(1)}}^T$	${\beta^{(2)}}^T$

In this work stochasticity enters the neural mass models in the form of additive white noise. Therefore, the classical Runge-Kutta scheme [Runge, 1895, Kutta, 1901, Butcher, 1963, Butcher, 1987] usually utilized to iterate the ordinary differential equations has to be extended to the stochastic Runge-Kutta (SRK) method [Burrage and Burrage, 1996, Honeycutt, 1992, Hernandez and Spigler, 1993, Rößler, 2004, Bastani and Hosseini, 2007, Rößler, 2009, Küpper et al., 2011]. Following [Rößler, 2010], the generic Runge-Kutta iteration of strong order 1.5 of the stochastic differential equations for additive white noise is given by an extended butcher tableau shown in Table 2.1, leading to the following equation

$$Y_{n+1} = Y_n + \sum_{i=1}^{s} \alpha_i h_n k_i^{(0)} + \sum_{l=1}^{m}\sum_{i=1}^{s} \left(\beta_i^{(1)} I_l + \beta_i^{(2)} I_{l,0}/h_n\right) g_l(t_n + c_i^{(1)} h_n),$$

$$k_i^{(0)} = f\left(t_n + c_i^{(0)} h_n, Y_n + \sum_{j=1}^{s} A_{ij}^{(0)} h_n k_j^{(0)} + \sum_{l=1}^{m}\sum_{j=1}^{s} B_{ij}^{(0)} g_l(t_n + c_j^{(1)} h_n) \frac{I_{l,0}}{h_n}\right),$$

with the independent noise terms I_k and $I_{l,0}$ defined as

$$I_l = \xi_l, \qquad I_{l,0} = h_n(I_l + \zeta_l/\sqrt{3})/2 = h_n(\xi_l + \zeta_l/\sqrt{3})/2.$$

Here, ξ_i and ζ_i are $\mathcal{N}(0, h_n)$ distributed increments of two independent Wiener processes. For the classic fourth order Runge-Kutta scheme the coefficients may be set to:

Table 2.2: Butcher tableau of the fourth order SRK method

0									1			
0.5	0.5				1.5				2			
0.5	0	0.5			0	1.5			0			
1	0	0	1		0	0	0		0			
	1/6	1/3	1/3	1/6	1	0	0	0	1	-1	0	0

2.8 Computational methods and documentation

All models were implemented in C++ and run within MATLAB R2015a with a step size of 0.1ms. The simulation routines are available at github `https://github.com/miscco`. Each model has its own repository, that also contains the plotting routines for the figures depicted in the individual publications:

- Cortex model: `https://github.com/miscco/NM_Cortex`
- Thalamus model: `https://github.com/miscco/NM_Thalamus`
- Thalamocortical model: `https://github.com/miscco/NM_TC`
- Sleep regulation model: `https://github.com/miscco/NM_Cortex_SR`

Additionally, the full model descriptions are given in Chapter A, with a description of the symbols and their numerical values in Chapter B. For the bifurcation analysis, the ode files for xppaut are included in Chapter C.

Chapter 3

Cortical Slow Oscillations and K-Complexes

This chapter is devoted to the generation of KCs and SOs in a neural mass model. First, a short overview over previous conductance based models of the sleeping cortex is given. The second section introduces previous neural mass approaches at modeling the cortex, with a special emphasize on sleep/anesthesia. In the third section, the hybrid model that was presented in [Weigenand et al., 2014] is introduced. The final section analyses the cortical dynamics during NREM sleep and illustrates the ability of the model to reproduce sleep EEG to a high degree.

3.1 Conductance based models of the sleeping cortex

As discussed in Section 1.3, different mechanisms have been proposed to explain the periodic alteration the active and the silent state during cortical KCs and SOs. Previous studies employing detailed Hodgkin-Huxley model focused mainly on miniature postsynaptic currents, induced by spontaneous release of neurotransmitters during silent states [Timofeev et al., 2000, Bazhenov et al., 2002, Compte et al., 2003, Chauvette et al., 2010]. However, spontaneous activity in layer V intrinsically bursting neurons [Sanchez-Vives et al., 2010], self-sustained asynchronous irregular activity in layer V [Destexhe, 2009], and intrinsic oscillatory mechanisms in thalamocortical neurons [Hughes et al., 2002, Crunelli et al., 2011] were investigated. In all of the above scenarios subthreshold synaptic inputs are summed up leading to spontaneous action potential generation. Once a sufficient number of action potentials was initiated, spiking activities propagates along the entire population of neurons via dense lateral excitatory connections, initiating a cortical active state.

While the generation of the active state is clearly of synaptic origin, the mechanisms underlying its termination are less understood. Early modeling approaches indicate firing rate adaptation to lead to the termination of the active stat [Compte et al., 2003, Benita et al., 2012]. However, recent experimental results revealed that the downward transition (from the active to the silent state) in cortical networks is often better synchronized than the upward transition (from the silent to the active state), and shows no latency bias for any location or cell type [Volgushev et al., 2006]. This in vivo result could not be explained by existing models [Timofeev et al., 2000, Compte et al., 2003, Hill and Tononi,

2004], and suggested that synaptic inhibition might also be involved in the downward transition during SOs [Benita et al., 2012, Chen et al., 2012]. Recently it was shown that the normal pattern of the neocortical SO requires thalamic inputs to better synchronize activity across large cortical areas [Lemieux et al., 2014].

3.2 Neural mass models of the cortex

Based on the cortical architecture described in Section 1.2 the simplest realization of a cortical neural mass model compromises a pyramidal population responsible for the generation of the EEG and an inhibitory population that ensures stability. Incidentally the first neural mass models exhibited that exact configuration [Wilson and Cowan, 1973, Lopes da Silva et al., 1974, Jansen et al., 1993, Robinson et al., 1997, Liley et al., 1999, Steyn-Ross et al., 1999]. Later these models where extended to incorporate excitatory feedback loops through the spiny stellate cells, that amplifies cortical activity but also leads to a more realistic EEG signal [Jansen and Rit, 1995, Wendling et al., 2000, David et al., 2004, David et al., 2005, Moran et al., 2007, Sotero et al., 2010]. Finally, the inclusion of a fast inhibitory feedback loop through a fast inhibitory population has been shown to lead to consistent gamma band oscillations in the cortical model [Wendling et al., 2002, Moran et al., 2007, Moran et al., 2009, Ursino et al., 2010].

Historically wakefulness has been the main focus for population based models. Surprisingly, early approaches on other states of vigilance focused on anesthesia rather than natural sleep. Steyn-Ross et al. investigated the effect of general anesthetics on the steady state of a cortical neural mass model [Steyn-Ross et al., 1999]. Assuming a modulation of inhibitory synaptic time scales through the anesthetic agent, they found multiple stable states of the cortical neural mass and investigated spatial coherence and phase transitions in the system [Steyn-Ross et al., 2001, Steyn-Ross et al., 2003, Steyn-Ross et al., 2004, Wilson et al., 2010]. A similar approach was followed by other groups manipulating firing rates, inhibitory synaptic responses as well as synaptic efficacy through anesthetic agents [Bojak and Liley, 2005, Foster et al., 2008, Liley et al., 2011, Bojak et al., 2013, Liley and Walsh, 2013], also investigating a connection to the generation of seizures [Liley and Bojak, 2005]. Extending their work on anesthetics, Steyn-Ross et al. considered the effect of neuromodulators on excitatory connections and resting potential, finding bistability similar to the anesthetized cortex [Steyn-Ross et al., 2005, Wilson et al., 2006a]. Importantly the lower stable state showed excitability, that resembled KCs and SOs [Wilson et al., 2006b]. A spatially extended model allowed the investigation of emerging spatial patterns and their interaction with the intrinsic dynamics [Steyn-Ross et al., 2007, Steyn-Ross et al., 2009, Steyn-Ross et al., 2011, Steyn-Ross et al., 2013].

Similarly Robinson et al. investigated thalamocortical dynamics and the influence of synaptic gains on the dominant oscillatory frequencies. They could identify different parameter regimes, that corresponded to various oscillatory regimes [Robinson et al., 2002, Robinson et al., 2003, Robinson et al., 2004, Robinson et al., 2005, Breakspear et al., 2006, Kerr et al., 2008, Robinson et al., 2011, Roberts and Robinson, 2012]. However, while their approach is able to generate oscillations with different dominant frequencies, these oscillations are solely of synaptic origin leading to certain drawbacks. First, the amplitude of the oscillations does not change significantly between the wake

and the sleep regimes, which is in strong contrast to experimental data. Second, they generate continuous oscillations that does not reflect the event-like character of many sleep related phenomena e.g. KCs and thalamic spindle oscillations.

Recently the effect of firing rate adaptation was studied by [Loxley and Robinson, 2007], although not in the context of sleep. They investigated possible alterations of the firing rate function with respect to the maximal firing rate and the firing threshold. They could show, that this behavior leads to the emergence of limit cycle oscillations. However, in contrast to experimental data these limit cycle oscillations are highly regular and persistent, i.e. they could not generate isolated events in the sense of KCs or the high variability of SOs during NREM sleep.

The first hybrid model that investigated the effect of firing rate adaptation on a neural mass model was developed by [Ardekani et al., 2005, Molaee-Ardekani et al., 2007] to study anesthesia. They included different potassium channels, that were dependent on the firing rate of the excitatory population. However, their approach had different drawback. First, they utilize a classical neural mass approach based solely on the synaptic drive. As discussed in Section 2.3 this is only possible if the model is always close to the equilibrium, which however is not a valid assumption for anesthesia or sleep. Second, they included multiple currents into their approach, increasing the complexity of the model substantially and preventing a detailed analysis.

3.3 Hybrid approach

As discussed in Section 3.1 the transition into the down state is mainly of intrinsic origin due to firing rate adaptation. Therefore, it is not necessary to address the full layered structure of the cortex that was discussed in Section 1.2 and the model is restricted to the simplest case of a two population model. As the intrinsic current requires the calculation of the membrane voltage and during KCs and SOs the model is far from equilibrium, the Liley formulation [Liley et al., 1999], discussed in detail in Section 2.3, was chosen. Here, the excitatory population represents pyramidal (p) neurons in layer 5, accompanied by a generic inhibitory population (i). The ensuing connectivity is depicted in Fig. 3.1.

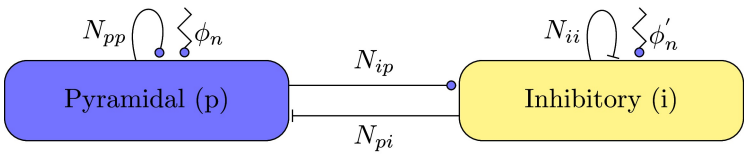

Figure 3.1: Connectivity of the Cortex. The two populations are all to all coupled. In addition to intrinsic activity both populations receive background noise from unspecified brain structures. Circles indicate excitatory synapses, butts inhibitory synapses.

As discussed above in Section 3.2 the abstract approach on spike frequency adaptation by [Loxley and Robinson, 2007] leads to highly regular limit cycle oscillations, that do not resemble KCs or SOs. Therefore, an current based hybrid approach similar to [Ardekani et al., 2005] was chosen. For the sake of simplicity, synaptic depression and other candidate mechanisms for additive feedback, like calcium dependent potassium currents are neglected. Following the results from [Compte et al., 2003] and [Benita et al., 2012] the pyramidal population is extended with a sodium dependent potassium

current

$$I_{\mathrm{KNa}} = \bar{g}_{\mathrm{KNa}} \frac{0.37}{1 + \left(\frac{38.7}{[\mathrm{Na}]}\right)^{3.5}} (V_p - E_K), \qquad [\dot{\mathrm{Na}}] = (\alpha_{\mathrm{Na}} Q_p(V_p) - \mathrm{Na}_{\mathrm{pump}}([\mathrm{Na}]))/\tau_{\mathrm{Na}} \tag{3.1}$$

Sodium influx responsible for the activation of I_{KNa} results from either spiking activity or through persistent I_{NaP} currents. It is not explicitly modeled, but assumed to be proportional to the firing rate Q_p. The coefficient α_{Na} can then be interpreted as the average sodium influx per spike. Extrusion of sodium is due to an active pump [Wang et al., 2003], which is detailed in Section A.1. The adaptation currents are primarily found in excitatory pyramidal cells and less so in inhibitory interneurons, which justifies the restriction of the parameter changes to the excitatory population. In analogy to the Hodgkin-Huxley model the current is connected to the pyramidal membrane voltage by a membrane capacity C_m leading to the following equations for the evolution of the membrane voltages of the cortical module

$$\begin{aligned} \tau_p \dot{V}_p &= -I_{\mathrm{L}}^p(V_p) - I_{\mathrm{AMPA}}(V_p, s_{ep}) - I_{\mathrm{GABA}}(V_p, s_{ep}) - C_m^{-1} \tau_p I_{\mathrm{KNa}}(V_p, [\mathrm{Na}]), \\ \tau_i \dot{V}_i &= -I_{\mathrm{L}}^i(V_i) - I_{\mathrm{AMPA}}(V_i, s_{ei}) - I_{\mathrm{GABA}}(V_i, s_{gi}). \end{aligned} \tag{3.2}$$

It is important to note. that this approach is qualitatively different to changes in the firing rate function, as utilized by [Molaee-Ardekani et al., 2007] and [Loxley and Robinson, 2007]. Gradually switching between two firing rates alters the overall shape of the sigmoid function in a multiplicative activity-dependent manner, whereas in this study an additive threshold modulation is employed.

3.4 Results

In the following section a bifurcation analysis is conducted, to analyze the dynamic repertoire of the cortical model and identify the resulting dynamic regimes. Importantly, while the bifurcation analysis is conducted in the noise free deterministic case, stochastic input is able to push the model from one regime into the other, if the parameters are chosen sufficiently close to the bifurcation. Therefore, the analysis provides the repertoire of *possible* modes, whereas the corresponding response to external stimuli as well as the behavior during the numerical simulations are captured in the following sections.

Later the effect of external stimulation on the generating mechanisms of KCs and slow oscillatory activity is investigated. Based on those findings the ability of the model to reproduce the EEG of sleep stages N2 and N3 is illustrated.

3.4.1 Dynamical structure

In order to characterize the dynamic repertoire of the cortical model a numerical bifurcation analysis of the noise-free system was conducted. The qualitative behavior of the model was most sensitive to changes in the inverse gain, σ_p, of the pyramidal population and the strength of the firing rate adaptation, $\bar{g}_{\mathrm{KNa}}$.

Incidentally, both parameters are known to be susceptible to neuromodulation, that changes the properties of neuronal populations over the sleep/wake cycle. Consequently, σ_p and $\bar{g}_{\mathrm{KNa}}$ were chosen as bifurcation parameters.

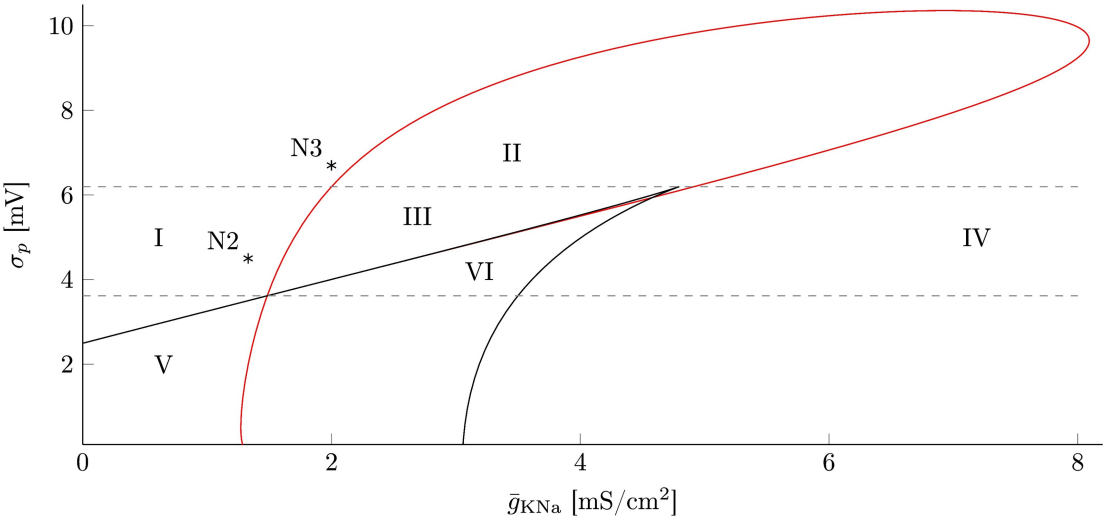

Figure 3.2: Bifurcation diagram of the cortex with respect to $\bar{g}_{\mathrm{KNa}}$ and σ_p. Overview over dynamic regimes of the cortical model, obtained via numerical bifurcation analysis of the cortex with respect to σ_p and $\bar{g}_{\mathrm{KNa}}$. Hopf bifurcations are drawn in red, while the black line depicts saddle-node bifurcations. The bottom gray line marks the intersection of Hopf and saddle curves, the top gray line the cusp bifurcation, where two saddle nodes coalesce. The labels N2 and N3 represent parameter settings used within this study for the respective sleep stages, as given in Table 3.2. Regions I-VI are described in the text and Table 3.1 (Parameters as in Table Table B.3).

As can be seen in Fig. 3.2 the dynamics of the system is shaped by two bifurcations. The first one is a fold created by two saddle node bifurcations (black), that vanishes in a cusp. Between the two saddle nodes there are three equilibrium states, leading to bistability or excitability, see Fig. 3.3a or Fig. 3.3b. This is in good agreement with previous analyses on stable states of the cortex [Steyn-Ross et al., 2005, Touboul et al., 2011, Robinson et al., 2011], as in the case of a fixed sodium concentration I_{KNa} is constant, and an increase in $\bar{g}_{\mathrm{KNa}}$ acts as a decrease in resting potential.

The second bifurcation is a Hopf arising at the upper stable branch (red), that is generated by the firing rate adaptation. Importantly, there is also a canard explosion, where the small amplitude limit cycle of the Hopf bifurcation transitions into a high-amplitude relaxation cycle. The canard phenomenon was first described by [Benoît et al., 1981] and later by [Krupa and Szmolyan, 2001, Szmolyan and Wechselberger, 2001, Wechselberger, 2005]. It is typical for systems where fast and slow subsystems interact and has already been described for different cases of firing adaptation in neurons [Guckenheimer et al., 1997, Gigante et al., 2007, Kopell et al., 2010, Curtu and Rubin, 2011, Rotstein et al., 2012]. The relaxation cycle vanishes at the left saddle-node via a homoclinic bifurcation. At the cusp both saddle nodes coalesce and the homoclinic bifurcation turns into a second Hopf point.

Based on those bifurcations on can define multiple dynamical regimes, see Table 3.1 for a short overview. Within region I a single stable state exists at depolarized membrane voltages where the cortex shows relatively high activity (see Fig. 3.3). Especially for small values of $\bar{g}_{\mathrm{KNa}}$ even large excitatory and inhibitory inputs only cause a passive response. A switch to the lower branch of the S-shaped curve in Fig. 3.3 (region IV, silent state) is not possible. Because of these properties the waking brain is assumed to operate within this regime.

Table 3.1: Dynamic regimes of the cortical module

Region	dynamical properties
I	single active state
II	limit cycles
III	limit cycles and relaxation cycles
IV	single silent state
V	bistability
VI	excitability

Overview over the different dynamical regimes, of the cortical model.

When crossing the curve of saddles to region V two new fixed points appear (see also Fig. 3.3a). The system becomes bistable, with a stable active and silent state. Positive and negative inputs can cause a switching between the two stable branches. A further increase in $\bar{g}_{\mathrm{KNa}}$ turns the upper branch (active state) unstable. However, within region VI there are still multiple equilibria leaving the system excitable. Here a stimulus can produce a large positive response, which was previously thought to be responsible for the generation of KCs as well as SOs [Wilson et al., 2005]. Only after the second saddle node is crossed the upper two equilibria vanish and a single stable state remains. This state is characterized by hyperpolarized membrane voltages leading to a quiescent cortex.

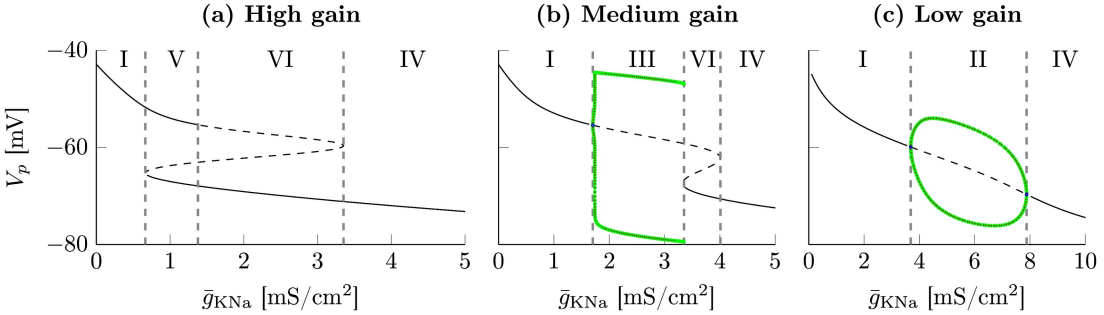

Figure 3.3: One-dimensional bifurcation diagrams for different gain levels. Low gain corresponds to high values of σ_p. Thick black lines depict stable fixed points, dashed lines unstable fixed points and green lines stable periodic solutions. The gray dashed lines mark bifurcations and separate the different regimes. (a) Two saddle-node bifurcations lead to excitability in region VI and bistability in region V. (b) A Hopf bifurcation appears (between I and III) in addition to the two saddle-nodes. The initial small amplitude limit cycle transitions into a high-amplitude relaxation cycle via a canard explosion. The high-amplitude periodic solutions vanish at the left saddle-node via a homoclinic bifurcation. The period of the relaxation oscillations goes to infinity as one approaches the homoclinic bifurcation.(c) Only the Hopf bifurcation remains, after the saddle nodes disappeared via a cusp bifurcation. Within region II there is no canard anymore. Parameters as in Table B.3.

Region III is characterized by periodic limit cycles or relaxation oscillations and, hence, high rhythmicity. The initial Hopf bifurcation is accompanied by a canard explosion: due to an exponentially small variation of the bifurcation parameter an abrupt transition from a medium-amplitude limit cycle to a high-amplitude relaxation cycle can take place. The corresponding one-dimensional bifurcation diagram is shown in Fig. 3.3b. The periodic solutions vanish at the left saddle-node via a homoclinic bifurcation, and the period of the relaxation oscillations goes to infinity as one approaches the homoclinic bifurcation.

Additionally, with increasing σ_p the amplitude of the limit cycle increases and ap-

proaches the form of relaxation oscillations. This explains the similarity between the limit cycles and relaxation oscillations. Both are shaped by the same homoclinic orbit.

At the cusp the two saddle nodes vanish and the homoclinic bifurcation turns into a second Hopf point. Without the homoclinic bifurcation there is no canard anymore. Therefore, in region II above the cusp bifurcation only limit cycles remain, illustrated in Fig. 3.3c, leading to high-amplitude oscillations.

3.4.2 Response to perturbations

While the bifurcation analysis provides the basic repertoire of the unperturbed model, its responsiveness with respect to perturbations, e.g. external stimuli or background noise, is crucial for its behavior. As mentioned before, within region I the cortex shows only a passive response. However, this changes for larger values of $\bar{g}_{\mathrm{KNa}}$, i.e. closer to the curve of Hopf points (red line in Fig. 3.2, separating region I from II and III).

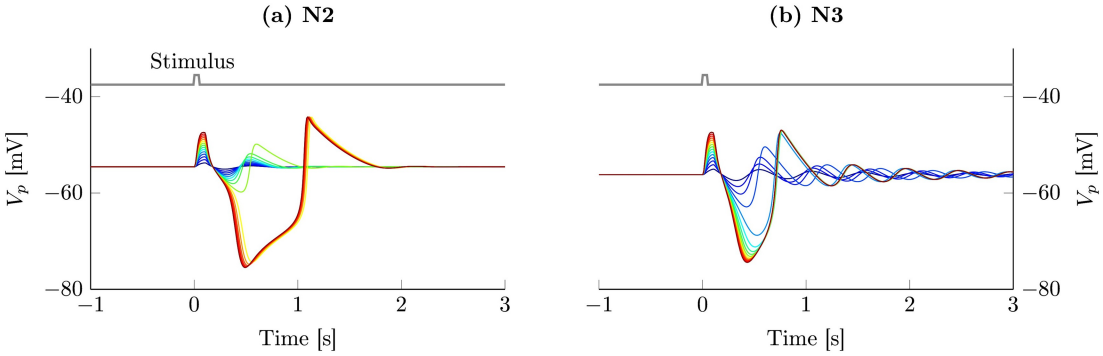

Figure 3.4: Response of the noise-free cortex to artificial stimuli. Excitatory bursts of 50 ms duration were applied to both populations. The spike rate of the stimuli ϕ_{stim} varies uniformly from 5 Hz (dark blue) to 100 Hz (dark red). The stimulus is shown in grey. (a) Bifurcation parameters are set to the mark N2 close to region III (see Table 3.2). There, a canard explosion leads to large amplitude responses that qualitatively resemble a typical evoked KC with its P200, N550 and P900 components. (b) Parameters are set to mark N3, so that the cortex is beyond the cusp close to region II (see Table 3.2). The canard vanished, leading to an even increase in the amplitude of the response.

There, the system is under the influence of the canard phenomenon and positive as well as negative inputs may cause a reverse spike due to a canard explosion, resembling a KC. Additionally, close to the curve of Hopf points the stable active state turns into a stable focus, i.e. the system behaves like a damped oscillator upon perturbation. In Fig. 3.4a the response to artificial stimuli ϕ_{stim} of varying strength is shown, when the cortex is set close to the Hopf bifurcation between region I and III.

Table 3.2: Cortical parameter configurations

Symbol	N2	N3	Unit	Description
σ_p	4.6	6.7	mV	inverse neural gain
$\bar{g}_{\mathrm{KNa}}$	1.33	2	$\mathrm{mS/cm^2}$	adaptation strength

This table depicts the chosen parameter configurations of sleep stages N2 and N3 for the isolated cortical model.

Stimuli of low strength lead to damped oscillations whose amplitudes are considerably larger than during the wake state but smaller than KCs or SOs. However, as the strength

of the stimuli increases the system is pushed into the canard explosion and the amplitude of the response increases rapidly. While in Fig. 3.4a there seems to be a threshold separating the two types of responses, it is actually a smooth transition given sufficiently small increases in stimulation strength.

On the other hand during slow wave sleep, the model is beyond the cusp bifurcation. As in that regime the canard has vanished in the cusp bifurcation, there is no canard explosion anymore. Consequently, increasing the strength of the stimulus leads to a more or less linear increase in the response of the cortex. This is in good agreement with slow wave activity, that is not distinguishable from the ongoing low amplitude background activity.

3.4.3 Reproduction of sleep EEG

We assume the canard explosion described above to be responsible for the generation of KCs during sleep stage N2. Importantly, this requires the cortex to be in the *active* state close to the Hopf bifurcation to region III, rather than being in the silent down state, which is in good agreement with multiple studies who report that during SWS of naturally sleeping animals more time is spent in up states than in down states [Steriade et al., 2001, Destexhe et al., 1999, Timofeev et al., 2001b, Chauvette et al., 2011, Ji and Wilson, 2006, Vyazovskiy et al., 2009].

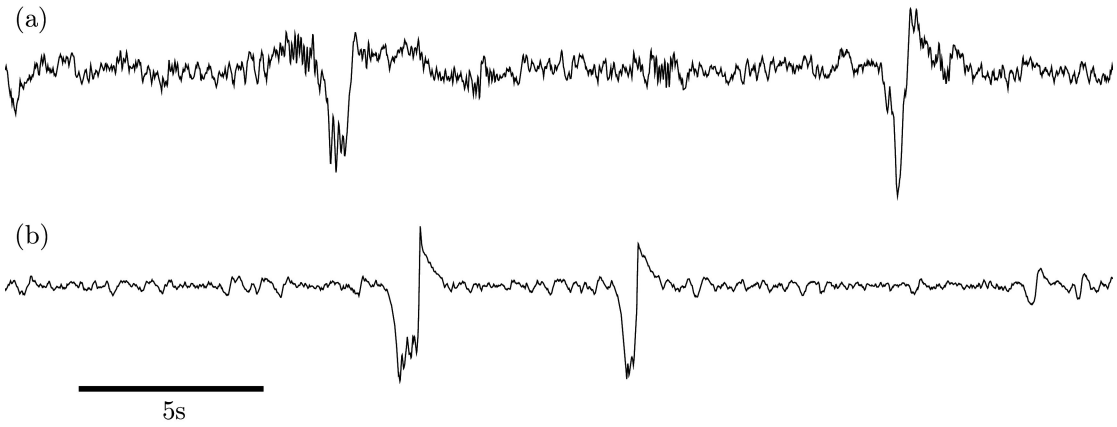

Figure 3.5: Comparison of human EEG with model output in regime N2. Qualitative comparison of (a) human EEG data of sleep stage N2 from electrode Cz with (b) the isolated cortical module in regime N2 (region IV in the bifurcation diagram in Fig. 3.2). The traces illustrate the medium-amplitude background oscillations and the stereotypical shape of spontaneous KCs at the EEG level. The model-KC is noise induced and represents a single relaxation cycle. An evoked KC in the noise-free case is shown in Fig. 3.4a. Model output is excitatory membrane voltage V_p, and both time series are z-scored (Parameters as in Table 3.2).

In Fig. 3.5 a comparison of experimental EEG data from sleep stage N2 with the model output in the N2 configuration from Table 3.2 is shown. There, the cortex is in the up state and shows the expected noise-driven medium-amplitude background oscillations Fig. 3.5. In addition, rare outliers in the background noise may push the model into large-amplitude deflections that closely resemble KCs seen in human EEG. The stochasticity involved in the generation of the KCs is in good agreement with the dynamics seen experimentally during sleep stage N2, where the medium-amplitude background oscillations are suddenly interrupted by large amplitude KCs. Similar to the data the

KCs in the model can show a single pronounced peak or a prolonged down state.

Close to the Hopf, an increase of the inverse gain, σ_p, leads to an *increase* in the amplitude of the background oscillations and they approach the shape of a relaxation cycle. Beyond the cusp the canard vanishes and isolated events in the sense of KCs are not possible anymore (see Fig. 3.4b). We hypothesize that during sleep stage N3 the cortex is beyond the cusp in region I close to the Hopf bifurcation to region II.

This behavior is well reflected in what is seen during sleep stage N3, where SOs appear as large amplitude oscillations, that are *not* separated from the ongoing background activity. Furthermore, it explains the high similarity between KCs and SOs, as they are both shaped by the same homoclinic orbit. In Fig. 3.6 a representative time series is shown with the parameters given in Table 3.2. There the cortex shows high amplitude oscillations around 0.8 Hz. In contrast to the N2 stage, the cortex does not produce KCs in the sense of isolated events that differ from the background oscillations. Rather, the response increases until it approaches the form of a KC, depending on the strength of the perturbation.

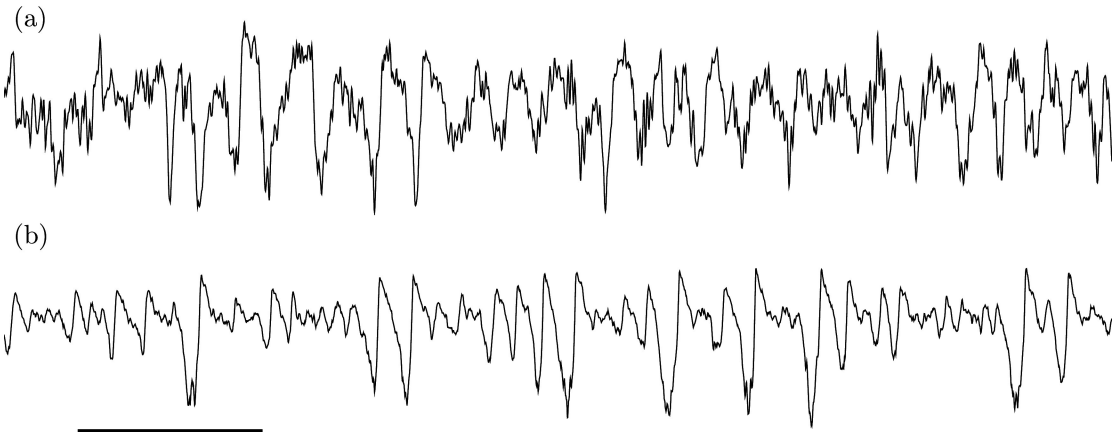

Figure 3.6: Comparison of human EEG with model output in regime N3. Qualitative comparison of (a) human EEG data of sleep stage N3 from electrode Cz with (b) the isolated cortical module in regime N3 (region I in the bifurcation diagram in Fig. 3.2). As the system is close to the Hopf bifurcation noise leads to quasiperiodic oscillations around the stable focus (up state). Large amplitude oscillations resemble KCs as both are shaped by the same homoclinic orbit. The model output is excitatory membrane voltage V_p, and both time series are z-scored (Parameters as in Table 3.2).

Together these findings give rise to a new interpretation of the sleep/wake transition. At the transition to sleep stage N2, the cortex approaches the Hopf bifurcation close to region III, which shifts the EEG trace to higher amplitudes and lower frequencies compared to wake activity. By virtue of a canard explosion this background activity is then interrupted by single, isolated relaxation cycles. As sleep deepens further, the cortex follows the route depicted in Fig. 3.2, while the amplitude of the background oscillations increases and ultimately approaches the form of a KC.

Chapter 4

Thalamic spindle oscillations

This chapter covers the generation of thalamic sleep spindles during NREM sleep in a neural mass model, that was published in [Schellenberger Costa et al., 2016b]. Similar to the previous work on cortical KCs and SOs in Chapter 3, this is accomplished by incorporating additional intrinsic mechanisms into the respective neural populations.In the first section a short overview over previous conductance based models of spindle generation is given. The second section then covers previous neural mass models of thalamocortical interaction mainly during wakefulness but also initial attempts at modeling sleep. Based on these findings, the hybrid model is presented in the third section. The fourth section analyses the dynamic repertoire of the model and investigates the different oscillatory modes the thalamus exhibits. Finally, the fifth section combines the cortical and thalamic neural mass models to close the thalamocortical loop and validate the full model against experimental EEG data from a stimulation study in humans.

4.1 Conductance based models of spindle generation

As discussed in Section 1.5, experimental data suggests a thalamic origin for sleep spindles [Morison and Bassett, 1945, Steriade and Deschênes, 1984, Contreras and Steriade, 1996, Timofeev and Steriade, 1996].

Early detailed Hodgkin-Huxley model focused on the generating mechanisms of spindle rhythmicity through low threshold spikes in RE neurons [Steriade et al., 1990, Destexhe et al., 1994a, Destexhe et al., 1994b, Destexhe et al., 1996b, Bazhenov et al., 1999], demonstrating the contribution of T-type clacium currents to the generation of LTSs. This was then expanded to the interaction between TC and RE cells [Destexhe et al., 1996a, Bazhenov et al., 1998b, Bazhenov et al., 1998a, Destexhe et al., 1998b, Bazhenov et al., 2000, Destexhe and Sejnowski, 2003]. They found that spindle oscillations were initiated in the RE cells, that then projected inhibitory input to the thalamic relay cells. The ensuing depolarization of the TC cells would lead to deinactivation of the T-type calcium currents and initiate a LTS in the thalamic relay cells.

The waxing and waning structure of spindle oscillations is regulated by the I_{h} currents, in the TC cells [Destexhe and Mainen, 1994, Destexhe et al., 1996a], as this counteracts the hyperpolarization necessary for the LTSs and finally leads to the end of the spindle oscillations in the TC cells. Later, excitation of the RE neurons then triggers the next cycle of spindle oscillations. Finally cortical feedback was considered regarding

the synchronization of the spindle oscillations [Destexhe et al., 1998a, Bazhenov et al., 2002, Destexhe and Sejnowski, 2003].

4.2 Thalamic neural mass models

The thalamus has always been one of the main focuses of neural mass models due to its strong influence on cortical dynamics [Lopes da Silva et al., 1974, Lopes da Silva, 1991]. Early work focused on the generation of EEG rhythms during wakefulness [Rennie et al., 2002, Robinson et al., 2004, Robinson et al., 2005, Sotero et al., 2007, Drover et al., 2010, Sotero et al., 2010, Freyer et al., 2011, Roberts and Robinson, 2012]. As sensory information is gated through the thalamus, it plays a pivotal role in the processing of sensory information and the generation of evoked responses in the EEG [Robinson et al., 2001, Nunez and Srinivasan, 2006, Sotero et al., 2007, Kerr et al., 2008].

The involvement in sensory processing also drew a lot of attention with respect to various diseases including epilepsy [Robinson et al., 2002, Suffczynski et al., 2004, Breakspear et al., 2006], Parkinson [Moran et al., 2011], Alzheimer [Bhattacharya et al., 2011, Bhattacharya et al., 2013] and depression [Kerr et al., 2011]. There are also several studies of the thalamus with respect to sleep. However, similar to the cortex, these studies focused mainly on generating continuous oscillations in the respective frequency bands through synaptic interactions [Robinson et al., 2003, Robinson et al., 2011, Roberts and Robinson, 2012]. While they were able to generate spindle band oscillations, they lacked the distinct spindle-like waveform and the event like character of thalamic sleep spindles.

More recently a hybrid approach was utilized to model spindle oscillations in a neural mass model [Żygierewicz et al., 1999, Żygierewicz, 2000, Żygierewicz et al., 2001]. Their model builds heavily on the results of the detailed conductance based models discussed in Section 4.1 incorporating T-type calcium currents as well as a modulating activity dependent h-current. While their model generated reasonable spindle oscillations, there were notable drawbacks. First, synaptic input was again treated independently from the population state, assuming the system to stay close to a steady state. Second, they incorporated additional activity dependent currents into the thalamic reticular population, that did not contribute to the generation of spindle oscillations but increased the complexity of the model considerably.

Their approach was recently adopted by [Cona et al., 2014]. Instead of incorporating the intrinsic currents directly, they utilized the activation function of the T-type calcium current to switch between a high-frequency and a low-frequency firing mode. However, their model is solely based on synaptic drive. Given the importance of strong hyperpolarization for the deinactivation of the T-type calcium current, this simplification is highly questionable. Furthermore, the gradual switching between two firing modes is not a good representation of bursting. Together this lead to a highly stereotypical EEG signal, that does not relate well to experimental data.

4.3 Hybrid approach

Similarly to the cortical module described in Chapter 3 the thalamic module is based on two populations, an excitatory and an inhibitory neural mass, representing a thalamic

relay (t) and the thalamic reticular (r) nucleus respectively. They are coupled via AMPA and GABA synapses, which have slightly different time constants than their cortical counterparts. As discussed in Section 1.4 the thalamic relay population does not possess self-connections and the isolated thalamus receives excitation mainly via sensory input that reaches only the thalamic relay population. Therefore, there is no additional noise input into the thalamic reticular population as well as no selfexcitation (See Fig. 4.1).

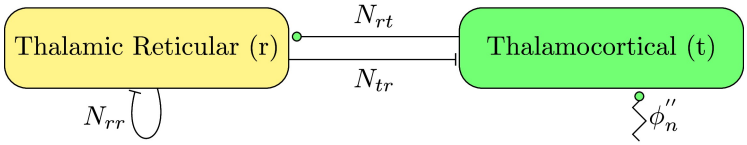

Figure 4.1: Connectivity of the Thalamus. The two thalamic nuclei form connections with each other, as well as a self connection within the thalamic reticular population. In addition to intrinsic activity the thalamic relay population receives background noise from unspecified brain structures, that is identified with sensory input. Circles indicate excitatory synapses, butts inhibitory synapses.

This approach utilizes the mechanisms established in the models by [Destexhe et al., 1996a, Bazhenov et al., 2002, Destexhe et al., 2003]. Consequently, both populations are equipped with a potassium leak current that leads to the observed hyperpolarization [Destexhe et al., 1996b].

$$I_{\mathrm{LK}} = \bar{g}_{\mathrm{LK}}(V_k - E_{\mathrm{K}}), \tag{4.1}$$

as well as a T-type calcium current

$$I_{\mathrm{T}} = \bar{g}_{\mathrm{T}} m_\infty^2 h(V_k - E_{\mathrm{Ca}}), \tag{4.2}$$

which deinactivate upon hyperpolarization and are essential for the generation of low-threshold spikes (LTSs) and rebound bursts. We use the description of I_{T} given in [Destexhe et al., 1996b] for the RE and the one in [Destexhe et al., 1998b] for the TC population.

As previously shown in [Destexhe et al., 1996a, Lüthi and McCormick, 1999, Destexhe et al., 2003, Timofeev and Bazhenov, 2005], the rhythmicity of spindle occurrence and the waxing and waning of the spindle amplitude is caused by an anomalous rectifier channel I_{h}.

$$I_{\mathrm{h}} = \bar{g}_{\mathrm{h}}(m_{\mathrm{h1}} + g_{inc} m_{\mathrm{h2}})(V_t - E_{\mathrm{h}}), \tag{4.3}$$

A sequence of LTS leads to the build-up of calcium, which increases the effective conductivity $\bar{g}_h = \bar{g}_h(m_{\mathrm{h1}} + g_{inc} m_{\mathrm{h2}})$ of I_{h}. The ensuing depolarization of the TC population increasingly counteracts its ability to produce a LTS and terminates the spindle oscillation [Lüthi and McCormick, 1998, Contreras et al., 1997].

Other currents, such as the calcium-dependent potassium currents I_{KCa} and I_{CAN}, are also known to play a role in spindle oscillations, but are omitted for simplicity. The thalamic module is summarized by

$$\begin{aligned} \tau_t \dot{V}_t &= -I_{\mathrm{L}}^t - I_{\mathrm{AMPA}}(s_{et}) - I_{\mathrm{GABA}}(s_{rt}) - C_m^{-1}\tau_t(I_{\mathrm{LK}}^t - I_{\mathrm{T}}^t - I_{\mathrm{h}}), \\ \tau_r \dot{V}_r &= -I_{\mathrm{L}}^r - I_{\mathrm{AMPA}}(s_{er}) - I_{\mathrm{GABA}}(s_{rr}) - C_m^{-1}\tau_r(I_{\mathrm{LK}}^r - I_{\mathrm{T}}^r). \end{aligned} \tag{4.4}$$

Parameter settings for the currents are identical to [Chen et al., 2012], with the exception

of the deactivation function h^t_∞ of the thalamic relay population, that is shifted towards more depolarized membrane voltages.

4.4 Dynamical structure

As suggested by the detailed conductance based models, incorporation of the intrinsic currents may lead to oscillations in the spindle band, due to deinactivation of T-type calcium currents. Here, $\bar{g}_h$ and $\bar{g}_{\mathrm{LK}}$ were chosen as bifurcation parameters, as hyperpolarization via I_{LK} is necessary for hyperpolarization and I_{h} is required for the waxing and waning structure.

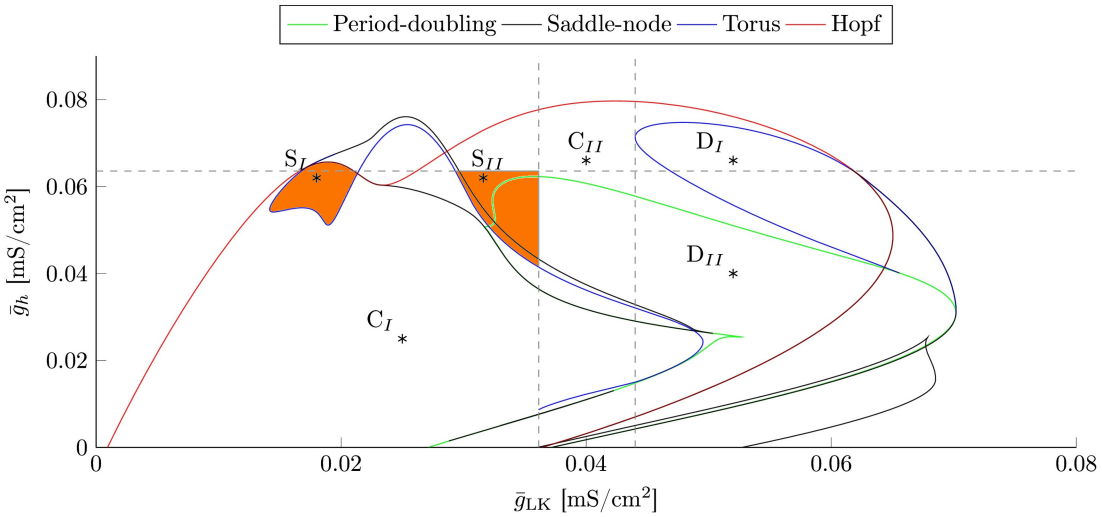

Figure 4.2: Two-dimensional bifurcation diagram of the thalamus. A Hopf bifurcation leads to the emergence of a stable limit cycle. The limit cycle loses its stability through torus bifurcations (blue) that arise from a blue sky catastrophe. this leads to spindle oscillations in the orange shaded regions. The left spindle regime ($\mathrm{S_I}$) is encased by a Hopf and a torus bifurcation, whereas the right spindle regime ($\mathrm{S_{II}}$) is constrained by two global bifurcations that are indicated by the dashed gray lines. The vertical line marks the emergence of the torus bifurcation, whereas the horizontal gray line marks the cusp bifurcation where the two saddle-nodes that accompany the left torus bifurcation vanish. The torus bifurcation on the right marks the transition from spindle oscillations to delta oscillations. The labeled points mark the parameter settings utilized in Fig. 4.3, which are given in Table 4.1.

A two-dimensional bifurcation analysis of the thalamic module reveals the existence of a Hopf bifurcation, as depicted in Fig. 4.2, which generates continuous oscillations in the spindle band due to deinactivation of the T-type calcium current (See Fig. 4.3-$\mathrm{C_I}$ and Fig. 4.3-$\mathrm{C_{II}}$). There is a distinct window for which the T-type current is able to generate oscillations. Consequently for large values of $\bar{g}_{\mathrm{h}}$ as well as too strong hyperpolarization via I_{LK}, the thalamus is unable to generate oscillations.

Table 4.1: Parameter settings for the isolated thalamus

Symbol	$\mathrm{S_I}$	$\mathrm{S_{II}}$	$\mathrm{D_I}$	$\mathrm{D_{II}}$	$\mathrm{C_I}$	$\mathrm{C_{II}}$	Unit
$\bar{g}_{\mathrm{LK}}$	0.018	0.032	0.052	0.052	0.025	0.04	mS/cm^2
$\bar{g}_{\mathrm{h}}$	0.062	0.062	0.066	0.04	0.025	0.066	mS/cm^2

Parameter settings of the isolated thalamus. This table lists the parameter values for the different dynamic regimes of the isolated thalamic module, that are utilized in Fig. 4.3.

The torus bifurcations emerge from a blue sky catastrophe that is generated by the slow-fast interaction between the fast T-type channels and their slow modulation via I_{h}, which is similar to other models that exhibit switching between tonic spiking and structured bursting activity [Shilnikov and Cymbalyuk, 2005, Mayer et al., 2006, Burke et al., 2012].

As depicted in Fig. 4.3-$\mathrm{S_I}$ and Fig. 4.3-$\mathrm{S_{II}}$ this leads to spindle like oscillations in the orange shaded regions in Fig. 4.2. The spindles exhibit an oscillation frequency of around 13 Hz. The spindle frequency depends on the strength of the T-type calcium current $\bar{g}_{\mathrm{T}}$. Importantly, spindle oscillations are initiated intrinsically. The thalamic module does *not* require modulatory input from external sources to initiate/terminate them.

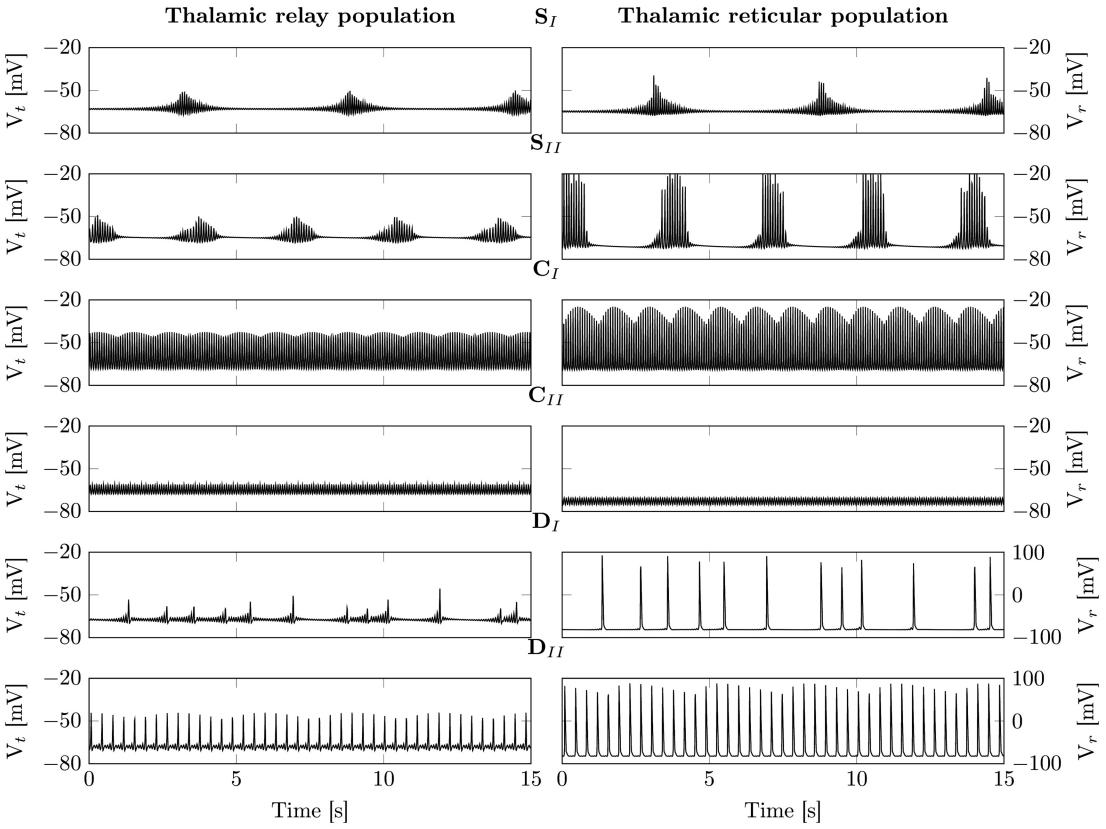

Figure 4.3: Dynamic modes of the isolated thalamic module. This figure illustrates the different dynamic modes the isolated thalamic module exhibits. The left panels depict the thalamic relay membrane voltage, whereas the right panels illustrate that of the thalamic reticular population. The parameter values are depicted in Fig. 4.2 and given in Table 4.1. $\mathrm{S_I}$ and $\mathrm{S_{II}}$: The isolated thalamus generates rhythmic spindle oscillations via a balanced interplay between I_{T} and I_{h}. $\mathrm{C_I}$ and $\mathrm{C_{II}}$: Outside of the spindle regime fast oscillations generated by the T-type calcium currents dominate and I_{h} is unable to sufficiently depolarize the thalamic relay population to cease them. $\mathrm{D_I}$ and $\mathrm{D_{II}}$: For strong hyperpolarization through I_{LK} the thalamic module switches into low frequency delta oscillations.

Activation of I_{h} is responsible for a refractory period that follows a spindle. As long as I_{h} activation persists, LTS generation is impeded and stronger perturbations are necessary to trigger spindle oscillations. Consequently, an increase in $\bar{g}_{\mathrm{h}}$ results in a larger inter-spindle interval. The left spindle regime ($\mathrm{S_I}$) is encased by the Hopf and the torus bifurcation, whereas the right spindle regime ($\mathrm{S_{II}}$) is constrained by two global bifurcations that are indicated by the dashed gray lines. The vertical line marks the emergence of the torus bifurcation, whereas the horizontal gray line marks the cusp bifurcation where the two saddle-nodes that accompany the left torus bifurcation vanish.

For strong hyperpolarization (high $\bar{g}_{\mathrm{LK}}$) the T-type calcium current leads to a single strong spike, rather an oscillation in the spindle band (See Fig. 4.3-$\mathrm{D_I}$ and Fig. 4.3-$\mathrm{D_{II}}$). There, the system transitions from medium frequency spindle oscillations to low frequency delta oscillations, e.g. Fig. 4.3-$\mathrm{D_I}$ and Fig. 4.3-$\mathrm{D_{II}}$. The labeled points mark the parameter settings utilized in Fig. 4.3 and are given in Table 4.1

4.5 Thalamocortical model

In this section we investigate the interplay between thalamus and cortex to reproduce the characteristics of different sleep stages. The cortex and the thalamus are coupled via long range afferents, that send excitatory input via Eq. (2.6) as depicted in Fig. 4.4.

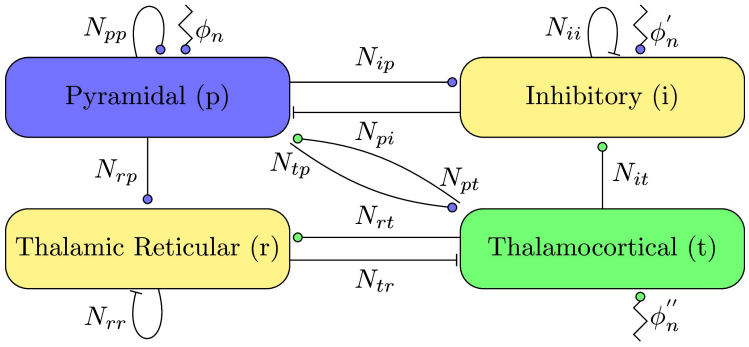

Figure 4.4: Connectivity of the thalamocortical system. Cortex and thalamus are interconnected via long range afferents, that originate from the cortical pyramidal and the thalamic relay population respectively. They both project on all populations of the other structure.

Please note, that this is a strong simplification of the cortical architecture discussed in Section 1.2. Physiologically, thalamic input would reach spiny stellate cells in layer 4 that feed the thalamic input into the pyramidal layer 5.

In the coupled system, the cortex and thalamus provide excitatory drive to each other. Consequently, the bifurcation parameters of both modules have to be adjusted to compensate for the additional input (See Table 4.2. For the thalamus the parameters were set within the right spindle regime from Fig. 4.2, as this lead to the best reproduction of both sleep stage N2 and N3.

Table 4.2: Parameter settings for the thalamocortical system

Symbol	N2	N3	Unit	Description
σ_p	4.7	6	mV	Neuronal gain
$\bar{g}_{\mathrm{KNa}}$	1.33	1.88	$\mathrm{mS/cm^2}$	Adaption strength
$\bar{g}_{\mathrm{LK}}$	0.034	0.034	$\mathrm{mS/cm^2}$	Potassium leak conductance
$\bar{g}_{\mathrm{h}}$	0.052	0.062	$\mathrm{mS/cm^2}$	h-current conductance

This table shows the different settings for the bifurcation parameters of the full model used throughout this study.

4.5.1 K-complexes and spindles during sleep stage N2

Given the parameter setting in Table 4.2, the cortical module is within a stable state, close to the Hopf bifurcation accompanied by the canard explosion. This leads to noise

driven medium amplitude background oscillations around the stable focus, that are interrupted by large amplitude deflections (KCs), which were discussed in Chapter 3.

At that parameter setting the thalamus in within the spindle regime and periodically creates spindle oscillations. As in the cortical module KCs occur at a low rate, spindle initiation and termination are closely linked to the time course of I_h, similar to the isolated thalamic module. Additionally, if the cortex generates a KC, the sudden drop of excitatory drive hyperpolarizes the RE and TC population, leading to deinactivation of I_{T}. The ensuing depolarization upon the transition back to the active state triggers a spindle sequence in turn. The spindle then projects back into the depolarizing phase of the KC. This is in good agreement with the grouping of spindles and KCs observed experimentally [Contreras and Steriade, 1995, Mölle et al., 2002].

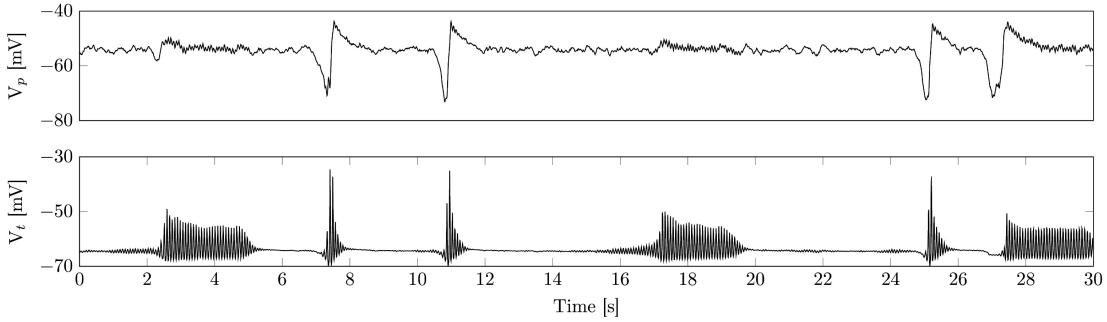

Figure 4.5: Thalamocortical simulation of sleep stage N2. Shown are membrane voltages of the cortical pyramidal (top) and the thalamic relay population (bottom). While the spindle oscillations are generally induced by fluctuations in background noise, there is also a grouping between cortical KCs and thalamic spindles (see 7 s-9 s and 10 s-12 s). The grouping stems from the lack of depolarizing input during a cortical KC.

Although less likely the model can also give rise to KCs triggered by a spindle. This can be achieved if thalamic input is sufficient to push the cortex into the canard explosion. The probability of a KC triggered by a spindle increases with the connection strength from the thalamic to the cortical module and the proximity of the cortical module to the canard. The parameters for the output in Fig. 4.5 are given in Table 4.2.

4.5.2 SOs and spindles during sleep stage N3

On the transition to sleep stage N3 the canard phenomenon vanishes in a cusp bifurcation and only a high amplitude limit cycle remains. As discussed in Section 3.4.1 Slow oscillations are noise driven oscillations around a stable focus, close to a Hopf bifurcation.

In contrast to sleep stage N2 spindle initiation and termination are now dominated by the modulatory input from the cortical module, that overrules the I_{h} rhythm. Rather than occurring rhythmically spindles are time-locked to the depolarized phase of a SO. In Fig. 4.6 an example time series is shown. Importantly, not every SO is able to trigger a spindle, as can be seen in Fig. 4.6 (9-12 s, 13-15 s). In a sequence of SOs the first generally triggers a spindle, which leads to an activation of I_{h}. This reduces spindle amplitude or even inhibits spindle initiation by the following SO.

While the cortex transitions into a different dynamic mode, it is not fully clear whether this is also true for the thalamus. There are two possible modes, that are indistinguishable i the EEG data. On one hand, the thalamus could be in a continuous oscillating regime, where the oscillations is silenced by strong cortical input. On the

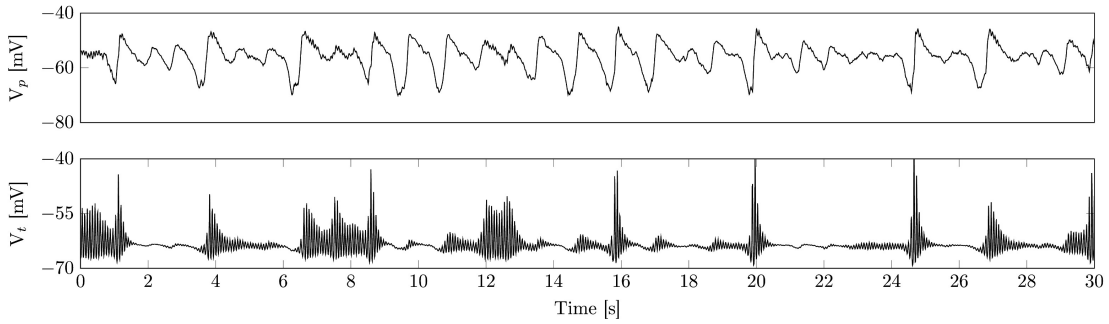

Figure 4.6: Thalamocortical simulation of sleep stage N3. Shown are membrane voltages of the cortical pyramidal (top) and the thalamic relay population (bottom). During N3 the model shows ongoing slow oscillatory activity. In contrast to sleep stage N2, SOs cannot be identified as isolated events. Furthermore, there are no isolated spindle oscillations and spindle activity is time-locked to SOs.

other hand it could still be in the genuine spindle regime with spindles time locked to the now more frequent slow oscillations.

4.5.3 Endogenous event triggered averages

To further validate the model, we determined averages of the generated EEG signal and fast spindle power time-locked to the negative peak of the endogenous KCs/SOs during N2 and N3. This method is often used to illustrate the grouping of spindles by SOs and morphological features of SOs, e.g. in [Ngo et al., 2013b, Ngo et al., 2013a, Mölle et al., 2002]. A comparison of model output and experimental data for N2 and N3 is depicted in Fig. 4.7.

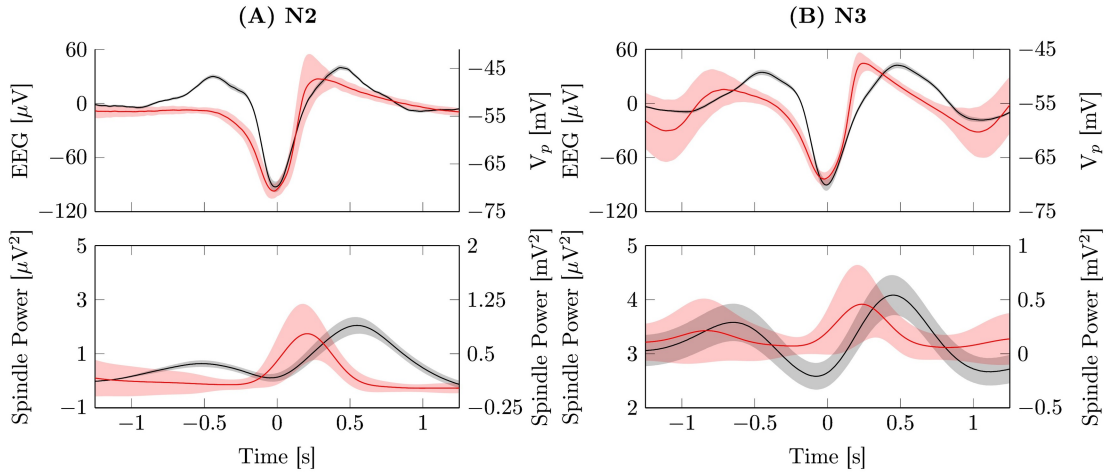

Figure 4.7: Event triggered average potentials. Averaged EEG signal (top) and fast spindle band power (bottom) time-locked to the negative peaks (t=0 s) of all detected events from electrode *Cz* (black, left axis) and model output (red, right axis). (A) Detected KCs from data scored as sleep stage N2 (Experiment: $227,45 \pm 19,22$, Model: 238 events). (B) SO average from data scored as sleep stage N3 (Experiment: $983,64 \pm 106,1$, Model: 654 events). Each simulation was run for 3600 s with parameters set according to Table 4.2.

As can be seen in Fig. 4.7, the grouping of spindles by SOs is present in the model. Spindle power is highest during the positive half-wave following the negative peak. However, there are some notable differences. Compared to the experimental data the initial depolarization preceding the transition to the down state is less prominent, leading to a shallower slope of the transition to the down state.

In the thalamocortical model the transition to the depolarized up state occurs considerably earlier with a time to peak of 300 ms, compared to 440 ms in the data. This stems from strong depolarizing input by thalamic spindle bursts, which start directly after the negative peak of a KC/SO and push the cortex further into the depolarized state.

These discrepancies in the timing are to be expected given the simplifications of the cortical architecture. Here more sophisticated models, that respect the full cortical processing of sensory information should yield a better agreement with the experimental data. However, our findings are still in line with other experimental studies, that find different timings of spindles for the supplementary motor area of the cortex [Andrillon et al., 2011].

4.5.4 Closed-loop auditory stimulation

In the following we show the ability of the model to reproduce data from a recent experiment in humans performing auditory closed-loop stimulation during NREM sleep [Ngo et al., 2013b]. The stimulation protocol is as follows: After the negative peak of a SO was detected, two auditory stimuli were applied phase-locked to the following positive peak of the depolarized up phase of the detected and the subsequent SO.

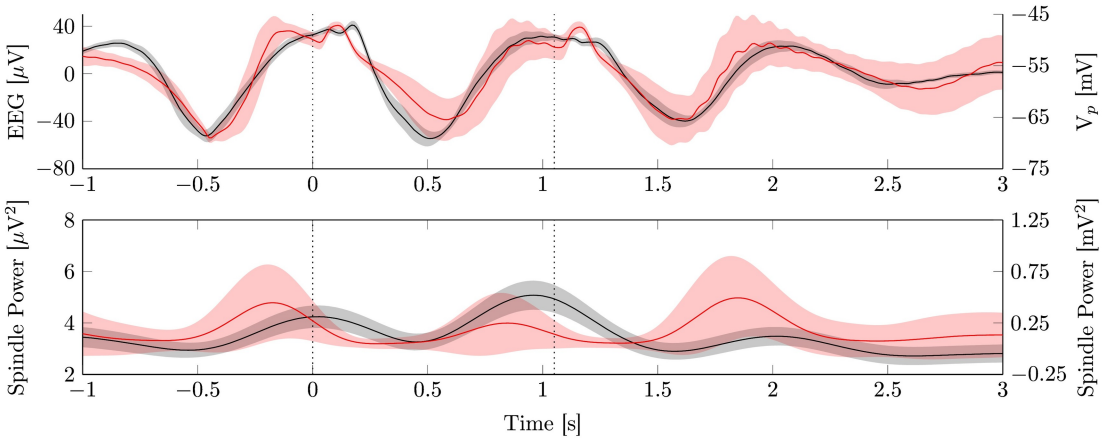

Figure 4.8: Closed loop stimulation. The upper panel depicts in black the mean (± SEM) evoked potentials of human EEG data from electrode *Cz* during closed loop stimulation, time locked to the first stimulus (11 subjects, 245.6 ± 38.1 stimuli). In red the reproduction of the stimulation protocol with the model is shown (mean ± SD, 88 stimuli). The dashed line marks the stimulus onset. The lower panel shows the corresponding fast spindle power.

In the experimental study the delay time between the negative peak and the ensuing positive half-wave peak was determined for every subject independently with an average of 470 ms. The second stimulus followed after a fixed interval of 1075 ms. Detection was then paused for 2.5 s. We accordingly determined the delay time from the model output, resulting in a delay of 450 ms for the N3 parameter setting. The second stimulus was chosen to occur 1075 ms after the first one and we also paused detection for 2.5 s. Stimuli are given as elevations in mean background noise of the thalamic relay population to 70 Hz for a duration of 80 ms.

In Fig. 4.8 we depict the averaged EEG signal and model output time-locked to the first stimulus ($t = 0$). There is a good agreement between model output and the experimental data. Especially the large amplitude, late components of the ERP are very

close to the original waveform. The early component of the evoked potential, the P200, can be seen in the experimental data after each stimulus, but it is more pronounced in the model output. This is most likely due to an oversimplification of the model to a single population, whereas in vivo the sensory input only projects into a fraction of the cortex

In addition, the evoked spindle responses of model and data also have similar time courses. In both cases spindle power is systematically increased during the depolarized up phases induced by the stimuli. However, the strong increase in spindle power seen in the data after the first stimulus is not visible in the model. We hypothesize this to stem from a recruitment effect, where the stimulus activates a larger fraction of the thalamus than the endogenous slow oscillation would. As our thalamic module is a point model without any spatial extent, these effects are excluded by construction.

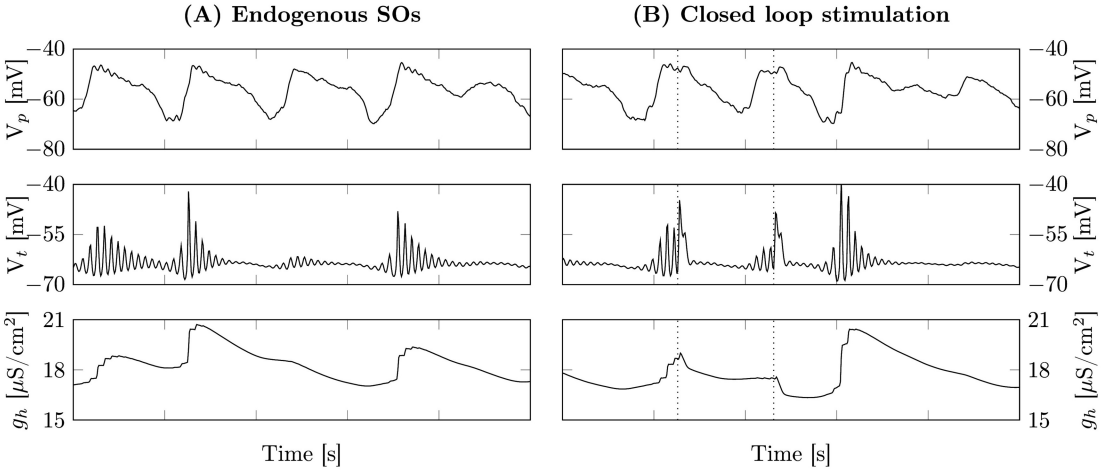

Figure 4.9: Stimulation disturbs refractoriness. The upper two panels depict the membrane voltages of the pyramidal and thalamic relay populations, respectively. In the third panel the effective conductivity g_h of the I_h current is shown. (A) Example time series of an unperturbed train of SOs during sleep stage N3. The first two SOs lead to an activation of I_h, that slowly declines back to baseline levels. As I_h activation is still well above baseline, the third SO is unable to trigger a spindle response. During the fourth SO I_h activation is sufficiently low so that a spindle occurs. (B) Shown is an example of closed loop stimulation during sleep stage N3, with the dashed lines indicating stimulus onset. In contrast to the endogenous case, the depolarization of the thalamic relay population induced by the stimulation leads to a rapid decrease in I_h activation, so that the following SO triggers a spindle. Parameters as in Table 4.2.

Interestingly, in the experimental data there is a drop in spindle power after the second stimulus is applied. This seems to be a refractoriness of the thalamus after the second slow oscillation, which has also been observed in [Ngo et al., 2015]. Despite the model showing such a refractory period in the isolated thalamus (See Fig. 4.3A), as well as during trains of endogenous SOs in the full model (See Fig. 4.9A), it lacks it upon stimulation (See Fig. 4.9B).

This happens because stimulation disturbs the I_h mediated spindle termination mechanism. As the stimulation depolarizes the TC population, the calcium concentration drops, as calcium influx through the I_T current stops and calcium leaks out with a time constant of 10 ms. Without the elevated calcium concentration, I_h deactivates back to baseline levels and immediately allows for a new full fledged spindle. This is exemplified by the effective conductivity $g_h = \bar{g}_\mathrm{h}(m_{\mathrm{h}1} + g_{inc} m_{\mathrm{h}2})$ of the I_h current depicted in Fig. 4.9.

The disturbance of the refractoriness by the external stimulation challenges our understanding how external input affects the intrinsic mechanisms. This finding suggests that the I_{h} current alone might not be sufficient to explain the refractoriness of spindle generation but requires other mechanisms such as firing rate adaptation in the RE population as suggested by [Żygierewicz et al., 2001].

Chapter 5

Sleep Regulation

In the previous two chapters we have analyzed the dynamics of the cortical and thalamic neural mass models and investigated how these dynamics lead to the observed EEG signals. However, while the bifurcation analysis provides the overall dynamical repertoire, a fixed choice of the bifurcation parameters was necessary for the individual simulations.

As discussed in Section 1.7, this is in strong contrast to physiology where, driven by sleep regulatory networks, the dynamics of the brain changes dynamically over the course of the night, rather than switching between isolated states. To remedy this drawback this chapter is devoted to the effect of sleep regulation on the cortical neural mass model presented in Chapter 3. In the first section the slightly different rate based formulation of the sleep regulatory networks is introduced. The second section then discusses the influence of neuromodulators released by the sleep regulatory network upon the bifurcation parameters of the cortex. Finally, the third section demonstrates the ability of the combined model to dynamically generate the EEG signal of the different sleep stages as well as wakefulness and reproduce the characteristics of the transition between them, which was published in [Schellenberger Costa et al., 2016a]

5.1 Population based models of sleep regulation

Early approaches on modeling the sleep-wake transition focused on homeostatic regulation [Borbély, 1982, Forger et al., 2015]. Only recently the faster cycling between NREM and REM sleep has been incorporated with varying levels of anatomical detail [Tamakawa et al., 2006, Diniz Behn et al., 2007, Phillips and Robinson, 2007, Diniz Behn and Booth, 2010, Rempe et al., 2010, Kumar et al., 2012]. These models describe the sleep-wake transition through firing rates of the involved neuronal populations. Depending on whether wake-promoting, REM-off or REM-on populations are active the system is assumed to be in a state of wakefulness, REM or NREM sleep. The transition between those stages is driven by synaptic interactions between the involved populations and the corresponding level of neurotransmitters, which is modulated by circadian and homeostatic drives.

For the sake of simplicity a reduced model was chosen [Diniz Behn and Booth, 2012], that accumulates populations which serve similar functionality into a single population neglecting more complex interactions [Rempe et al., 2010, Diniz Behn and Booth, 2010, Kumar et al., 2012], including those with the SCN and circadian modulation. This

results in a minimal model with only three populations (WAKE, NREM, and REM). See [Fleshner et al., 2011, Gleit et al., 2013] for extended models incorporating circadian modulation of the sleep regulatory network.

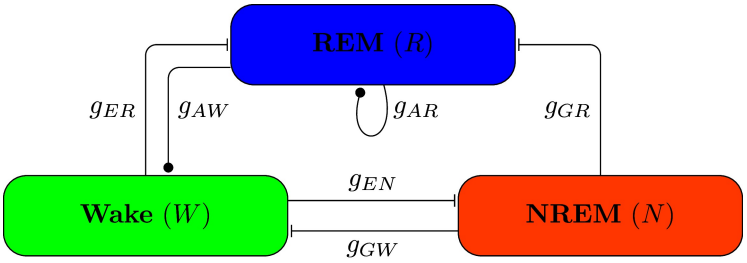

Figure 5.1: Connectivity within the sleep regulatory network. The sleep regulatory network consists of three populations, Wake (W), NREM (N), and REM (R), that are associated with a specific neuromodulator, which is noradrenalin (E) for Wake, acetylcholine (A) for REM, and GABA (G) for the NREM population. They interact mainly through inhibition, with the interaction strength given by the synaptic weights g.

In contrast to the neural mass framework introduced in the previous section, they use an equivalent formulation related to the Wilson-Cowan formalism [Wilson and Cowan, 1973]. They directly utilize the firing rates $F_k(V_k)$ rather than the membrane voltages V_k as their system variables [Diniz Behn et al., 2007, Diniz Behn and Booth, 2010, Diniz Behn and Booth, 2012]. To provide a direct link to their work, this formulation is kept and the firing rate of population k is denoted as F_k for the sleep regulatory model.

The firing rate F_k of the presynaptic population k elicits the release of neurotransmitter X into the synaptic cleft. The change of neurotransmitter concentration C_X is given by

$$\tau_X \dot{C}_X = \tanh(F_k/\gamma_X) - C_X. \tag{5.1}$$

Here, X depicts the type of neurotransmitter (i.e. E for noradrenalin, G for GABA or A for acetylcholine), γ_X the gain of neurotransmitter release and τ_X the corresponding time constant. In their study on the reduced model Diniz Behn et al. assumed $\tau_k \gg \tau_X$, approximating the change in neurotransmitter concentration to be instantaneous. However, given that the time constant of the cortical model is in the range of milliseconds this assumption is not valid anymore.

Varying levels of neurotransmitters then change the postsynaptic activity

$$\tau_k \dot{F}_k = Q_k^{SR}\left(\sum_X g_{X,k} C_X\right) - F_k, \tag{5.2}$$

with the time constant τ_k and weights $g_{X,k}$ that scale the strength of the synaptic responses. It is important to note, that due to the long timescale τ_k the synaptic inputs are assumed to act instantaneous. This is equivalent to Eq. 2.8 for $\alpha_m = \delta(t)$. The formulation of the firing rate function Q_k^{SR} utilized by Diniz Behn et al. is mathematically equivalent to

$$Q_k^{SR}(Y) = \frac{F_k^{\max}}{1 + \exp(-(Y - \beta_k)/\alpha_k)}. \tag{5.3}$$

Here β_k denotes the firing rate threshold, α_k the corresponding inverse gain and Y the sum of the weighted neurotransmitter inputs. Note that for the NREM population the threshold is dependent on the homeostatic sleep drive h through $\beta_N = kh$, where k

scales the influence of the sleep drive.

Following the two-process model originally proposed by [Borbély, 1982], the transition between sleep and wakefulness is driven by an homeostatic sleep drive $h(t)$. It builds up during wakefulness, due to high activity F_W of the wake population and declines during sleep, when F_W is low. Assuming a maximal strength of h^{max}, this can be described by

$$\dot{h} = \frac{h^{max} - h}{\tau_h^w}\mathcal{H}(F_W - \theta_h) - \frac{h}{\tau_h^s}\mathcal{H}(\theta_h - F_W), \tag{5.4}$$

where $\mathcal{H}$ stands for the Heaviside function, θ_h defines the sleep/wake transition point and τ_h^i depicts the time constants for increase and decline of h during sleep and wakefulness respectively.

It is important to note, that in this work the term *neurotransmitter* is used only in the context of the sleep regulatory network. There noradrenalin, GABA and acetylcholine act as transmitters eliciting a synaptic response. Given the assumption that GABA from the sleep regulatory network is released on extrasynaptic sites in the cortical model, *neurotransmitters* from the sleep regulatory network only *modulate* the activity of the pyramidal population. Consequently, the term *neuromodulator* is utilized in the context of the cortical model.

5.2 Action of neuromodulators

According to the findings presented in Chapter 3, changes in the inverse neural gain σ_p and the adaptation strength $\bar{g}_{\mathrm{KNa}}$ lead to the transition between wakefulness and sleep stages N2/N3. As discussed in Section 1.7 they are subject to neuromodulation by certain neuromodulators, as depicted in Table 5.1.

Table 5.1: Neuromodulators and cortical bifurcation parameters

	Wake	NREM	REM
Acetylcholine	low	low	high
Noradrenalin/Serotonin	high	low	increasing
extrasynaptic GABA	low	high	high
$\bar{g}_{\mathrm{KNa}}$	low	high	low
σ_p	low	high	low

Qualitative levels of neuromodulators and their influence on the cortical bifurcation parameters.

Acetylcholine blocks potassium currents [McCormick, 1989, McCormick and Huguenard, 1992], such as I_{KNa} and reduces firing rate adaptation of cortical neurons [Madison et al., 1987, Barkai and Hasselmo, 1994, Hasselmo and Barkai, 1995, Liljenström and Hasselmo, 1995]. Likewise, serotonin [Colino and Halliwell, 1987, Davies et al., 1987] and noradrenaline [Madison and Nicoll, 1982, Madison and Nicoll, 1986] have been shown to affect firing rate adaptation. In contrast, extrasynaptic release of GABA increases activation of potassium currents [Saint et al., 1990, Gage, 1992].

Consequently $\bar{g}_{\mathrm{KNa}}$ increases during the transition into NREM sleep and declines during REM and wakefulness, see Table 5.1 for an overview. As there are no quantitative measurements, our choice of the dependency between the neuromodulator concentrations

and $\bar{g}_{\mathrm{KNa}}$ is arbitrary. For the sake of simplicity, we assume the following relationship for the strength of firing rate adaptation

$$\tau_g \dot{g}_{\mathrm{KNa}} = \bar{g}_{\mathrm{KNa}}(1 - 0.95C_A)(1 - 0.6C_E)(2C_G) - g_{\mathrm{KNa}}. \tag{5.5}$$

Please note, that we utilize g_{KNa} for the dynamically modulated conductivity, whereas $\bar{g}_{\mathrm{KNa}}$ describes its default value.

The neural gain, on the other hand, is increased by acetylcholine [Barkai and Hasselmo, 1994, Disney et al., 2007, Gulledge et al., 2009, Soma and Shimegi, 2012], serotonin [Zhang and Arsenault, 2005], and noradrenalin [McCormick, 1989, Timmons et al., 2004]. With σ_p acting as the inverse gain, it is maximal during NREM sleep and at the lowest during REM and wakefulness (see Table 5.1). Due to the lack of quantitative measurements which might hint to a more complex dependency, we work with the most simple assumption, namely a linear dependency between σ_p and the neuromodulator concentrations

$$\tau_\sigma \dot{\sigma}_p = \bar{\sigma}_p - (4C_E + 2C_A) - \sigma_p. \tag{5.6}$$

As the sleep regulatory network deals with normalized concentrations of the respective neuromodulators, we assume that the cortical levels are identical to those within the sleep regulatory network. This leads to the following model architecture

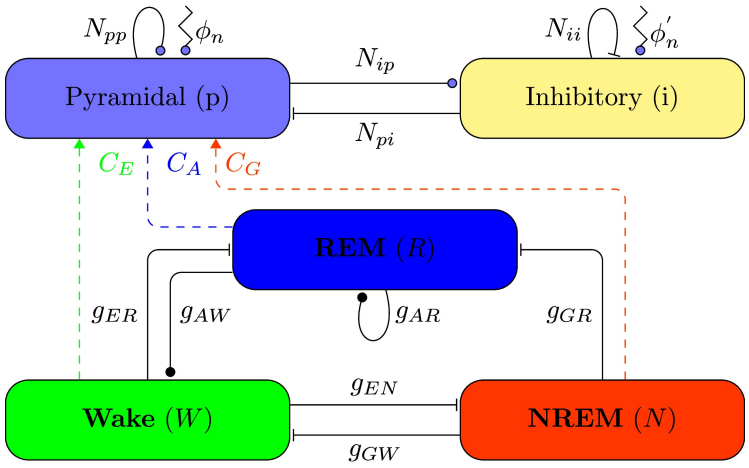

Figure 5.2: Connectivity between sleep regulatory network and cortex. The sleep regulatory network consists of three populations, Wake (W), NREM (N), and REM (R), that are associated with a specific neuromodulator, which is noradrenalin (E) for Wake, acetylcholine (A) for REM, and GABA (G) for the NREM population. They interact mainly through inhibition, with the interaction strength given by the synaptic weights g. The sleep regulatory network modulates activity of the pyramidal population through the respective neuromodulators C. The different types of neuromodulatory input are indicated by colored triangles connected through dashed lines. The cortical submodule is as given in Chapter 3.

5.3 Results

Here, we will recapitulate our results in comparison to the reduced Diniz Behn model and relate them to changes of the bifurcation parameters of the cortex model. As illustrated in Fig. 5.3, the system is primarily in a state of wakefulness, accompanied by high levels of noradrenalin, during which the homeostatic sleep drive increases. Given sufficiently

large sleep pressure the cortex will then transition into NREM sleep, characterized by elevated levels of GABA. As can be seen in Fig. 5.2 the NREM population also inhibits REM sleep. However, inhibition through GABA is weaker than that by noradrenalin during wakefulness ($|g_{GR}| > |g_{ER}|$), which leads to a slow increase in REM activity that ultimately switches the system into REM sleep.

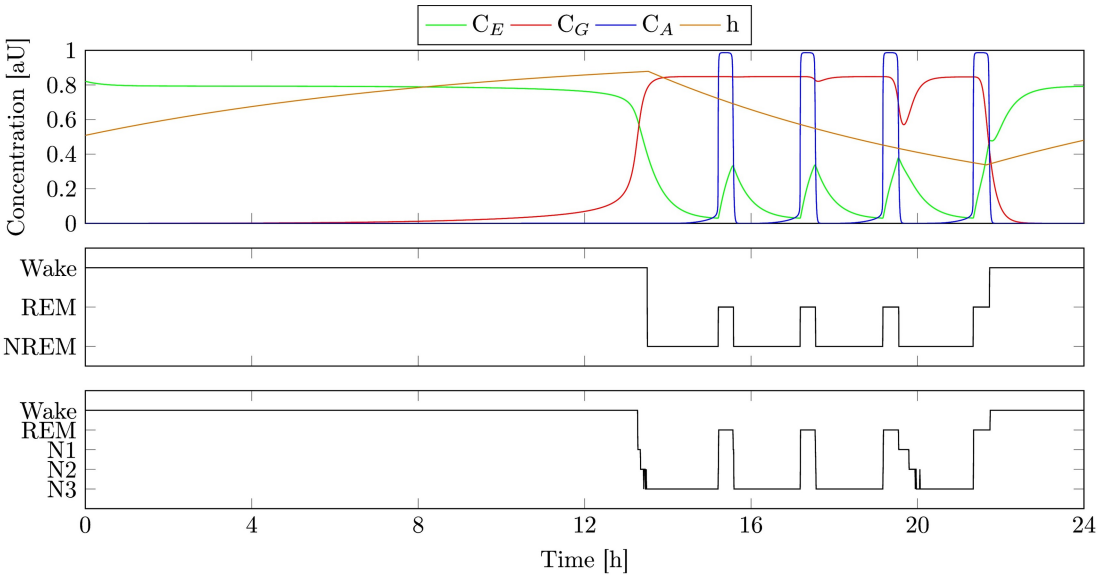

Figure 5.3: Activity of the sleep regulatory network. In the upper panel the concentration of the different neurotransmitters in the sleep regulatory network is shown over the course of one day, together with the homeostatic sleep drive. The concentrations are directly related to the firing rates of the different populations. In the mid panel the hypnogram according to Diniz Behn and Booth [Diniz Behn and Booth, 2012] is shown, which is based on the activity of the sleep regulatory network. In contrast, the lower panel depicts the hypnogram based on scoring of the activity of the pyramidal population, following the AASM rules for the EEG. There, we further subdivide NREM sleep into stages N1-N3.

The high levels of acetylcholine during REM sleep promote release of noradrenalin. As noradrenalin suppresses the REM population, REM sleep is terminated through reciprocal interaction between the Wake and the REM population. The ultradian cycling between NREM and REM sleep continues until the homeostatic sleep drive is sufficiently low. At that point the Wake population takes over and the system transitions from REM sleep to wakefulness. Following Diniz Behn and Booth wakefulness is defined as states with $C_E > 0.4$, REM through $C_A > 0.4$, and all other states as NREM. As described below, we utilize the activity of the cortical model to score the different sleep stages similar to experimental sleep research.

Due to its simplicity the presented sleep regulatory network exhibits differences with regard to human sleep EEG. In the model, the ultradian rhythm is uniform over the night, with equal portions of NREM and REM sleep for every cycle. This is in contrast to human sleep EEG, where NREM sleep is dominant in the first half of the night, whereas REM sleep occupies the better part of the second half. In the chosen 3 population regulatory network, the duration of REM episodes is directly linked to those of NREM through the reciprocal interaction with the Wake population. Initiation of REM sleep is due to declining levels of noradrenalin during NREM, whereas termination of REM is driven by increasing levels of noradrenalin (Fig. 5.3). Therefore, prolonging a REM episode would also lead to a longer NREM stage.

Furthermore, as there is only one NREM population, the model is not able to capture the deepening of NREM sleep within an ultradian cycle, which can be observed in the human EEG. This is exemplified in the lower panel of the Fig. 5.3, where the classification of sleep stages is based on the activity of the cortex. Except for the last ultradian cycle, where the NREM population shows a distinct drop in activity, the transition into sleep stage N3 is nearly instant, whereas in human sleep, N2 occupies a majority of NREM sleep (Fig. 1.1 for comparison). Interestingly the last ultradian cycle shows a prolonged transition from N1 over N2 to finally sleep stage N3. This is due to reduced sleep pressure h, that results in a reduced activity of the NREM population. Here a more sophisticated model, where NREM promoting populations are silenced during REM sleep might lead to more realistic results.

5.3.1 Modulation of the bifurcation parameters

As discussed above, the varying levels of neuromodulators affect the two bifurcation parameters g_{KNa} and σ_p. The combination of the three different neuromodulators leads to an increase of both parameters during NREM sleep and a decline during REM and wakefulness (See Fig. 5.4). Given the slow timescale of the sleep regulatory network, the bifurcation parameters can be assumed as quasi-static, so that our findings on the isolated cortex in Chapter 3 are still valid for the coupled system and we can use the same bifurcation diagram. At the same time, the cortical model does not influence the sleep regulatory network directly and the analysis from [Diniz Behn and Booth, 2012] is unaffected.

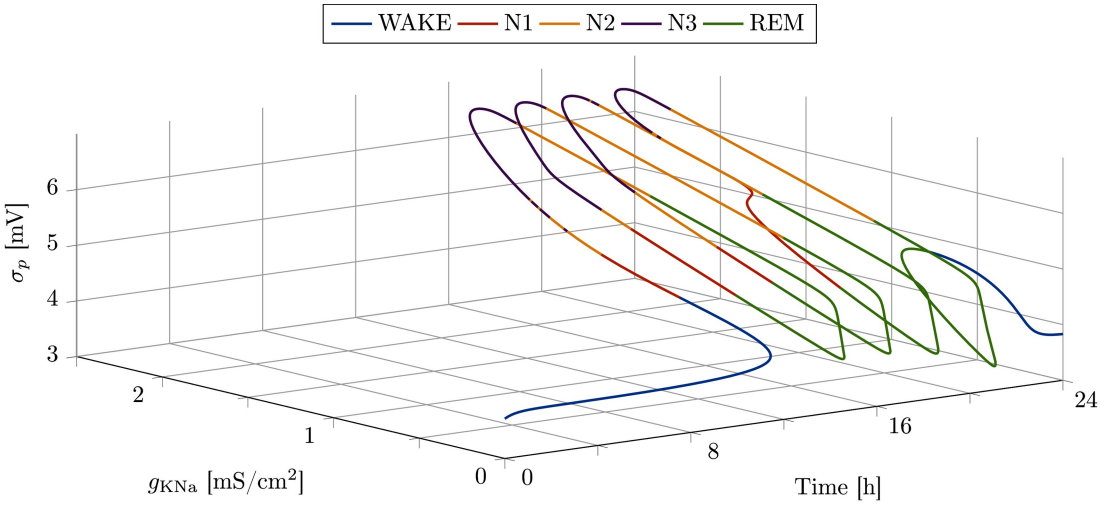

Figure 5.4: Trajectory of the bifurcation parameters. The figure illustrates the time course of the two bifurcation parameters, modulated by the sleep regulatory network. To better relate the change of the bifurcation parameters to the activity of the cortical populations, the trajectory is color-coded with respect to the scored sleep stage. During NREM sleep, both g_{KNa} and σ_p increase, to drop again during REM sleep. Over the night, the system undergoes four ultradian cycles, with the last cycle being strongly influenced by the drop in NREM activity.

During wakefulness the model is close to the z-axis around $\sigma_p = 4$ and g_{KNa}=0, which corresponds to a parameter configuration of the wake state given by a similar model of Steyn-Ross et al. [Steyn-Ross et al., 2005]. During the transitions into NREM sleep, declining levels of noradrenaline lead to an increase in σ_p and g_{KNa}. At the same time GABA activates potassium channels, increasing g_{KNa}. When the model switches into

REM sleep, rising levels of acetylcholine rapidly decrease the adaptation strength g_{KNa}. In addition, neural gain is increased by acetylcholine and noradrenalin, leading to smaller values of σ_p. Over the night the ultradian cycle is repeated multiple times (See Fig. 5.5).

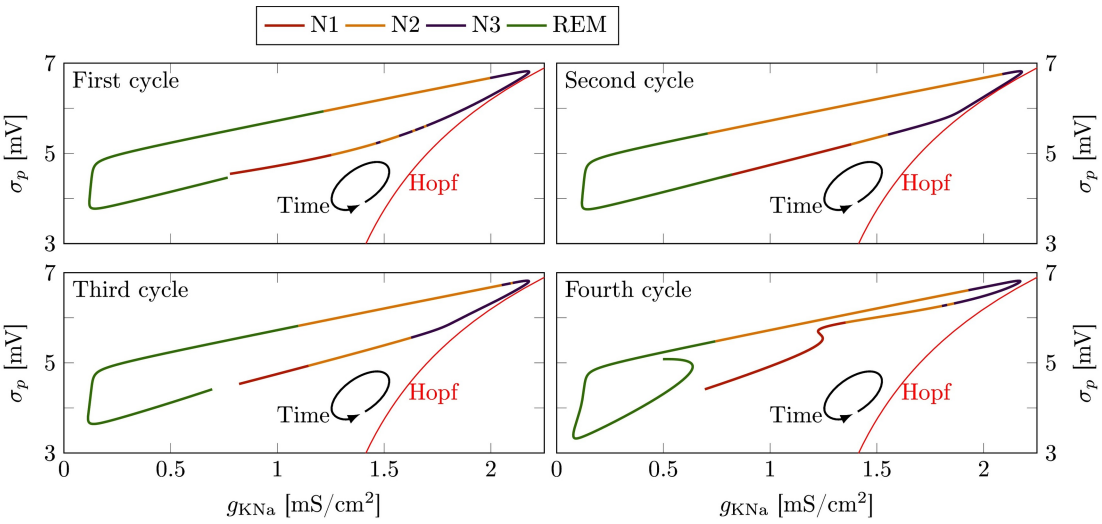

Figure 5.5: Trajectory of the ultradian cycles. The panels depict the four ultradian cycles, the model fulfills during a night. Notably, the last ultradian cycle differs considerably from the others, as it is influenced by reduced NREM activity. This leads to a slower increase in g_{KNa}. The resulting trajectory is farther away from the Hopf bifurcation leading to a prolonged period of N1 and a slower transition phase into slow wave sleep (N3). As indicated the time flows counterclockwise.

However, there are notable differences between the respective ultradian cycles, that are not reflected in the classification of Diniz Behn and Booth. Especially during the last cycle, the activity of the NREM populations is significantly decreased after the REM episode (See Fig. 5.5). Importantly, this leads to a different trajectory in the bifurcation diagram of the cortex model, that directly affects the dynamics of the cortical populations, resulting in a different scoring in the EEG based hypnogram in Fig. 5.3. Due to decreased levels of GABA, the firing rate adaptation g_{KNa} recovers slowly. This puts the cortex in a trajectory farther away from the Hopf bifurcation, where it is unable to generate a canard explosion, leading to a prolonged period of N1 (See Fig. 5.6).

In the wake state, the cortex is far away from the Hopf bifurcation in a single active state. When the homeostatic sleep drive intensifies, the NREM population activates. This leads to an release of extrasynaptic GABA and the cortex approaches the Hopf bifurcation as both g_{KNa} and σ_p increase (See Fig. 5.4 red line). As NREM sleep deepens further, the canard vanishes in a cusp bifurcation, with only the limit cycle of the Hopf bifurcation remaining. At the onset of REM sleep, rising levels of acetylcholine block firing rate adaptation through g_{KNa}, pushing the cortex away from the Hopf bifurcation. Without its influence, the model returns to high frequency oscillations generated by synaptic interactions.

5.3.2 Effect of sleep regulation on the EEG

Cortical activity modulated by the sleep regulatory network is shown in Fig. 5.7. In the wake state, the cortex is in a depolarized stable equilibrium. Without influence of the Hopf bifurcation synaptic interactions dominate and it generates the typical high frequency low amplitude oscillations observed in the EEG during the day (Fig. 5.8-Wake).

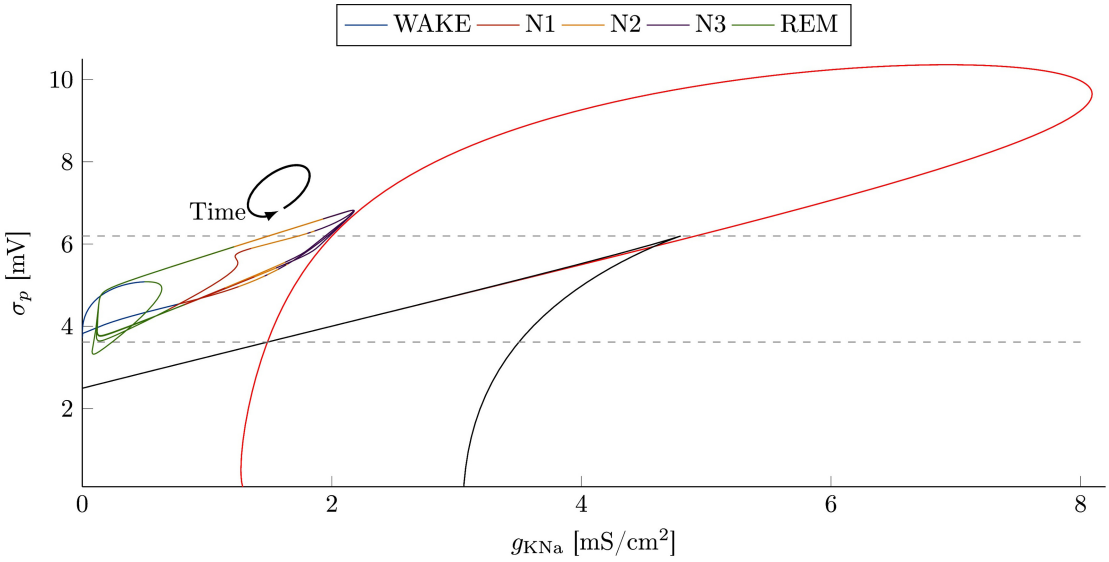

Figure 5.6: Trajectory in the bifurcation diagram. This figure depicts the projection of the time course of the bifurcation parameters onto the bifurcation diagram from Chapter 3. The trajectory of the cortex model is color-coded with respect to the classification of the sleep stages. With the cortex moving closer to the Hopf bifurcation, the high frequency oscillations during wakefulness turn into low frequency large amplitude oscillations. During REM sleep increasing concentrations of acetylcholine push the model back to the lower left leading to higher frequency oscillations. It should be noted, that the projection does not reflect the time spend at the given point.

During the early part of the wake-sleep transition, the system is increasingly affected by the ghost of the homoclinic orbit generated by the Hopf bifurcation. After perturbations through the background noise, the system does not directly return to the equilibrium, but follows a trajectory that is shaped by the homoclinic orbit. This results in a slow down in oscillation frequency and an increase in amplitude, corresponding to sleep stage N1 (Fig. 5.8-N1).

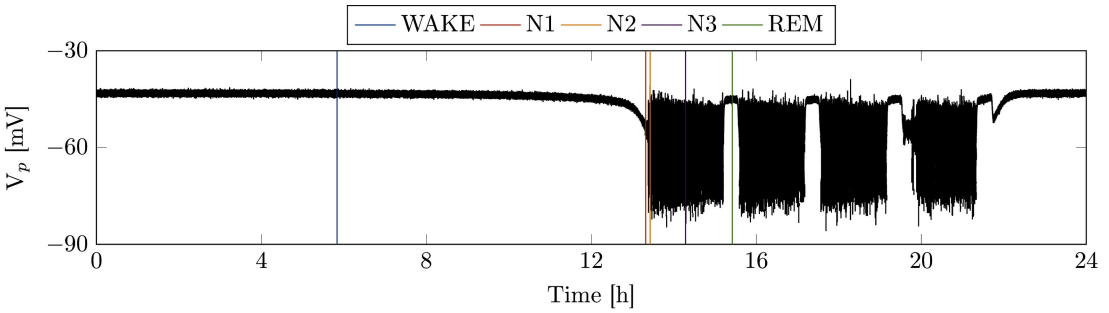

Figure 5.7: Modulation of cortical activity over the day. Here, we illustrate the effect of modulation by the sleep regulatory network on the activity of the cortical model represented by the averaged membrane voltage of the pyramidal population V_p. After a period of wakefulness, the model transitions into NREM sleep, characterized by large amplitude oscillations. NREM episodes are interrupted by REM sleep, that resembles wakefulness. After 4 cycles of the ultradian rhythm, the cortex returns to a state of wakefulness. The vertical lines indicate the position of the respective episodes depicted in Fig. 5.8.

As sleep deepens further, the cortex moves closer to the Hopf bifurcation, where the canard phenomenon described in Section 3.4.1 emerges through the interaction between the fast cortical activity and the slow firing rate adaptation. As shown in Section 3.4.3 the low frequency background oscillations may be interrupted by large amplitude deflections, which resemble K-complexes. They are initiated by background noise that pushes the

system into the attractor of the canard, resulting in a single canard cycle around the silent hyperpolarized state (Fig. 5.8-N2).

With increasing σ_p the canard vanishes in a cusp bifurcation (marked by the upper dotted line in Fig. 5.4) and only a limit cycle remains. The previously isolated K-complexes are replaced by continuous noise driven large amplitude oscillations which resemble slow oscillatory activity during sleep stage N3 (Fig. 5.8-N3). Importantly, at no time the system actually crosses the Hopf bifurcation, but rather approaches it. Otherwise the highly regular limit cycle oscillations would generate pathologically seizure behavior.

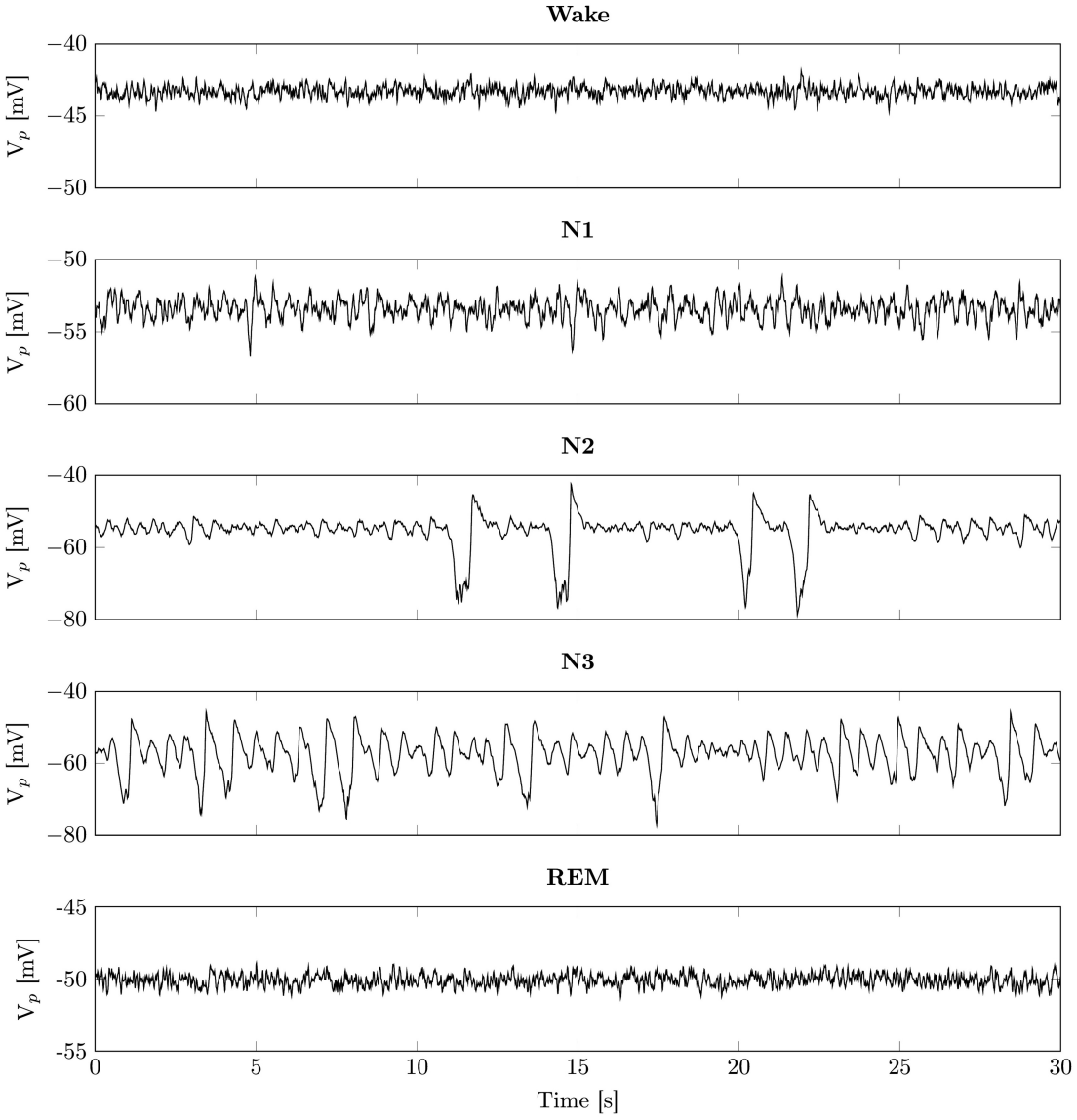

Figure 5.8: Individual sleep stages generated by the model. The individual panels depict example epochs from Fig. 5.7, that correspond to different sleep stages following the classification scheme by the AASM [Iber et al., 2007]. Activity during REM sleep resembles wakefulness, with the exception, that the cortex is relatively hyperpolarized. The panels N1-N3 show NREM sleep of increasing depth, with K-complexes emerging during N2 and slow wave activity during N3. Please note the different scales of the y axis especially for N2 and N3.

When the sleep regulatory network switches to REM sleep, the increasing levels of acetylcholine push the cortex away from the Hopf bifurcation. Without its influence the cortex returns to low amplitude high frequency oscillations which are typical for REM sleep (Fig. 5.8-REM). The transition between the different sleep stages is depicted in

Fig. 5.9. It occurs rapidly as close proximity to the limit cycle is necessary for slow wave activity, and blockage of g_{KNa} through acetylcholine moves the system perpendicularly to the Hopf bifurcation. (Fig. 5.6).

5.3.3 Transition between sleep stages

In human sleep research, the classification into different sleep stages is based on electrophysiological measurements. However, in the Diniz Behn and Booth model as well as the related literature, there is no correlate of such activity. Here, we can directly relate the EEG signal generated by the activity in the cortical model to the ongoing activity in the sleep regulatory network. Therewith, we can provide a classification that directly relates activity of the sleep regulatory network to experimental measurements. We follow the more recent classification scheme provided by the American Academy of Sleep Medicine (AASM) [Iber et al., 2007], although the classical rules by Rechtschaffen and Kales [Kales and Rechtschaffen, 1968] would apply equally. It should be noted, that our classification is solely based on the EEG part of the manual, as our model cannot generate EOG or EMG activity. The sleep scoring based on the activity of the pyramidal population is shown in Fig. 5.3.

The transitions between the different sleep stages are heavily dependent on two sets of time scales. The first are the time scales of neurotransmitter release in the sleep regulatory network, τ_E, τ_G, and τ_A respectively. They are directly related to the intrinsic dynamics of the sleep regulatory network. Given the large timescales the sleep regulatory populations act upon, the behavior of the model is more sensitive to changes in τ_X than to changes in cortical timescales. The larger the time constants, the slower the transition between the different sleep stages.

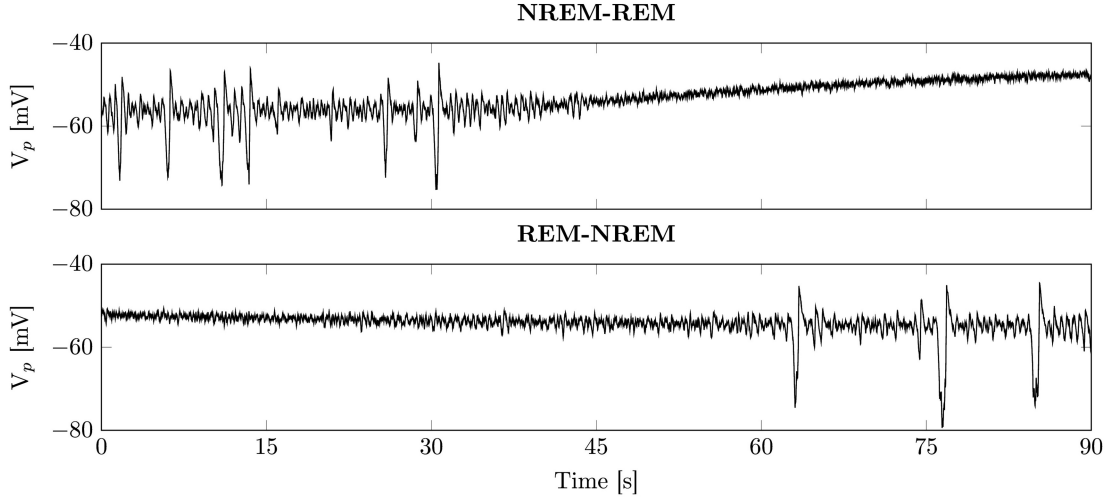

Figure 5.9: Transition between sleep stages. This figure demonstrates the ability of the cortex model to rapidly switch between NREM and REM sleep. During NREM the cortex is close to the Hopf bifurcation leading to low frequency large amplitude oscillations. When the system transits into REM sleep, the increasing levels of acetylcholine block potassium channels, pushing the cortex away from the Hopf. Immediately the slow oscillatory activity vanishes and gives rise to high frequency low amplitude oscillations typical for REM sleep. For brevity the transition between wakefulness and NREM sleep is omitted, as it is identical to the REM-NREM transition.

The other set are the time constants of the bifurcation parameters τ_g and τ_σ in

Eq. (5.5) and Eq. (5.6) respectively. Here, we assume them to be in the range of tens to hundreds of milliseconds, which yielded the best results. It might be difficult to directly measure them in vivo, as they cover rather unspecific processes, e.g. neuronal gain is affected by many neuromodulators which might have different time scales individually. For the sake of simplicity we have also assumed that activation and inactivation of neuromodulators has the same time constant.

Importantly the two time constants τ_g and τ_σ cover different aspects of the sleep transitions. The change in firing rate adaptation g_{KNa} is crucial for the generation of large amplitude oscillations, as its axis is mostly orthogonal to the line of Hopf points. Therefore, τ_g has a strong influence on the ability of the model to rapidly switch into and out of NREM sleep, which is depicted in Fig. 5.9.

In contrast, changes in σ_p move the system on a trajectory parallel to the Hopf bifurcation. Therefore, it does not determine *whether* the cortex is able to generate large amplitude oscillations, but rather if they are generated through a canard explosion or through a limit cycle. Therefore, τ_σ mainly affects the speed, the system transitions from early NREM sleep (N2) to late NREM sleep (N3). However, as sleep is scored in epochs of 30s, physiological values of τ_σ have only a minimal effect on the hypnogram (data not shown). To effectively change the distribution between N2 and N3, τ_σ would have to be in the range of minutes to hours, which suggests that the lack of N2 is not of cortical origin but due to over simplification of the sleep regulatory network.

Note, that τ_g and τ_σ cannot be chosen arbitrarily, as the line of Hopf points is not fully parallel to the σ_p axis. Therefore, if τ_σ is sufficiently large compared to τ_g, the cortex might cross the Hopf bifurcation at a smaller g_{KNa} and generate unrealistic limit cycle oscillations.

Chapter 6

Conclusions

This work focuses on the development of neural mass models of the sleeping brain. Based on results from detailed conductance based models and physiological data, a hybrid approach was utilized, that extended previous neural mass model of wakefulness with Hodgkin-Huxley currents. By means of a bifurcation analysis the dynamical repertoire of the respective cortical and thalamic modules was investigated. Based on these findings we could describe how these intrinsic mechanisms lead to the generation of K-complexes, slow oscillations and thalamic sleep spindles in the human EEG. To better understand how the bifurcation parameters change during the sleep wake transition and over the night, we investigated the effect of neuromodulation through a sleep regulatory network on the cortical model. In the following section key aspects of the obtained results are discussed in greater detail. The second section then identifies new research opportunities that arise from this work. Finally, this chapter concludes with a general summary of this work.

6.1 Discussion

The results obtained in this work provide evidence that challenges the current view in the literature on certain topics, especially concerning the KCs and SOs, as well as the discrimination between N2 and N3 in sleep regulation. On the other hand there are obvious trade-offs where the models employed here cannot explain certain aspects of the data. In the following we will first discuss KCs and SOs and the underlying bistability observed in individual neurons, as well as other oscillatory activity of the cortex. Then thalamic spindle oscillations and the current limitation of the thalamic model are discussed as well as sleep regulation and neuromodulation.

6.1.1 Characterization of KCs and SOs

In Chapter 3 an extended neural mass model of the sleeping cortex explored, relating its multiple dynamical regimes to different NREM sleep stages. A bifurcation analysis revealed the existence of a fold as well as a Hopf bifurcation accompanied by a canard phenomenon. Based on a comparison of the impulse response within the different settings, it was argued that the deflections generated by the canard explosion are identical to KCs seen in the EEG during natural sleep, leading to the spike-like nature of the KCs. Increasing the bifurcation parameter σ_p the canard vanishes, explaining the damped os-

cillatory behavior of SOs. This analysis provides a clear theoretical distinction between KCs and SOs and their generating mechanisms. However, as both the limit and the relaxation cycle are shaped by the same underlying homoclinic orbit, the actual transition is rather smooth even in the noise-free deterministic system (see Fig. 3.4). Therefore, it might be challenging to find this distinction within experimental data.

The bifurcation analysis revealed different parameter regimes that show characteristics of sleep stage N2 and N3 and illustrated that the model is able to reproduce the EEG of both sleep stages to a high degree. These findings suggest an alternative scenario for the sleep wake transition, that challenges the current view of a bistable cortex. Rather than entering a bistable regime the cortex stays primarily within the active state. As sleep deepens, it approaches the Hopf bifurcation, leading to an increase in amplitude and slowing of noise-driven background oscillations. Eventually, as the cortex approaches the Hopf bifurcation further, large amplitude deflections, i.e. KCs arise. At the transition to sleep stage N3 the canard phenomenon vanishes due to the cusp bifurcation. The remaining Hopf bifurcation is responsible for the generation of noise-driven SOs. Isolated events as in sleep stage N2 are not possible within that regime.

The waveform of a KC has been described as being biphasic, consisting of a large negative deflection (down state) followed by a pronounced depolarization (up state) - or triphasic, comprising an initial positive bump followed by a down state and an up state. Menicucci et al. [Menicucci et al., 2013] analyzed the shapes of KCs in N2 and N3 and found that on average a triphasic pattern, up-down-up, is present in both sleep stages. The cortical model does not show this sequence for sleep stage N2. *In vivo*, sleep stage N2 is rarely stationary and spans varying depths of sleep, as well as transitions to other sleep stages. In contrast, the parameter setting chosen in Section 3.4.3 depicts idealized N2 at a single point in time, to separate it from wakefulness and N3. Choosing a parameter setting closer to N3 will naturally give rise to a depolarization preceding the down state. The model predicts that biphasic KCs should be found mostly in early N2 or very late N2, as in the second half of the night after the major SWS episodes.

Parameter settings within region II or III lead to highly regular relaxation oscillations or limit cycles, that do *not* resemble human EEG. Therefore, it is crucial that the cortex must be within region I *close* to region II or III to reproduce the experimental data. In a study on resting state networks [Deco and Jirsa, 2012] found the awake brain to be in a state of criticality, which leads to an increased responsiveness. Similarly, in the model the sleeping cortex is close to a phase transition, suggesting that the concept of criticality is not restricted to wakefulness but carries over to sleep. Due to the presence of noise, bifurcations do not lead to clear-cut qualitative changes of the dynamics [Curto et al., 2009]. Stochasticity can shift critical points or induce behavior that is not seen in the deterministic case, such as noise-induced transitions.

6.1.2 Bistability and relaxation oscillations

Bistability of the cortex during slow wave sleep is inferred via bimodality in the distribution of individual cells' membrane potential. In local field potentials, one can observe a markedly conserved waveform of individual SO events [Crunelli and Hughes, 2009], but bimodality is already less visible. It is known that collective dynamics can exhibit, e.g. limit-cycle regimes, but at the same time emerge from irregular and high-dimensional

neuronal activity, which is only apparent at small-scales [Boustani and Destexhe, 2010].

A main result of the analysis of the cortical model is that on the macroscopic level the cortex is not necessarily in a bistable regime during natural deep sleep. The properties of KCs and SOs at the EEG level support the view of a monostable active cortex close to a Hopf and a saddle node bifurcation. Importantly, the characterization is made on the *population* level. While the switching between up and down states on the cellular level points to relaxation oscillations or bistability with noise-driven transitions, relatively regular oscillation at the cellular level may appear less regular at the EEG level, due to varying spatial synchrony [Amzica and Steriade, 1998]. Relaxation oscillations in the EEG usually correspond to pathological conditions like epilepsy.

In summary, the spectrum of observed slow oscillatory phenomena cannot be fully captured by the concepts of bimodality or relaxation oscillations. The analysis corroborates that the KC can be identified with a single, isolated relaxation cycle and slow wave activity, including prolonged episodes of low-amplitude fast oscillations, stems from noise-driven oscillations around a stable focus. Furthermore, while down states occur frequently they are still transients in the up state dominated cortex.

6.1.3 Mechanisms of firing rate adaptation

In the present work other adaptation mechanisms like multiplicative feedback arising due to synaptic depression or depletion of extra-cellular calcium or inhibitory modulation [Sanchez-Vives et al., 2010] have been ignored. However, the additive activity-dependent feedback investigated here is sufficient to account for a multitude of phenomena in healthy and pathological conditions. Furthermore, one can expect that the bifurcation structure of the cortical system, i.e. presence of saddle-nodes, Hopf and homoclinic bifurcation, will persist in alternative settings. Thus, the main conclusions do not depend on the particular choice of the feedback mechanism.

Firing rate adaptation might also play a role for spindle generation. In [Żygierewicz et al., 2001] the thalamic reticular population featured two calcium dependent currents, that regulated its activity. It might be possible, that the suppression of spindle generation is partially due to such adaptation mechanisms, which are currently not included in the thalamic model. They may also contribute to the refractoriness that was discussed in Section 4.5.4, as the thalamic reticular population might become unable to generate sufficient hyperpolarization for spindle initiation in the thalamic relay population.

6.1.4 Other oscillatory activity in the EEG

The cortical model deals primarily with the characteristics of EEG signals during natural sleep. However, the presented bifurcation analysis is useful in a broader context. Similar activity is found e.g. during anesthesia, coma and in isolated cortical preparations. It becomes increasingly clear that there exists a continuum of slow oscillatory states, which are mainly characterized by the fraction of time spent in up or down states, the temporal regularity with which state transitions occur and the response to external stimuli.

The phenomenon of up and down states in intracellular recordings is commonly associated with the notion of bistability or relaxation oscillations. However, it is important to note that most results on SOs were obtained in deeply anesthetized animals or slice prepa-

rations. Under these conditions, the system is down state dominated, i.e. down states last longer than up states, the occurrence of up states is often highly rhythmic [Deco et al., 2009, Chauvette et al., 2011] or up states are infrequent and transient [Poskanzer and Yuste, 2011]. These regimes are also present in the cortical model, namely in regions III, V and VI.

Generally, SOs produced by anesthesia are much more regular than during natural sleep [Chauvette et al., 2011, Amzica and Steriade, 1998]. Under ketamine-xylazine anesthesia neurons spend twice the time in silent states compared to natural SWS [Chauvette et al., 2011], and in the auditory cortex of awake rats prolonged up states are not even observed at all [Hromadka et al., 2013]. Furthermore, SO properties differ from one anesthetic to the other [Amzica and Steriade, 1997a]. Ketamine-xylazine anesthesia produces a uniform and continuous SO state [Ruiz-Mejias et al., 2011], whereas with urethane epochs of stable SOs are short-lived and desynchronized periods may occur spontaneously [Clement et al., 2008]. This is similar to SWS where one finds waxing and waning of slow wave complexes interleaved with periods reminiscent of wakefulness [Destexhe et al., 1999].

In contrast, [Cash et al., 2009] pointed out that a KC during light sleep is not always embedded in an ongoing SO, but is mostly an isolated event. Clearly, in N2 the active state dominates. Similarly, many studies report that during SWS of naturally sleeping animals more time is spent in up states than in down states [Destexhe et al., 1999, Steriade et al., 2001, Timofeev et al., 2001b, Ji and Wilson, 2006, Vyazovskiy et al., 2009, Chauvette et al., 2011] Furthermore, it has been reported that SWS contains many episodes of low-amplitude fast oscillations, lasting several seconds and resembling the active state [Destexhe et al., 2003]. This evidence points to natural sleep being up state dominated.

6.1.5 Mechanisms of spindle generation

The thalamic model emphasizes the role of I_{T} and I_{h} currents in the generation of thalamic spindle oscillations, which is in good agreement with the experimental findings. It is currently unclear, whether the two observed spindle regimes correspond to slow and fast spindles. In that regard more sophisticated models are required. The combined thalamocortical model reproduces the grouping of spindles and KCs/SOs, observed in human EEG [Mölle et al., 2002], which is thought to play a crucial role in the consolidation of memory [Mölle et al., 2006, Diekelmann and Born, 2010]. Additionally, it exhibits refractoriness of spindle oscillations, i.e. not every SO in a train of endogenous SOs triggers a spindle. Although adding extra currents increases dimensionality and parameter space, the model still preserves the overall simplicity and computational efficacy common to neural mass models.

Relative to the negative deflection of a KC, spindles consistently start earlier than in the data. Furthermore, the depolarizing up phase of endogenous KCs and SOs arrives earlier in the model than in the data. A comparison with the results from the isolated cortical module shows, that this is mostly due to strong depolarizing input from the thalamus. While there is no clear explanation for this discrepancy between experimental data and the model, there is a high probability, that this is due to simplifications of the cortical architecture. As discussed in Section 1.2 thalamic input does not reach the

pyramidal neurons in layer 5 directly, but is relayed by spiny stellate cells in layer 4. Respecting the more sophisticated architecture of the cortex should lead to a certain delay as well as attenuation of the thalamic input to the pyramidal population.

6.1.6 Auditory stimulation and refractoriness

The thalamocortical model was able to reproduce natural NREM sleep, but also the cortical response to auditory stimulation [Ngo et al., 2013b], that is gated through the thalamus. A recent experimental study suggests that the refractoriness of thalamic spindles is a limiting factor for the impact of auditory stimulation upon memory consolidation [Ngo et al., 2015]. They found, that longer trains of stimuli do *not* provide any benefit in memory consolidation compared to the two stimulus protocol. Remarkably, in the experiment the first stimulus triggers a strong spindle response, whereas the following stimuli show a diminished effect. This clearly indicates the importance of the grouping of spindles and SOs for the consolidation of memory. In contrast to these experimental findings, auditory stimulation in the model alleviates the refractoriness of the thalamic module, leading to spindle oscillations with similar amplitude following every stimulus. This is because of strong depolarization of the thalamic populations by the stimulus interrupts the thalamic I_{h} rhythm. While not shown in this work, other forms of stimuli lead to the same effect. This provides a challenge for the understanding of how auditory or more general sensory stimulation is processed during sleep and how it interacts with spindle generation.

6.1.7 Effect of neuromodulators and sleep regulation

The goal of Chapter 5 was to combine two different yet related modeling frameworks. On the one hand sleep regulatory networks with their complex interactions, that govern the transition between different states of vigilance. On the other hand EEG generating models, with a special emphasize on sleep. The interaction is based on the modulatory effect of the neurotransmitters released by the sleep regulatory network, e.g. noradrenalin, GABA, and acetylcholine, on key parameters of the cortical neural mass model to regulate the transition between its different dynamics modes [McCormick and von Krosigk, 1992, Hughes et al., 2002, Steriade, 2004, Weigenand et al., 2014].

It was shown, that the combined model is able to generate key patterns observed in the EEG over a full day, transitioning between the different sleep stages independently from external input. While physiological studies provide a very clear grand picture of the qualitative effect the neuromodulators have on the different parameters (see Table 5.1), the literature lacks quantitative measurements of these changes. Therefore, we choose a simple dependency between g_{KNa}, σ_p, and the neuromodulators as a starting point for Eq. (5.5) and Eq. (5.6). Here, neurophysiological measurements might help to elucidate the dependency of those bifurcation parameters on the respective neuromodulators and provide a better fit of their relationship. Also different neuromodulators were subsumed in the presented model, e.g. noradrenalin and serotonin for the wake population. While these neuromodulators generally act similarly there are subtle differences that may play an important role.

6.1.8 Distribution of NREM and REM sleep.

In the original model from Diniz Behn and Booth [Diniz Behn and Booth, 2012], the NREM and REM episodes are uniformly distributed over the duration of the night. This is in contrast to human sleep data, where NREM sleep occupies the majority of the first half of the night and vice versa. Inclusion of the circadian rhythm through activity in the SCN has been shown to introduce a distribution of the REM bout durations [Fleshner et al., 2011, Gleit et al., 2013]. However, this increases the complexity of the sleep regulatory network significantly. Also the reduction to a single REM population with reciprocal interactions employed in this study might be critical, as other mechanisms beyond reciprocal interaction have been hypothesized to be involved in REM sleep regulation [Brown et al., 2008, Lu et al., 2006, Luppi et al., 2006, Sapin et al., 2009], which are also subject to circadian modulation. This requires more detailed models of both the REM sleep regulation as well as the circadian rhythm to elucidate the mechanisms underlying the distribution of REM sleep.

It is also possible to scale the strength of REM sleep related weights g_{ER} and g_{AW} in the sleep regulatory network with the homeostatic sleep drive h, to prolong REM episodes over the night (data not shown). However, given the high level of simplification in the chosen sleep regulatory model, it is questionable whether there is a physiological process corresponding to this scaling. The aim of this study is to provide a minimal physiologically plausible model of sleep regulation in a neural mass model. Therefore, we believe that rather than fixing minor aspects of an oversimplified sleep regulatory network, one should relate to more sophisticated models, e.g. [Rempe et al., 2010, Diniz Behn and Booth, 2010, Kumar et al., 2012].

6.1.9 Subdivision of NREM sleep.

Currently the literature on sleep regulatory network focuses on two cardinal rhythms, the sleep-wake transition as well as NREM-REM cycling. However, in human sleep there is a further subdivision of NREM sleep into the sleep stages N1-N3, which corresponds to increasing depth of sleep and are characterized by unique features in the EEG. While the model can generate EEG activity that shows the characteristics of all stages of NREM sleep (See Fig. 5.8), N1 and N2 only appear as transients during the transition to sleep stage N3. In human sleep, N1 occupies only a minimal fraction of the night and is indeed assumed transient, whereas N2 accounts for the majority of sleep.

The small influence the timescales of the bifurcation parameters have on the hypnogram suggests that it is not possible to represent both N2 and N3 by a single population to fully reproduce human sleep EEG. Here, more sophisticated models, that include the subdivision of NREM sleep into two distinct sleep stages N2 and N3, will be necessary to fully capture sleep dynamics. Similar to REM sleep, the distribution of NREM varies over the night. This includes not only the total amount of NREM compared to REM, but also the distribution between N2 and N3. Modulation by the circadian rhythm might also play a crucial role, as changes in REM bout duration also affect NREM distribution.

Finally, the assumption, that all neuromodulators manipulate the bifurcation parameters on the same time scale might not be valid and those different time scales might play an important role in the transition between the different sleep stages.

6.2 Outlook

The presented models already reproduce sleep EEG to a high degree. However, there are still various possible approaches for improvement. These are mostly related to extensions of the current model that could remedy some of its drawbacks or lead to new applications. Below some of the more important topics are discussed.

6.2.1 Extended cortical architecture

As mentioned in the discussion in Section 6.1.5 the cortical architecture depicted in Section 1.2 might play a crucial role in the time course of the spindle response during external sensory stimulation. Moreover, while the work on the combined model in Chapter 5 resulted in a realistic reproduction of the EEG over a day, the cortical model presented here is not on par with the state of the art for wake EEG. This concerns both the inclusion of more synapse types for excitation and inhibition as well as the overall cortical architecture. Here more realistic models [Ursino et al., 2010, Sotero et al., 2010] might be extended to reproduce both wake and sleep EEG, especially regarding higher frequency bands [Wendling et al., 2002]. However, it should be mentioned that due to the asynchronous cortical activity during wakefulness and the resulting low amplitude oscillations, most advanced neural mass models are not of the Liley type and require an extensive redesign to be applicable for sleep. Another architectural enhancement concerns the spatial extension of the cortex, which has been shown to play an important role in the generation of ultra-slow oscillations [Steyn-Ross et al., 2011] and Turing patterns [Steyn-Ross et al., 2013].

6.2.2 Mechanisms of firing rate adaptation

As discussed in Section 2.4 the mechanism of the firing rate adaptation utilized in this work is only one of many candidates, that might play a role in the sleep wake transition [Benda and Herz, 2003]. Most prominent examples of other mechanisms are calcium dependent potassium channels [Benita et al., 2012] and or synaptic depression [Kilpatrick and Bressloff, 2010a, Kilpatrick and Bressloff, 2010b]. While it is questionable, whether different mechanisms of firing rate adaptation would change the dynamical structure of the cortical model, they might play an important role in the thalamic model. This, includes both the individual time course of a spindle oscillation as well as the refractoriness of the thalamus after consecutive slow oscillations, that was observed in the data [Ngo et al., 2015].

6.2.3 Sleep regulation of the thalamus

The combined model presented in Chapter 5 only considered the cortical neural mass. However, the thalamus is also affected by neuromodulators [McCormick and Huguenard, 1992, Destexhe and Mainen, 1994, Destexhe et al., 1994a, Varela, 2014], which might play an important role in the transition between sleep stages N2 and N3. In addition to providing a better fit of the relevant bifurcation parameters, this might also help to elucidate the role of the different spindle regimes present in the thalamic model depicted in Fig. 4.2 in the context of fast and slow spindle oscillations.

6.2.4 Validation of other sleep regulatory networks

The combined model provides a direct relation between the activity of a sleep regulatory network and a generating model of human EEG. As sleep regulation affects the cortical model only indirectly though a slow modulation of the bifurcation parameters, the sleep regulatory network can be replaced by a different one, making it a useful tool for validating other sleep regulatory models.

Similar to the estimation of effective connectivity in the dynamic causal modeling framework [Kiebel et al., 2008], the EEG signal generated by the cortical model can be utilized to infer a mapping from human EEG data to the bifurcation parameters and therewith levels of neuromodulators. As this translates to the activity of the sleep regulatory network, it provides insights into activity of regulatory networks that otherwise might not be easily measured in vivo.

6.2.5 Pathological brain states and interventions

The work presented here focuses on natural sleep. However, there is a multitude of sleep related pathological conditions, that might be investigated with this model e.g. narcolepsy or insomnia. Here, a comparison with experimental data might help to better understand how the brain deviates from the healthy sleep wake transition and predict treatment opportunities..

In addition to pathological conditions, the model model can provide predictions for pharmacological interventions that either target the bifurcation parameters or neuromodulators, e.g. the model suggests that the application of a cholinergic antagonist during REM sleep should lead to the emergence of slow oscillatory activity. Interestingly it was shown that during anesthesia application of of acetylcholine can lead to wake-like activity in animals [Metherate et al., 1992, Steriade et al., 1993b, Steriade, 1993, Goard and Dan, 2009]. Furthermore, anesthetic agents and neuromodulators have similar targets [Nicoll et al., 1990, Patel et al., 1999, Talley and Bayliss, 2002], which could be incorporated in the model as an additional way of modifying the bifurcation parameters. Also some anesthetics target other properties of the neuronal populations, e.g. GABAergic efficacy [Steyn-Ross et al., 2001, Steyn-Ross et al., 2003, Hutt, 2012, Hashemi et al., 2015]. It would be interesting to see, whether this can be incorporated into the model.

6.2.6 Minimal models

In contrast to the possible research questions discussed above that call for extended models with more physiological detail, the mathematically most interesting questions is that of model reduction. While models presented here strove to be as clear and simple as possible, they still include a certain level of detail, that might not be necessary to capture the core mechanisms. This is related to the so called “normal form” of a bifurcation, which represents the minimal model that exhibits that dynamical behavior [Guckenheimer et al., 1984, Kuznetsov, 1998] and which is -at least locally- topologically equivalent to a more complex model that shows the same bifurcation.

For example the Morris-Lecar model [Morris and Lecar, 1981] has been shown to have a rich repertoire of bifurcations [Wilson, 1999, Tsumoto et al., 2006]. In a similar fashion the Hindmarsh-Rose model of a bursting neuron [Hindmarsh and Rose, 1984] is

able to generate the transition between tonic spiking and bursting patterns [Shilnikov and Cymbalyuk, 2005, Mayer et al., 2006] comparable to what the thalamus model does.

6.3 Summary

In sum, the results presented here exemplify that the hybrid approach employed in this work is an useful extension of the neural mass framework when the dynamics of the neural population are dominated by intrinsic mechanisms rather than synaptic drive. The hybrid models developed here reproduce the EEG signal of the sleeping thalamocortical system to a high degree, requiring only minimal computational resources. Furthermore, the simplicity of the approach allows a detailed mathematical analysis of the dynamical repertoire of the underlying brain structures, that provides new insights into the generating mechanisms of sleep related EEG phenomena. By utilizing physiologically motivated mechanisms, the models can be directly related to experimental measurements, which simplifies experimental validation. Moreover, by considering the action of neuromodulators, the models may act as an useful validation layer for arbitrary sleep regulatory networks by means of the EEG signal. Finally, the inclusion of the thalamus enables the treatment of sensory stimulation, that has played an increasingly important role as a noninvasive means of manipulating natural sleep.

Appendix A: Equations

A.1 Cortex

The cortical model is described by the following stochastic differential equations:

$$
\begin{aligned}
\tau_p \dot{V}_p &= -I_{\mathrm{L}}(V_p) - I_{\mathrm{AMPA}}(V_p, s_{ep}) - I_{\mathrm{GABA}}(V_p, s_{ip}) - C_m^{-1}\tau_p I_{\mathrm{KNa}}(V_p, [\mathrm{Na}]) \\
\tau_i \dot{V}_i &= -I_{\mathrm{L}}(V_i) - I_{\mathrm{AMPA}}(V_i, s_{ei}) - I_{\mathrm{GABA}}(V_i, s_{ii}) \\
\ddot{\phi}_c &= \nu^2 \left(Q_p(V_p) - \phi_p\right) - 2\nu\dot{\phi}_c \\
\ddot{s}_{ep} &= \gamma_e^2 \left(N_{pp}Q_p(V_p) + N_{pt}\phi_t + \phi_n - s_{ep}\right) - 2\gamma_e \dot{s}_{ep} \\
\ddot{s}_{ei} &= \gamma_e^2 \left(N_{ip}Q_p(V_p) + N_{it}\phi_t + \phi_n' - s_{ei}\right) - 2\gamma_e \dot{s}_{ei} \\
\ddot{s}_{ip} &= \gamma_g^2 \left(N_{pi}Q_i(V_i) - s_{ip}\right) - 2\gamma_g \dot{s}_{ip} \\
\ddot{s}_{ii} &= \gamma_g^2 \left(N_{ii}\,Q_i(V_i) - s_{ii}\right) - 2\gamma_g \dot{s}_{ii} \\
[\dot{\mathrm{Na}}] &= \left(\alpha_{\mathrm{Na}} Q_p(V_p) - \mathrm{Na}_{\mathrm{pump}}([\mathrm{Na}])\right)/\tau_{\mathrm{Na}}
\end{aligned}
$$

A.2 Thalamus

The thalamic model is described by the following stochastic differential equations:

$$
\begin{aligned}
\tau_t \dot{V}_t &= -I_{\mathrm{L}}^t(V_t) - I_{\mathrm{AMPA}}(V_t, s_{et}) - I_{\mathrm{GABA}}(V_t, s_{rt}) - C_m^{-1}\tau_t(I_{\mathrm{LK}}^t(V_t) - I_{\mathrm{T}}^t(V_t) - I_{\mathrm{h}}(V_t)), \\
\tau_r \dot{V}_r &= -I_{\mathrm{L}}^r(V_r) - I_{\mathrm{AMPA}}(V_r, s_{er}) - I_{\mathrm{GABA}}(V_r, s_{rr}) - C_m^{-1}\tau_r(I_{\mathrm{LK}}^r(V_r) - I_{\mathrm{T}}^r(V_r)) \\
\ddot{\phi}_t &= \nu^2(Q_t(V_t) - \phi_t) - 2\nu\dot{\phi}_t \\
\ddot{s}_{et} &= \gamma_e^2(N_{tp}\phi_c + \phi_n - s_{et}) - 2\gamma_e \dot{s}_{et} \\
\ddot{s}_{er} &= \gamma_e^2(N_{rt}Q_t(V_t) + N_{rp}\phi_c - s_{er}) - 2\gamma_e \dot{s}_{er} \\
\ddot{s}_{rt} &= \gamma_r^2(N_{tr}Q_r(V_r) - s_{rt}) - 2\gamma_r \dot{s}_{rt} \\
\ddot{s}_{rr} &= \gamma_r^2(N_{rr}Q_r(V_r) - s_{rr}) - 2\gamma_r \dot{s}_{rr} \\
\dot{h}_{\mathrm{T}}^t &= (h_\infty^t - h_{\mathrm{T}}^t)/\tau_h^t \\
\dot{h}_{\mathrm{T}}^r &= (h_\infty^r - h_{\mathrm{T}}^r)/\tau_h^r \\
\dot{m}_{\mathrm{h1}} &= (m_\infty^{\mathrm{h}}(1 - m_{\mathrm{h2}}) - m_{\mathrm{h1}})/\tau_m^{\mathrm{h}} - k_3 P_{\mathrm{h}} m_{\mathrm{h1}} + k_4 m_{\mathrm{h2}} \\
\dot{m}_{\mathrm{h2}} &= k_3 P_{\mathrm{h}} m_{\mathrm{h1}} - k_4 m_{\mathrm{h2}} \\
[\dot{\mathrm{Ca}}] &= \alpha_{\mathrm{Ca}} I_{\mathrm{T}}^t - ([\mathrm{Ca}] - [\mathrm{Ca}_0])/\tau_{\mathrm{Ca}}
\end{aligned}
$$

A.3 Currents and gating functions

The sodium pump and firing rate function are described by:

$$
\begin{aligned}
\mathrm{Na}_{\mathrm{pump}}([\mathrm{Na}]) &= R_{\mathrm{pump}} \left(\frac{[\mathrm{Na}]^3}{[\mathrm{Na}]^3 + 3375} - \frac{[\mathrm{Na}_0]^3}{[\mathrm{Na}_0]^3 + 3375} \right) \\
Q_k(V_k) &= \frac{Q_k^{\max}}{1 + \exp(-(V_k - \theta)/\sigma_k)}
\end{aligned}
$$

The currents are given by the following equations:

$$
\begin{aligned}
I_{\mathrm{L}} &= (V_k - E_{\mathrm{L}}) \\
I_{\mathrm{AMPA}} &= g_{\mathrm{AMPA}} s_{ek} (V_k - E_{\mathrm{AMPA}}) \\
I_{\mathrm{GABA}} &= g_{\mathrm{GABA}} s_{ik} (V_k - E_{\mathrm{GABA}}) \\
I_{\mathrm{KNa}} &= \bar{g}_{\mathrm{KNa}} \frac{0.37}{1 + \left(\frac{38.7}{[\mathrm{Na}]}\right)^{3.5}} (V_p - E_{\mathrm{K}}) \\
I^k_{\mathrm{LK}} &= \bar{g}_{\mathrm{LK}} (V_k - E_{\mathrm{K}}) \\
I^k_{\mathrm{T}} &= \bar{g}^k_{\mathrm{T}} m^k_\infty m^k_\infty h^k (V_k - E_{\mathrm{Ca}}), \\
I_{\mathrm{h}} &= \bar{g}_{\mathrm{h}} (m_{\mathrm{h1}} + g_{inc} m_{\mathrm{h2}}) (V_t - E_{\mathrm{h}})
\end{aligned}
$$

Gating functions are taken as:

$$
\begin{aligned}
m^t_\infty &= \frac{1}{1 + \exp(-(V_t + 59)/6.2))} \\
m^r_\infty &= \frac{1}{1 + \exp(-(V_r + 52)/7.4))} \\
h^t_\infty &= \frac{1}{1 + \exp((V_t + 81)/4))} \\
h^r_\infty &= \frac{1}{1 + \exp((V_r + 80)/5))} \\
\tau^t_h &= (30.8 + (211.4 + \exp((V_t + 115.2)/5))/(1 + \exp((V_t + 86)/3.2)))/3^{1.2} \\
\tau^r_h &= (85 + 1/(\exp((V_r + 48)/4) + \exp(-(V_r + 407)/50)))/3^{1.2} \\
m^{\mathrm{h}}_\infty &= \frac{1}{1 + \exp((V_t + 75)/5.5))} \\
\tau^{\mathrm{h}}_m &= (20 + 1000/(\exp((V_t + 71.5)/14.2) + \exp(-(V_t + 89)/11.6))) \\
P_{\mathrm{h}} &= k_1 [\mathrm{Ca}]^{n_P} / (k_1 [\mathrm{Ca}]^{n_P} + k_2)
\end{aligned}
$$

A.4 Sleep regulatory network

The sleep regulatory network is described by:

$$
\begin{aligned}
\tau_W \dot{F}_W &= Q_W \left(g_{GW} C_G + g_{AW} C_A\right) - F_W \\
\tau_N \dot{F}_N &= Q_N \left(g_{EN} C_N\right) - F_N \\
\tau_R \dot{F}_R &= Q_R \left(g_{ER} C_E + g_{GR} C_G + g_{AR} C_A\right) - F_R \\
\tau_E \dot{C}_E &= \tanh(F_W/\gamma_E) - C_E \\
\tau_G \dot{C}_G &= \tanh(F_N/\gamma_G) - C_G \\
\tau_A \dot{C}_A &= \tanh(F_R/\gamma_A) - C_A \\
\dot{h} &= \frac{h^{\max} - h}{\tau^w_h} \mathcal{H}(F_W - \theta_h) - \frac{h}{\tau^s_h} \mathcal{H}(\theta_h - F_W)
\end{aligned}
$$

The firing rate function for the sleep regulatory network is given as:

$$
Q_k(Y) = \frac{F^{\max}_k}{1 + \exp(-(Y - \beta_k)/\alpha_k)}
$$

Appendix B: Parameters

B.1 Symbol descriptions

Here, we describe the different symbols used in the thalamocortical model and sleep regulation module and give their values.

Table B.1: Symbol description thalamocortical model

C_m	Membrane capacitance
$Q_k^{\max}$	Maximal firing rate of population k
θ	Firing threshold (half activation)
σ_k	Default gain coefficient of the firing rate function of population k (inverse neural gain)
τ_k	Membrane time constant of population k
τ_σ	Time constant of neural gain modulation
τ_g	Time constant of the modulation of the firing rate adaptation
γ_m	Synaptic rate constant of synapse type m
N_{kl}	Connectivity constant for presynaptic population l to postsynaptic population k
g_X	Weight of channel X
$\bar{g}_X$	Conductivity of channel X
E_X	Nernst reversal potential of channel X
α_{Na}	Sodium influx through firing rate
τ_{Na}	Time constant of sodium extrusion
R_{pump}	Strength of the sodium pump
Na_0	Resting state sodium equilibrium
α_{Ca}	calcium influx through firing rate
τ_{Ca}	Time constant of calcium extrusion
Ca_0	Resting state calcium equilibrium
k	Reaction velocity of calcium binding
g_{inc}	Increase of conductance by binding
ϕ^{sd}	Standard deviation of background noise

Table B.2: Symbol description sleep regulatory network

τ_K	Membrane time constant of population K
τ_X	Membrane time constant of neuromodulator X
$F_K^{\max}$	Maximal firing rate of population K
β_K	Firing threshold of population K (Half activation)
α_K	Default slope of the firing rate function of population K
γ_X	Synaptic rate constant of neuromodulator X
g_{XK}	Synaptic weight of neuromodulator X acting on postsynaptic population K
$h^{\max}$	Maximal sleep drive
θ_h	Sleep drive threshold
τ_h^w	Time constant of sleep drive build up during wakefulness
τ_h^s	Time constant of sleep drive decline during sleep
κ	NREM firing threshold modulation parameter

B.2 Parameter values

This table defines all parameter values of the cortical model that are not subject to the bifurcation analysis or defined elsewhere.

Table B.3: Parameter values cortex

Symbol	Value	Unit
C_m	1	μF/cm^2
τ_p, τ_i	30	ms
$Q_p^{\max}$	$30{\cdot}10^{-3}$	ms^{-1}
$Q_i^{\max}$	$60{\cdot}10^{-3}$	ms^{-1}
θ_p, θ_i	-58.5	mV
$\bar{\sigma}_p$	7	mV
$\bar{\sigma}_i$	6	mV
τ_σ	100	ms
γ_e	$70{\cdot}10^{-3}$	ms^{-1}
γ_g	$58.6{\cdot}10^{-3}$	ms^{-1}
N_{pp}	120	-
N_{ip}	72	-
N_{pi}	90	-
N_{ii}	90	-
N_{pt}	2.5	-
N_{it}	2.5	-
g_{AMPA}	1	ms
g_{GABA}	1	ms
$\bar{g}_{\mathrm{KNa}}$	1.33	mS/cm^2
τ_g	10	ms
E_{L}^p	-66	mV
E_{L}^i	-64	mV
E_{K}	-100	mV
E_{AMPA}	0	mV
E_{GABA}	-70	mV
α_{Na}	2	mM/mA ms
τ_{Na}	1.7	ms
$\mathrm{Na}_{\mathrm{eq}}$	9.5	mM
R_{pump}	0.09	mM ms^{-1}
ϕ_n^{sd}	2	ms^{-1}

This table defines all parameter values of the thalamic model that are not subject to the bifurcation analysis or defined elsewhere.

Table B.4: Parameter values thalamus

Symbol	Value	Unit
C_m	1	μF/cm^2
τ_k	20	ms
$Q_k^{\max}$	$400{\cdot}10^{-3}$	ms^{-1}
θ	-58.5	mV
σ_k	6	mV
γ_e	$70{\cdot}10^{-3}$	ms^{-1}
γ_r	$100{\cdot}10^{-3}$	ms^{-1}
N_{rt}	3	-
N_{tr}	5	-
N_{rr}	19	-
N_{tp}	2.6	-
N_{rp}	2.6	-
g_{AMPA}	1	ms
g_{GABA}	1	ms
$\bar{g}_{\mathrm{T}}^t$	3	mS cm^{-2}
$\bar{g}_{\mathrm{T}}^r$	2.3	mS cm^{-2}
$\bar{g}_{\mathrm{h}}$	0.51	mS cm^{-2}
E_{L}^k	-70	mV
E_{K}	-100	mV
E_{AMPA}	0	mV
E_{GABA}	-70	mV
E_{Ca}	120	mV
E_{h}	-40	mV
α_{Ca}	$51.8{\cdot}10^{-6}$	mM/mA ms
τ_{Ca}	10	ms
Ca_0	$2.4{\cdot}10^{-4}$	mM
k_1	$2.5{\cdot}10^{7}$	mM^{-1} ms^{-1}
k_2	$4{\cdot}10^{-4}$	ms^{-1}
k_3	0.1	ms^{-1}
k_4	$1{\cdot}10^{-3}$	ms^{-1}
n_P	4	-
g_{inc}	2	-
ϕ_n	2	ms^{-1}

This table defines all parameter values of the sleep regulatory network that are not defined elsewhere. It should be noted, that in the original manuscript by [Diniz Behn and Booth, 2012] the parameter values for the sleep regulatory network are given in seconds or hours. However, since we combine the cortical and the sleep regulatory model, we have to decide on one time unit.

Table B.5: Parameter values sleep regulatory network

Symbol	Value	Unit
τ_W	$1500{\cdot}10^3$	ms
τ_N	$600{\cdot}10^3$	ms
τ_R	$60{\cdot}10^3$	ms
τ_E	$2.5{\cdot}10^3$	ms
τ_G	$1{\cdot}10^3$	ms
τ_A	$1{\cdot}10^3$	ms
$F_W^{\max}$	$6.5{\cdot}10^{-3}$	ms^{-1}
$F_N^{\max}$	$5{\cdot}10^{-3}$	ms^{-1}
$F_R^{\max}$	$5{\cdot}10^{-3}$	ms^{-1}
β_W	-0.4	ms^{-1}
β_R	-0.9	ms^{-1}
α_W	0.5	ms^{-1}
α_N	0.175	ms^{-1}
α_R	0.13	ms^{-1}
γ_E	$5{\cdot}10^{-3}$	ms^{-1}
γ_G	$4{\cdot}10^{-3}$	ms^{-1}
γ_A	$2{\cdot}10^{-3}$	ms^{-1}
g_{GW}	-1.68	-
g_{AW}	1	-
g_{GR}	-1.3	-
g_{AR}	1.6	-
g_{ER}	-4	-
g_{EN}	-2	-
$h^{\max}$	1	-
θ_h	$2{\cdot}10^{-3}$	ms^{-1}
τ_h^w	$34830{\cdot}10^3$	ms
τ_h^s	$30600{\cdot}10^3$	ms
κ	1.5	-

Appendix C: Bifurcation analysis

C.1 Cortex

Here, we give the model definition of the cortex for xppaut. Note there is an additional linebreak due to editing, in Napump that might cause problems for the parser.

```
# Cortical model description for xppaut
# Bifurcation parameter
parameter g_KNa   = 0
parameter sigma_p = 4

# Membrane capacity
!C_m    = 1

# Membrane time constant
!tau   = 30

# Weights/conductivities
!g_AMPA = 1
!g_GABA = 1

# Reversal potentials
!E_L    = -64
!E_K    =-100
!E_AMPA = 0
!E_GABA = -70

# Sigmoid parameters
# Maximal firing rates
!Qmax_p = 0.03
!Qmax_i = 0.06

# Inhibitory slope
!sigma_i= 6

# Firing threshold
!theta = -58.5

# Scaling parameter for sigmoidal mapping
!C=(pi/sqrt(3))

# Synaptic time constants
!gamma_e=0.07
!gamma_g=0.0586

# Sodium parameters
!Na_eq  =9.5
!alpha_Na=2
!tau_Na  = 1.3
!R_pump  =0.09
```

```
# Connectivities
!N_pp = 120
!N_ip = 72
!N_pi = 90
!N_ii = 90

# Function definition
# Sodium pump
Napump(Na)= Rpump * ( Na*Na*Na / (Na*Na*Na + 3375)
          - Naeq*Naeq*Naeq / (Naeq*Naeq*Naeq + 3375))

# Firing rate functions
Qp(Vp)= Qmaxp / (1 + exp(-C*(Vp - theta) / sigmap))
Qi(Vi)= Qmaxi / (1 + exp(-C*(Vi - theta) / sigmai))

# Currents
# Leak current
I_L(V)= (V - E_L)

# Synaptic currents
I_AMPA(V,s)= g_AMPA * s * (V - E_AMPA)
I_GABA(V,s)= g_GABA * s * (V - E_GABA)

# Sodium current
IKNa(Vp,Na) = gKNa * 0.37 / (1 + (38.7 / Na)^3.5) * (Vp - E_K)

# ODE_s
Vp'  = (-I_L(Vp)-I_AMPA(Vp,s_ep)-I_GABA(Vp,s_gp))/tau-1/C_m*I_KNa(Vp,Na)
Vi'  = (-I_L(Vi)-I_AMPA(Vi,s_ei)-I_GABA(Vi,s_gi))/tau
Na'  = (alphaNa * Qp(Vp) -Napump(Na))/tauNa
s_ep' = x_ep
s_ei' = x_ei
s_gp' = x_gp
s_gi' = x_gi
x_ep' = gamma_e * gamma_e * (N_pp * Qp(Vp) - s_ep) - 2 * gamma_e * x_ep
x_ei' = gamma_e * gamma_e * (N_ip * Qp(Vp) - s_ei) - 2 * gamma_e * x_ei
x_gp' = gamma_g * gamma_g * (N_pi * Qi(Vi) - s_gp) - 2 * gamma_g * x_gp
x_gi' = gamma_g * gamma_g * (N_ii * Qi(Vi) - s_gi) - 2 * gamma_g * x_gi

# Initial parameters
init Vp=-64, Vi=-64, Na=9.5

# XPPAUT settings
@ total=3000,dt=1,meth=rungekuta
@ YLO=-80,YHI=-40,XLO=0,XHI=3000
@ parmin=0,parmax=10.2
@ autoxmin=0,autoxmax=10,autoymin=-100,autoymax=0
@ ds=1e-2,dsmin=1e-5,dsmax=0.05
@ nmax=4000,npr=0,ntst=600,epsl=1e-9,epss=1e-7,epsu=1e-7
done
```

C.2 Thalamus

Here, we give the model definition of the thalamus for xppaut. Note there are additional linebreaks due to editing, in Vt' and Vr' that might cause problems for the parser.

```
# Thalamic model description for xppaut
# Bifurcation parameters
param g_LK=0.02
param g_h=0.06

# Membrane capacity
!C_m = 1

# Membrane time constant
!tau=20.0

# Weights/conductivities
!g_T_t=3.0
!g_T_r=2.3

!g_AMPA=1.0
!g_GABA=1.0

# Reversal potentials
!E_L   =-70
!E_K   =-100
!E_Ca  =120
!E_h   =-40
!E_AMPA=0
!E_GABA=-70

# Sigmoid parameters
# Maximum firing rate
!Q_max=400E-3

# Slope for sigmoid
!sigma=6

# Sigmoid threshold
!theta=-58.5

# Scaling parameter for sigmoidal mapping
!C=(pi/sqrt(3))

# PSC rise time in ms^-1
!gamma_t=70E-3
!gamma_r=100E-3

# Calcium dynamic
!alpha_Ca=-51.8E-6
!tau_Ca=10
!Ca_0=2.4E-4
```

```
# Parameters of h-current
!k1   = 2.5E_7
!k2   = 4E-4
!k3   = 1E-1
!k4   = 1E-3
!n_P  = 4
!g_inc= 2

# Connectivities
!N_er=3
!N_rt=5
!N_rr=25

# Functions
# Firing rates
Qt(Vt)=Q_max/(1+exp(-C*(Vt-theta)/sigma))
Qr(Vr)=Q_max/(1+exp(-C*(Vr-theta)/sigma))

# Activation functions
m_inf_T_t(Vt)=1/(1+exp(-(Vt+59)/6.2))
m_inf_T_r(Vr)=1/(1+exp(-(Vr+52)/7.4))
h_inf_T_t(Vt)=1/(1+exp((Vt+81)/4))
h_inf_T_r(Vr)=1/(1+exp((Vr+80)/5))

tau_h_T_t(Vt)=(30.8+(211.4+exp((Vt+115.2)/5))/(1+exp((Vt+86)/3.2)))/3^1.2
tau_h_T_r(Vr)=(85+1/(exp((Vr+48)/4)+exp(-(Vr+407)/50)))/3^1.2

m_inf_h(Vt)=1/(1+exp((Vt+75)/5.5))
tau_m_h(Vt)=(20+1000/(exp((Vt+71.5)/14.2)+exp(-(Vt+89)/11.6)))

# Synaptic currents
I_AMPA(V,s)= g_AMPA * s * (V - E_AMPA)
I_GABA(V,s)= g_GABA * s * (V - E_GABA)

# Leak currents
I_L(V)=(V-E_L)
I_LK(V)=g_LK*(V-E_K)

# Calicum current
I_T_t(Vt,h_T_t)=g_T_t*m_inf_T_t(Vt)*m_inf_T_t(Vt)*h_T_t*(Vt-E_Ca)
I_T_r(Vr,h_T_r)=g_T_r*m_inf_T_r(Vr)*m_inf_T_r(Vr)*h_T_r*(Vr-E_Ca)

# h-current
I_h(Vt,m_h,m_h2)=g_h*(m_h+g_inc*m_h2)*(Vt-E_h)

# Protein binding
P_h(Ca)=(k1*Ca*Ca*Ca*Ca/(k1*Ca*Ca*Ca*Ca+k2))
```

```
# System equation
Vt'=-(I_L(Vt)+I_GABA(Vt,s_rt))/tau
    -1/C_m*(I_LK(Vt)+I_T_t(Vt,h_T_t)+I_h(Vt,m_h,m_h2))
Vr'=-(I_L(Vr)+I_AMPA(Vr,s_er)+I_GABA(Vr,s_rr))/tau
    -1/C_m*(I_LK(Vr)+I_T_r(Vr,h_T_r))
Ca'=(alpha_Ca*I_T_t(Vt,h_T_t)-(Ca-Ca_0)/tau_Ca)
h_T_t'=(h_inf_T_t(Vt)-h_T_t)/tau_h_T_t(Vt)
h_T_r'=(h_inf_T_r(Vr)-h_T_r)/tau_h_T_r(Vr)
m_h'=((m_inf_h(Vt)*(1-m_h2)-m_h)/tau_m_h(Vt)-k3*P_h(Ca)*m_h+k4*m_h2)
m_h2'=(k3*P_h(Ca)*m_h-k4*m_h2)
s_er'=x_er
s_rt'=x_rt
s_rr'=x_rr
x_er'=gamma_t*gamma_t*(N_er*Qt(Vt)-s_er)-2*gamma_t*x_er
x_rt'=gamma_r*gamma_r*(N_rt*Qr(Vr)-s_rt)-2*gamma_r*x_rt
x_rr'=gamma_r*gamma_r*(N_rr*Qr(Vr)-s_rr)-2*gamma_r*x_rr

# Initial parameters
init Vt=-70,Vr=-70,Ca=2.4E-4

# XPPAUT settings
@ total=3000,dt=1,meth=rungekuta
@ YLO=-80,YHI=-40,XLO=0,XHI=3000
@ parmin=0,parmax=0.2
@ autoxmin=0,autoxmax=0.2,autoymin=-100,autoymax=0
@ ds=1e-2,dsmin=1e-5,dsmax=0.5
@ nmax=400,npr=0,ntst=600,epsl=1e-9,epss=1e-7,epsu=1e-7
done
```

Bibliography

[Achermann and Borbély, 1997] Achermann, P. A. and Borbély, A. A. (1997). Low-frequency (< 1 Hz) oscillations in the human sleep electroencephalogram. *Neuroscience*, 81(1):213–22.

[Adomian, 1990] Adomian, G. (1990). *Nonlinear Stochastic Systems Theory and Applications to Physics*, volume 70. Springer Netherlands.

[Ali et al., 2001] Ali, A. B., Rossier, J., Staiger, J. F., and Audinat, E. (2001). Kainate receptors regulate unitary IPSCs elicited in pyramidal cells by fast-spiking interneurons in the neocortex. *The Journal of Neuroscience*, 21(9):2992–2999.

[Amari, 1974] Amari, S.-i. (1974). A method of statistical neurodynamics. *Kybernetik*, 215:201–215.

[Amzica and Steriade, 1997a] Amzica, F. and Steriade, M. (1997a). Cellular substrates and laminar profile of sleep K-complex. *Neuroscience*, 82(3):671–686.

[Amzica and Steriade, 1997b] Amzica, F. and Steriade, M. (1997b). The K-complex: its slow (<1-Hz) rhythmicity and relation to delta waves. *Neurology*, 49(4):952–9.

[Amzica and Steriade, 1998] Amzica, F. and Steriade, M. (1998). Electrophysiological correlates of sleep delta waves. *Electroencephalography and Clinical Neurophysiology*, 107(2):69–83.

[Andrillon et al., 2011] Andrillon, T., Nir, Y., Staba, R. J., Ferrarelli, F., Cirelli, C., Tononi, G., and Fried, I. (2011). Sleep spindles in humans: insights from intracranial EEG and unit recordings. *The Journal of Neuroscience*, 31(49):17821–17834.

[Ardekani et al., 2005] Ardekani, B. M., Senhadji, L., and Shamsollahi, M. B. (2005). Inserting the Effects of Ion Channels in Mean Field Models: Application to generation of anesthetic slow waves. In *EUROCON*, volume 00, pages 378–381.

[Aserinsky and Kleitman, 1953] Aserinsky, E. and Kleitman, N. (1953). Regularly Occurring Periods of Eye Motility, and Concomitant Phenomena, during Sleep. *Science*, 118(3062):273–274.

[Aston-Jones and Bloom, 1981] Aston-Jones, G. and Bloom, F. E. (1981). Activity of norepinephrine-containing locus coeruleus neurons in behaving rats anticipates fluctuations in the sleep-waking cycle. *The Journal of Neuroscience*, 1(8):876–86.

[Bal and McCormick, 1996] Bal, T. and McCormick, D. A. (1996). What stops synchronized thalamocortical oscillations? *Neuron*, 17(2):297–308.

[Banks et al., 2000] Banks, M. I., White, J. A., and Pearce, R. A. (2000). Interactions between Distinct GABAA Circuits in Hippocampus. *Neuron*, 25(2):449–457.

[Barkai and Hasselmo, 1994] Barkai, E. and Hasselmo, M. E. (1994). Modulation of the input/output function of rat piriform cortex pyramidal cells. *Journal of Neurophysiology*, 72(2):644–658.

[Bartos et al., 2007] Bartos, M., Vida, I., and Jonas, P. (2007). Synaptic mechanisms of synchronized gamma oscillations in inhibitory interneuron networks. *Nature Reviews. Neuroscience*, 8(1):45–56.

[Bastani and Hosseini, 2007] Bastani, A. F. and Hosseini, S. M. (2007). A new adaptive Runge-Kutta method for stochastic differential equations. *Journal of Computational and Applied Mathematics*, 206(2):631–644.

[Bazhenov et al., 2005] Bazhenov, M., Rulkov, N. F., Fellous, J.-M., and Timofeev, I. (2005). Role of network dynamics in shaping spike timing reliability. *Physical Review E - Statistical, Nonlinear, and Soft Matter Physics*, 72(4):1–5.

[Bazhenov et al., 1998a] Bazhenov, M., Timofeev, I., Steriade, M., and Sejnowski, T. J. (1998a). Cellular and network models for intrathalamic augmenting responses during 10-Hz stimulation. *Journal of Neurophysiology*, 79(5):2730–2748.

[Bazhenov et al., 1998b] Bazhenov, M., Timofeev, I., Steriade, M., and Sejnowski, T. J. (1998b). Computational models of thalamocortical augmenting responses. *The Journal of Neuroscience*, 18(16):6444–6465.

[Bazhenov et al., 1999] Bazhenov, M., Timofeev, I., Steriade, M., and Sejnowski, T. J. (1999). Self-sustained rhythmic activity in the thalamic reticular nucleus mediated by depolarizing GABAA receptor potentials. *Nature Neuroscience*, 2(2):168–174.

[Bazhenov et al., 2000] Bazhenov, M., Timofeev, I., Steriade, M., and Sejnowski, T. J. (2000). Spiking-bursting activity in the thalamic reticular nucleus initiates sequences of spindle oscillations in thalamic networks. *Journal of Neurophysiology*, 84(2):1076–1087.

[Bazhenov et al., 2002] Bazhenov, M., Timofeev, I., Steriade, M., and Sejnowski, T. J. (2002). Model of thalamocortical slow-wave sleep oscillations and transitions to activated States. *The Journal of Neuroscience*, 22(19):8691–8704.

[Benda and Herz, 2003] Benda, J. and Herz, A. V. M. (2003). A universal model for spike-frequency adaptation. *Neural Computation*, 15(11):2523–64.

[Benita et al., 2012] Benita, J. M., Guillamon, A., Deco, G., and Sanchez-Vives, M. V. (2012). Synaptic depression and slow oscillatory activity in a biophysical network model of the cerebral cortex. *Frontiers in Computational Neuroscience*, 6:64.

[Benoît et al., 1981] Benoît, E., Callot, J. L., Diener, F., and Diener, M. (1981). Chasse au canard. *Collectanea Mathematica*, 31-32((1-3)):37–119.

[Berger and Phillips, 1995] Berger, R. J. and Phillips, N. H. (1995). Energy conservation and sleep. *Behavioural Brain Research*, 69(1-2):65–73.

[Besedovsky et al., 2012] Besedovsky, L., Lange, T., and Born, J. (2012). Sleep and immune function. *Pflugers Archiv European Journal of Physiology*, 463(1):121–137.

[Bhattacharya et al., 2013] Bhattacharya, B. S., Cakir, Y., Serap-Sengor, N., Maguire, L. P., and Coyle, D. (2013). Model-based bifurcation and power spectral analyses of thalamocortical alpha rhythm slowing in Alzheimer's Disease. *Neurocomputing*, 115:11–22.

[Bhattacharya et al., 2011] Bhattacharya, B. S., Coyle, D., and Maguire, L. P. (2011). A thalamo-cortico-thalamic neural mass model to study alpha rhythms in Alzheimer's disease. *Neural Networks*, 24(6):631–45.

[Bojak et al., 2013] Bojak, I., Day, H. C., and Liley, D. T. J. (2013). Ketamine, Propofol, and the EEG: A Neural Field Analysis of HCN1-Mediated Interactions. *Frontiers in Computational Neuroscience*, 7(April):22.

[Bojak and Liley, 2005] Bojak, I. and Liley, D. T. J. (2005). Modeling the effects of anesthesia on the electroencephalogram. *Physical Review E*, 71(4):041902.

[Bonjean et al., 2012] Bonjean, M., Baker, T., Bazhenov, M., Cash, S. S., Halgren, E., and Sejnowski, T. J. (2012). Interactions between Core and Matrix Thalamocortical Projections in Human Sleep Spindle Synchronization. *The Journal of Neuroscience*, 32(15):5250–5263.

[Bonjean et al., 2011] Bonjean, M., Baker, T., Lemieux, M., Timofeev, I., Sejnowski, T. J., and Bazhenov, M. (2011). Corticothalamic feedback controls sleep spindle duration in vivo. *The Journal of Neuroscience*, 31(25):9124–9134.

[Booth and Diniz Behn, 2014] Booth, V. and Diniz Behn, C. G. (2014). Physiologically-based modeling of sleep-wake regulatory networks. *Mathematical Biosciences*, 250(1):54–68.

[Borbély, 1982] Borbély, A. A. (1982). A two process model of sleep regulation. *Human Neurobiology*.

[Born et al., 1997] Born, J., Lange, T., Hansen, K., Mölle, M., and Fehm, H.-L. (1997). Sleep and Circadian Rhythm on Human Circulating Immune Cells. *Journal of Immunology*, 158(9):4454–4464.

[Boustani and Destexhe, 2010] Boustani, S. E. and Destexhe, A. (2010). Brain dynamics at multiple scales: can one reconcile the apparent low-dimensional chaos of macroscopic variables with the seemingly stochastic behavior of single neurons? *International Journal of Bifurcation and Chaos*, 20(6):1687–1702.

[Braitenberg and Schüz, 1991] Braitenberg, V. and Schüz, A. (1991). Statistics and Geometry. In Mayhew, editor, *Anatomy of the Cortex*, volume 179, pages 203–204.

[Braitenberg and Schüz, 2013] Braitenberg, V. and Schüz, A. (2013). *Anatomy of the cortex: statistics and geometry*, volume 18. Springer Science & Business Media.

[Breakspear et al., 2006] Breakspear, M., Roberts, J. A., Terry, J. R., Rodrigues, S., Mahant, N., and Robinson, P. A. (2006). A unifying explanation of primary generalized seizures through nonlinear brain modeling and bifurcation analysis. *Cerebral Cortex*, 16(9):1296–313.

[Brown and Adams, 1980] Brown, D. A. and Adams, P. R. (1980). Muscarinic suppression of a novel voltage-sensitive K+ current in a vertebrate neurone. *Nature*, 283(5748):673–676.

[Brown et al., 2008] Brown, R. E., McKenna, J. T., Winston, S., Basheer, R., Yanagawa, Y., Thakkar, M. M., and McCarley, R. W. (2008). Characterization of GABAergic neurons in rapid-eye-movement sleep controlling regions of the brainstem reticular formation in GAD67–green fluorescent protein knock-in mice. *European Journal of Neuroscience*, 27(2):352–363.

[Brunel et al., 2007] Brunel, N., Van Rossum, M. C. W., and Lapicque, L. (2007). Quantitative investigations of electrical nerve excitation treated as polarization. *Biological Cybernetics*, 97(5-6):341–349.

[Budde et al., 1997] Budde, T., Biella, G., Munsch, T., and Pape, H.-C. (1997). Lack of regulation by intracellular Ca2+ of the hyperpolarization- activated cation current in rat thalamic neurones. *The Journal of Physiology*, 503:79–85.

[Burke et al., 2012] Burke, J., Desroches, M., Barry, A. M., Kaper, T. J., and Kramer, M. A. (2012). A showcase of torus canards in neuronal bursters. *Journal of Mathematical Neuroscience*, 2(1):3.

[Burrage and Burrage, 1996] Burrage, K. and Burrage, P. M. (1996). High Strong Order Explicit Runge-Kutta Methods for Stochastic Ordinary Differential Equations. *Applied Numerical Mathematics*, 22(1-3):81–101.

[Butcher, 1963] Butcher, J. C. (1963). Coefficients for the study of Runge-Kutta integration processes. *Journal of the Australian Mathematical Society*, 3(May):185–201.

[Butcher, 1987] Butcher, J. C. (1987). *The Numerical Analysis of Ordinary Differential Equations: Runge-Kutta and General Linear Methods*. Wiley-Interscience, New York, NY, USA.

[Buzsáki, 1998] Buzsáki, G. (1998). Memory consolidation during sleep: a neurophysiological perspective. *Journal of Sleep Research*, 7 Suppl 1:17–23.

[Buzsáki, 2006] Buzsáki, G. (2006). *Rhythms of the Brain*. Oxford University Press.

[Buzsáki and Lopes da Silva, 2012] Buzsáki, G. and Lopes da Silva, F. H. (2012). High frequency oscillations in the intact brain. *Progress in Neurobiology*, 98(3):241–249.

[Buzsáki and Wang, 2012] Buzsáki, G. and Wang, X.-J. (2012). Mechanisms of gamma oscillations. *Annual Review of Neuroscience*, 35(March):203–25.

[Carlen et al., 2000] Carlen, P. L., Skinner, F. K., Zhang, L., Naus, C., Kushnir, M., and Perez Velazquez, J. L. (2000). The role of gap junctions in seizures. *Brain Research Reviews*, 32(1):235–41.

[Carlson and Giordano, 2011] Carlson, K. D. and Giordano, N. (2011). Interplay of the magnitude and time-course of postsynaptic Ca(2 +) concentration in producing spike timing-dependent plasticity. *Journal of Computational Neuroscience*, 30(3):747–58.

[Cash et al., 2009] Cash, S. S., Halgren, E., Dehghani, N., Rossetti, A. O., Thesen, T., Wang, C., Devinsky, O., Kuzniecky, R., Doyle, W., Madsen, J. R., Bromfield, E., Eross, L., Halasz, P., Karmos, G., Csercsa, R., Wittner, L., Ulbert, I., Eröss, L., and Halász, P. (2009). The human K-complex represents an isolated cortical down-state. *Science*, 324(5930):1084–1087.

[Castellani et al., 2009] Castellani, G. C., Bazzani, A., and Cooper, L. N. (2009). Toward a microscopic model of bidirectional synaptic plasticity. *Proceedings of the National Academy of Sciences of the United States of America*, 106(33):14091–5.

[Castellani et al., 2001] Castellani, G. C., Quinlan, E. M., Cooper, L. N., and Shouval, H. Z. (2001). A biophysical model of bidirectional synaptic plasticity: dependence on AMPA and NMDA receptors. *Proceedings of the National Academy of Sciences of the United States of America*, 98(22):12772–7.

[Chauvette et al., 2011] Chauvette, S., Crochet, S., Volgushev, M., and Timofeev, I. (2011). Properties of Slow Oscillation during Slow-Wave Sleep and Anesthesia in Cats. *The Journal of Neuroscience*, 31(42):14998–15008.

[Chauvette et al., 2010] Chauvette, S., Volgushev, M., and Timofeev, I. (2010). Origin of Active States in Local Neocortical Networks during Slow Sleep Oscillation. *Cerebral Cortex*, pages 1–15.

[Chen et al., 2012] Chen, J.-Y., Chauvette, S., Skorheim, S., Timofeev, I., and Bazhenov, M. (2012). Interneuron-mediated inhibition synchronizes neuronal activity during slow oscillation. *The Journal of Physiology*, 590(Pt 16):3987–4010.

[Cirelli and Tononi, 2008] Cirelli, C. and Tononi, G. (2008). Is sleep essential? *PLoS Biology*, 6(8):1605–1611.

[Clement et al., 2008] Clement, E. A., Richard, A., Thwaites, M., Ailon, J., Peters, S., and Dickson, C. T. (2008). Cyclic and Sleep-Like Spontaneous Alternations of Brain State Under Urethane Anaesthesia. *PLoS One*, 3(4):e2004.

[Cobb et al., 1995] Cobb, S. R., Buhl, E. H., Halasy, K., Paulsen, O., and Somogyi, P. (1995). Synchronization of neuronal activity in hippocampus by indivicual GABAergic interneurons. *Nature*, 378(6552):75–8.

[Colino and Halliwell, 1987] Colino, A. and Halliwell, J. V. (1987). Differential modulation of three separate K-conductances in hippocampal CA1 neurons by serotonin. *Nature*, 328(6125):73–7.

[Compte et al., 2003] Compte, A., Sanchez-Vives, M. V., McCormick, D. A., and Wang, X.-J. (2003). Cellular and network mechanisms of slow oscillatory activity (<1 Hz) and wave propagations in a cortical network model. *Journal of Neurophysiology*, 89(5):2707–2725.

[Cona et al., 2014] Cona, F., Lacanna, M., and Ursino, M. (2014). A thalamo-cortical neural mass model for the simulation of brain rhythms during sleep. *Journal of Computational Neuroscience*, 37:125–148.

[Contreras et al., 1992] Contreras, D., Curró Dossi, R., and Steriade, M. (1992). Bursting and tonic discharges in two classes of reticular thalamic neurons. *Journal of Neurophysiology*, 68(3):973–977.

[Contreras et al., 1997] Contreras, D., Destexhe, A., Sejnowski, T. J., and Steriade, M. (1997). Spatiotemporal patterns of spindle oscillations in cortex and thalamus. *The Journal of Neuroscience*, 17(3):1179–1196.

[Contreras and Steriade, 1995] Contreras, D. and Steriade, M. (1995). Cellular basis of EEG slow rhythms: a study of dynamic corticothalamic relationships. *The Journal of Neuroscience*, 15(1):604–622.

[Contreras and Steriade, 1996] Contreras, D. and Steriade, M. (1996). Spindle oscillation in cats: the role of corticothalamic feedback in a thalamically generated rhythm. *The Journal of Physiology*, 490 (Pt 1(Pt 1):159–179.

[Cox et al., 2012] Cox, R., Hofman, W. F., and Talamini, L. M. (2012). Involvement of spindles in memory consolidation is slow wave sleep-specific. *Learning & Memory*, 19(7):264–267.

[Crunelli et al., 2011] Crunelli, V., Errington, A. C., Hughes, S. W., and Tóth, T. I. (2011). The thalamic low-threshold Ca2+ potential: a key determinant of the local and global dynamics of the slow (<1 Hz) sleep oscillation in thalamocortical networks. *Philosophical Transactions of the Royal Society A: Mathematical, physical, and engineering sciences*, 369(1952):3820–39.

[Crunelli and Hughes, 2009] Crunelli, V. and Hughes, S. W. (2009). The slow rhythm of non-REM sleep: a dialogue between three cardinal oscillators. *Nature Neuroscience*, 13(1):9–17.

[Curto et al., 2009] Curto, C., Sakata, S., Marguet, S., Itskov, V., and Harris, K. D. (2009). A simple model of cortical dynamics explains variability and state dependence of sensory responses in urethane-anesthetized auditory cortex. *The Journal of Neuroscience*, 29(34):10600–12.

[Curtu and Rubin, 2011] Curtu, R. and Rubin, J. E. (2011). Interaction of Canard and Singular Hopf Mechanisms in a Neural Model. *SIAM Journal on Applied Dynamical Systems*, 10(4):1443–1479.

[da Costa and Martin, 2011] da Costa, N. M. and Martin, K. A. C. (2011). How thalamus connects to spiny stellate cells in the cat's visual cortex. *The Journal of Neuroscience*, 31(8):2925–37.

[Daan et al., 1984] Daan, S., Beersma, D. G. M., and Borbély, A. A. (1984). Timing of human sleep: recovery process gated by a circadian pacemaker. *The American Journal of Physiology*, 246(2 Pt 2):R161———R183.

[Datta and MacLean, 2007] Datta, S. and MacLean, R. R. (2007). Neurobiological Mechanisms for the Regulation of Mammalian Sleep-Wake Behavior: Reinterpretation of Historical Evidence and Inclusion of Contemporary Cellular and Molecular Evidence. *Neuroscience & Biobehavioral Reviews*, 31(5):775–824.

[David et al., 2004] David, O., Cosmelli, D., and Friston, K. J. (2004). Evaluation of different measures of functional connectivity using a neural mass model. *NeuroImage*, 21(2):659–673.

[David and Friston, 2003] David, O. and Friston, K. J. (2003). A neural mass model for MEG/EEG: coupling and neuronal dynamics. *NeuroImage*, 20(3):1743–1755.

[David et al., 2005] David, O., Harrison, L. M., and Friston, K. J. (2005). Modelling event-related responses in the brain. *NeuroImage*, 25(3):756–70.

[Davies et al., 1987] Davies, M. F., Deisz, R. A., Prince, D. A., and Peroutka, S. J. (1987). Two distinct effects of 5-hydroxytryptamine on single cortical neurons. *Brain Research*, 423(1-2):347–52.

[Deco and Jirsa, 2012] Deco, G. and Jirsa, V. K. (2012). Ongoing cortical activity at rest: criticality, multistability, and ghost attractors. *The Journal of Neuroscience*, 32(10):3366–75.

[Deco et al., 2008] Deco, G., Jirsa, V. K., Robinson, P. A., Breakspear, M., and Friston, K. J. (2008). The dynamic brain: from spiking neurons to neural masses and cortical fields. *PLoS Computational Biology*, 4(8):e1000092.

[Deco et al., 2009] Deco, G., Martí, D., Ledberg, A., Reig, R., Vives, M. V. S., and Sanchez-Vives, M. V. (2009). Effective reduced diffusion-models: a data driven approach to the analysis of neuronal dynamics. *PLoS Computational Biology*, 5(12):e1000587.

[DeFelipe et al., 2002] DeFelipe, J., Alonso-Nanclares, L., and Arellano, J. I. (2002). Microstructure of the neocortex: Comparative aspects. *Journal of Neurocytology*, 31(3-5 SPEC. ISS.):299–316.

[Denenberg and Thoman, 1981] Denenberg, V. H. and Thoman, E. B. (1981). Evidence for a functional role for active (REM) sleep in infancy. *Sleep*, 4(2):185–191.

[Destexhe, 2009] Destexhe, A. (2009). Self-sustained asynchronous irregular states and Up-Down states in thalamic, cortical and thalamocortical networks of nonlinear integrate-and-fire neurons. *Journal of Computational Neuroscience*, 27(3):493–506.

[Destexhe et al., 1996a] Destexhe, A., Bal, T., McCormick, D. A., and Sejnowski, T. J. (1996a). Ionic mechanisms underlying synchronized oscillations and propagating waves in a model of ferret thalamic slices. *Journal of Neurophysiology*, 76(3):2049–2070.

[Destexhe et al., 1994a] Destexhe, A., Contreras, D., Sejnowski, T. J., and Steriade, M. (1994a). A model of spindle rhythmicity in the isolated thalamic reticular nucleus. *Journal of Neurophysiology*, 72(2):803–18.

[Destexhe et al., 1994b] Destexhe, A., Contreras, D., Sejnowski, T. J., and Steriade, M. (1994b). Modeling the control of reticular thalamic oscillations by neuromodulators. *Neuroreport*, 5(17):2217–2220.

[Destexhe et al., 1998a] Destexhe, A., Contreras, D., and Steriade, M. (1998a). Mechanisms underlying the synchronizing action of corticothalamic feedback through inhibition of thalamic relay cells. *Journal of Neurophysiology*, 79(2):999–1016.

[Destexhe et al., 1999] Destexhe, A., Contreras, D., and Steriade, M. (1999). Spatiotemporal analysis of local field potentials and unit discharges in cat cerebral cortex during natural wake and sleep states. *The Journal of Neuroscience*, 19(11):4595–4608.

[Destexhe et al., 1996b] Destexhe, A., Contreras, D., Steriade, M., Sejnowski, T. J., and Huguenard, J. R. (1996b). In vivo, in vitro, and computational analysis of dendritic calcium currents in thalamic reticular neurons. *The Journal of Neuroscience*, 16(1):169–185.

[Destexhe and Mainen, 1994] Destexhe, A. and Mainen, Z. F. (1994). Synthesis of Models for Excitable Membranes, Synaptic Transmission and Neuromodulation Using a Common Kinetic Formalism. *Journal of Computational Neuroscience*, 1(3):195–230.

[Destexhe et al., 1998b] Destexhe, A., Neubig, M., Ulrich, D., and Huguenard, J. R. (1998b). Dendritic low-threshold calcium currents in thalamic relay cells. *The Journal of Neuroscience*, 18(10):3574–3588.

[Destexhe et al., 2003] Destexhe, A., Rudolph, M., and Paré, D. (2003). The high-conductance state of neocortical neurons in vivo. *Nature Reviews. Neuroscience*, 4(9):739–751.

[Destexhe and Sejnowski, 2003] Destexhe, A. and Sejnowski, T. J. (2003). Interactions between membrane conductances underlying thalamocortical slow-wave oscillations. *Physiological Reviews*, 83(4):1401–53.

[Diekelmann and Born, 2010] Diekelmann, S. and Born, J. (2010). The memory function of sleep. *Nature Reviews. Neuroscience*, 11(2):114–126.

[Dingledine et al., 1999] Dingledine, R., Borges, K., Bowie, D., and Traynelis, S. F. (1999). The Glutamate Receptor Ion Channels. *Pharmacological Reviews*, 51(1).

[Diniz Behn and Booth, 2010] Diniz Behn, C. G. and Booth, V. (2010). Simulating microinjection experiments in a novel model of the rat sleep-wake regulatory network. *Journal of Neurophysiology*, 103(4):1937–1953.

[Diniz Behn and Booth, 2012] Diniz Behn, C. G. and Booth, V. (2012). A fast-slow analysis of the dynamics of REM sleep. *SIAM Journal on Applied Dynamical Systems*, 11(1):212–242.

[Diniz Behn et al., 2007] Diniz Behn, C. G., Brown, E. N., Scammell, T. E., and Kopell, N. J. (2007). Mathematical model of network dynamics governing mouse sleep – wake behavior. *Journal of Neurophysiology*, 97:3828–3840.

[Disney et al., 2007] Disney, A. A., Aoki, C., and Hawken, M. J. (2007). Gain modulation by nicotine in macaque v1. *Neuron*, 56:701–713.

[Do et al., 2013] Do, J., Kim, J.-I., Bakes, J., Lee, K., and Kaang, B.-k. (2013). Functional roles of neurotransmitters and neuromodulators in the dorsal striatum. *Learning & Memory*, 20(1):21–28.

[Drover et al., 2010] Drover, J. D., Schiff, N. D., and Victor, J. D. (2010). Dynamics of coupled thalamocortical modules. *Journal of Computational Neuroscience*, pages 605–616.

[Dutar and Nicoll, 1988] Dutar, P. and Nicoll, R. A. (1988). A physiological role for GABAB receptors in the central nervous system. *Nature*, 332(6160):156–158.

[El Boustani et al., 2007] El Boustani, S., Pospischil, M., Rudolph-Lilith, M., and Destexhe, A. (2007). Activated cortical states: Experiments, analyses and models. *Journal of Physiology Paris*, 101(1-3):99–109.

[Ermentrout and Terman, 2010] Ermentrout, G. B. and Terman, D. H. (2010). *Mathematical Foundations of Neuroscience*. Springer-Verlag New York.

[Evans et al., 2012] Evans, R. C., Morera-Herreras, T., Cui, Y., Du, K., Sheehan, T., Hellgren Kotaleski, J., Venance, L., and Blackwell, K. T. (2012). The effects of NMDA subunit composition on calcium influx and spike timing-dependent plasticity in striatal medium spiny neurons. *PLoS Computational Biology*, 8(4):e1002493.

[Fishbein and Gutwein, 1977] Fishbein, W. and Gutwein, B. M. (1977). Paradoxical sleep and memory storage processes. *Behavioral Biology*, 19(4):425–464.

[Fitzhugh, 1961] Fitzhugh, R. (1961). Impulses and Physiological States in Theoretical Models of Nerve Membrane. *Biophysical Journal*, 1(6):445–466.

[Fleidervish et al., 1996] Fleidervish, I. A., Friedman, A., and Gutnick, M. J. (1996). Slow inactivation of Na current and slow cumulative spike adaptation in mouse and guinea-pig neocortical neurones in slices. *Journal of Physiology*, 493(1):83–97.

[Fleshner et al., 2011] Fleshner, M., Booth, V., Forger, D. B., and Diniz Behn, C. G. (2011). Circadian regulation of sleep-wake behaviour in nocturnal rats requires multiple signals from suprachiasmatic nucleus. *Philosophical Transactions of the Royal Society A: Mathematical, physical, and engineering sciences*, 369(1952):3855–3883.

[Forger et al., 2015] Forger, D. B., Jewett, M. E., and Kronauer, R. E. (2015). A Simpler Model of the Human Circadian Pacemaker. *Journal of Biological Rhythms*, 14(6):533–538.

[Foster et al., 2008] Foster, B. L., Bojak, I., and Liley, D. T. J. (2008). Population based models of cortical drug response: insights from anaesthesia. *Cognitive Neurodynamics*, 2(4):283–96.

[Foster, 1901] Foster, H. H. (1901). The Necessity for a New Standpoint in Sleep Theories. *The American Journal of Psychology*, 12(2):145–177.

[Frerking et al., 1999] Frerking, M., Petersen, C. C. H., and Nicoll, R. A. (1999). Mechanisms underlying kainate receptor-mediated disinhibition in the hippocampus. *Proceedings of the National Academy of Sciences of the United States of America*, 96(22):12917–12922.

[Freyer et al., 2011] Freyer, F., Roberts, J. A., Becker, R., Robinson, P. A., Ritter, P., and Breakspear, M. (2011). Biophysical mechanisms of multistability in resting-state cortical rhythms. *The Journal of Neuroscience*, 31(17):6353–61.

[Fuhrmann et al., 2002] Fuhrmann, G., Markram, H., Tsodyks, M. V., and Spike, M. T. (2002). Spike Frequency Adaptation and Neocortical Rhythms. *Journal of Neurophysiology*, 88(2):761–770.

[Fuller et al., 2007] Fuller, P. M., Saper, C. B., and Lu, J. (2007). The pontine REM switch: past and present. *The Journal of Physiology*, 584(Pt 3):735–741.

[Gage, 1992] Gage, P. W. (1992). Activation and modulation of neuronal K+ channels by GABA. *Trends in Neurosciences*, 15(2):46–51.

[Gais and Born, 2004] Gais, S. and Born, J. (2004). Low acetylcholine during slow-wave sleep is critical for declarative memory consolidation. *Proceedings of the National Academy of Sciences of the United States of America*, 101(7):2140–4.

[Gais et al., 2002] Gais, S., Mölle, M., Helms, K., and Born, J. (2002). Learning-dependent increases in sleep spindle density. *The Journal of Neuroscience*, 22(15):6830–4.

[Gardiner, 2004] Gardiner, C. W. (2004). *Handbook of Stochastic Methods*, volume 37. Springer-Verlag.

[Gigante et al., 2007] Gigante, G., Mattia, M., and Giudice, P. (2007). Diverse Population-Bursting Modes of Adapting Spiking Neurons. *Physical Review Letters*, 98(14):148101.

[Gleit et al., 2013] Gleit, R. D., Diniz Behn, C. G., and Booth, V. (2013). Modeling interindividual differences in spontaneous internal desynchrony patterns. *Journal of Biological Rhythms*, 28(5):339–55.

[Goard and Dan, 2009] Goard, M. and Dan, Y. (2009). Basal forebrain activation enhances cortical coding of natural scenes. *Nature Neuroscience*, 12(11):1444–9.

[Graupner and Brunel, 2012] Graupner, M. and Brunel, N. (2012). Calcium-based plasticity model explains sensitivity of synaptic changes to spike pattern, rate, and dendritic location. *Proceedings of the National Academy of Sciences of the United States of America*.

[Gray, 1918] Gray, H. (1918). *Anatomy of the human body*. Lea & Febiger, Philadelphia, 20th edition.

[Groch et al., 2013] Groch, S., Wilhelm, I., Diekelmann, S., and Born, J. (2013). The role of REM sleep in the processing of emotional memories: evidence from behavior and event-related potentials. *Neurobiology of Learning and Memory*, 99:1–9.

[Gu and Stornetta, 2007] Gu, Y. and Stornetta, R. L. (2007). Synaptic plasticity, AMPA-R trafficking, and Ras-MAPK signaling. *Acta Pharmacologica Sinica*, 28(7):928–936.

[Guckenheimer et al., 1997] Guckenheimer, J., Harris-Warrick, R., Peck, J., and Willms, A. (1997). Bifurcation, Bursting, and Spike Frequency Adaptation. *Journal of Computational Neuroscience*, 4(3):257–277.

[Guckenheimer et al., 1984] Guckenheimer, J., Holmes, P., and Slemrod, M. (1984). Nonlinear Oscillations Dynamical Systems, and Bifurcations of Vector Fields.

[Guillery and Sherman, 2002] Guillery, R. W. and Sherman, S. M. (2002). Thalamic relay functions and their role in corticocortical communication: Generalizations from the visual system. *Neuron*, 33(2):163–175.

[Gulledge et al., 2009] Gulledge, A. T., Bucci, D. J., Zhang, S. S., Matsui, M., and Yeh, H. H. (2009). M1 receptors mediate cholinergic modulation of excitability in neocortical pyramidal neurons. *The Journal of Neuroscience*, 29(31):9888–9902.

[Hashemi et al., 2015] Hashemi, M., Hutt, A., and Sleigh, J. W. (2015). How the cortico-thalamic feedback affects the EEG power spectrum over frontal and occipital regions during propofol-induced sedation. *Journal of Computational Neuroscience*, 39(2):155–179.

[Hasselmo and Barkai, 1995] Hasselmo, M. E. and Barkai, E. (1995). Cholinergic modulation of activity-dependent synaptic plasticity in the piriform cortex and associative memory function in a network biophysical simulation. *The Journal of Neuroscience*, 15(10):6592–604.

[Hernandez and Spigler, 1993] Hernandez, D. B. and Spigler, R. (1993). Convergence and stability of implicit Runge-Kutta methods for systems with multiplicative noise. *BIT Numerical Mathematics*, 33(July 1992):654–669.

[Hill and Tononi, 2004] Hill, S. L. and Tononi, G. (2004). Modeling Sleep and Wakefulness in the Thalamocortical System. *Journal of Neurophysiology*, 93(3):1671–1698.

[Hindmarsh and Rose, 1984] Hindmarsh, J. L. and Rose, R. M. (1984). A model of neuronal bursting using three coupled first order differential equations. *Proceedings of the Royal Society of London. Series B, Biological sciences*, 221(1222):87–102.

[Hodgkin, 1957] Hodgkin, A. L. (1957). Ionic movements and electrical activity in giant nerve fibers.

[Hodgkin and Huxley, 1952a] Hodgkin, A. L. and Huxley, A. F. (1952a). A Quantitative Description of Membrane Current and its Application to Conduction and Excitation in Nerves. *The Journal of Physiology*, 117:500–544.

[Hodgkin and Huxley, 1952b] Hodgkin, A. L. and Huxley, A. F. (1952b). Currents carried by sodium and potassium ions through the membrane of the giant axon of Loligo. *The Journal of Physiology*, 116(4):424–448.

[Holcman and Tsodyks, 2006] Holcman, D. and Tsodyks, M. V. (2006). The emergence of Up and Down states in cortical networks. *PLoS Computational Biology*, 2(3):e23.

[Honeycutt, 1992] Honeycutt, R. L. (1992). Stochastic runge-kutta algorithms. I. White noise. *Physical Review A*.

[Hopf, 1942] Hopf, E. F. F. (1942). Abzweigung einer periodischen Lösung von einer stationären Lösung eines Differentialsystems. *Berichten der Mathematisch-Physischen Klasse der Sächsischen Akademie der Wissenschaften zu Leipzig*, XCIV:1–22.

[Hromadka et al., 2013] Hromadka, T., Zador, A., and DeWeese, M. R. (2013). Up states are rare in awake auditory cortex. *Journal of Neurophysiology*, 109(8):1989–1995.

[Huber et al., 2004a] Huber, R., Felice Ghilardi, M., Massimini, M., and Tononi, G. (2004a). Local sleep and learning. *Nature*, 430(6995):78–81.

[Huber et al., 2004b] Huber, R., Hill, S. L., Holladay, C., Biesiadecki, M., Tononi, G., and Cirelli, C. (2004b). Sleep homeostasis in Drosophila melanogaster. *Sleep*, 27(4):628–639.

[Hughes et al., 2002] Hughes, S. W., Cope, D. W., Blethyn, K. L., and Crunelli, V. (2002). Cellular mechanisms of the slow (<1 Hz) oscillation in thalamocortical neurons in vitro. *Neuron*, 33(6):947–958.

[Huguenard and McCormick, 1992] Huguenard, J. R. and McCormick, D. A. (1992). Simulation of the currents involved in rhythmic oscillations in thalamic relay neurons. *Journal of Neurophysiology*, 68(4):1373–1383.

[Hunt and Castillo, 2012] Hunt, D. L. and Castillo, P. E. (2012). Synaptic plasticity of NMDA receptors: mechanisms and functional implications. *Current Opinion in Neurobiology*.

[Hutt, 2012] Hutt, A. (2012). The population firing rate in the presence of GABAergic tonic inhibition in single neurons and application to general anaesthesia. *Cognitive Neurodynamics*, 6(3):227–237.

[Iber et al., 2007] Iber, C., Ancoli-Israel, S., Chesson Jr., A. L., and Quan, S. F. (2007). The AASM Manual for the Scoring of Sleep and Associated Events: Rules Terminology and Technical Specifications 1st ed.

[Isomura et al., 2006] Isomura, Y., Sirota, A., Özen, S., Montgomery, S., Mizuseki, K., Henze, D. A., and Buzsáki, G. (2006). Integration and Segregation of Activity in Entorhinal-Hippocampal Subregions by Neocortical Slow Oscillations. *Neuron*, 52(5):871–882.

[Itô, 1944] Itô, K. (1944). Stochastic integral. *Proceedings of the Imperial Academy*, 20(8):519–524.

[Itô, 1951] Itô, K. (1951). On a formula concerning stochastic differentials. *Nagoya Mathematical Journal*, 3(3):55–66.

[Itô, 1984] Itô, K. (1984). Foundations of Stochastic Differential Equations in Infinite Dimensional Spaces. *Society for Industrial and Applied Mathematics*, 26.

[Izhikevich, 2007] Izhikevich, E. M. (2007). *Dynamical Systems in Neuroscience: The Geometry of Excitability and Bursting*. Massachusetts Institute of Technology.

[Izhikevich et al., 2004] Izhikevich, E. M., Gally, J. A., and Edelman, G. M. (2004). Spike-timing dynamics of neuronal groups. *Cerebral Cortex*, 14(8):933–44.

[Jansen and Rit, 1995] Jansen, B. H. and Rit, V. G. (1995). Electroencephalogram and visual evoked potential generation in a mathematical model of coupled cortical columns. *Biological Cybernetics*, 73(4):357–366.

[Jansen et al., 1993] Jansen, B. H., Zouridakis, G., and Brandt, M. E. (1993). A neurophysiologically-based mathematical model of flash visual evoked potentials. *Electrical Engineering*, 283(3):275–283.

[Jefferys et al., 2012] Jefferys, J. G. R., Menendez de la Prida, L., Wendling, F., Bragin, A., Avoli, M., Timofeev, I., and Lopes da Silva, F. H. (2012). Mechanisms of physiological and epileptic HFO generation. *Progress in Neurobiology*, 98(3):250–264.

[Jenkins and Dallenbach, 1924] Jenkins, J. G. and Dallenbach, K. M. (1924). Obliviscence during Sleep and Waking. *The American Journal of Psychology*, 35(4):605–612.

[Ji and Wilson, 2006] Ji, D. and Wilson, M. A. (2006). Coordinated memory replay in the visual cortex and hippocampus during sleep. *Nature Neuroscience*, 10(1):100–107.

[Jones, 1975] Jones, E. G. (1975). Some aspects of the organization of the thalamic reticular complex. *The Journal of Comparative Neurology*, 162(3):285–308.

[Jones, 1985] Jones, E. G. (1985). *The Thalamus*. Springer US, New York, 1 edition.

[Jones, 2001] Jones, E. G. (2001). The thalamic matrix and thalamocortical synchrony. *Trends in Neurosciences*, 24(10):595–601.

[Jones, 2002] Jones, E. G. (2002). Thalamic circuitry and thalamocortical synchrony. *Philosophical Transactions of the Royal Society B: Biological Sciences*, 357(1428):1659–1673.

[Kales and Rechtschaffen, 1968] Kales, A. and Rechtschaffen, A. (1968). *A manual of standardized terminology, techniques and scoring system for sleep stages of human subjects*. U. S. National Institute of Neurological Diseases and Blindness, Neurological Information Network.

[Kampa et al., 2004] Kampa, B. M., Clements, J., Jonas, P., and Stuart, G. J. (2004). Kinetics of Mg2+ unblock of NMDA receptors: implications for spike-timing dependent synaptic plasticity. *The Journal of Physiology*, 556(Pt 2):337–345.

[Kerr et al., 2011] Kerr, C. C., Kemp, A. H., Rennie, C. J., and Robinson, P. A. (2011). Thalamocortical changes in major depression probed by deconvolution and physiology-based modeling. *NeuroImage*, 54(4):2672–82.

[Kerr et al., 2008] Kerr, C. C., Rennie, C. J., and Robinson, P. A. (2008). Physiology-based modeling of cortical auditory evoked potentials. *Biological Cybernetics*, 98(2):171–184.

[Kiebel et al., 2008] Kiebel, S. J., Garrido, M. I., Moran, R. J., and Friston, K. J. (2008). Dynamic causal modelling for EEG and MEG. *Cognitive Neurodynamics*, 2(2):121–136.

[Kilpatrick and Bressloff, 2010a] Kilpatrick, Z. P. and Bressloff, P. C. (2010a). Effects of synaptic depression and adaptation on spatiotemporal dynamics of an excitatory neuronal network. *Physica D: Nonlinear Phenomena*, 239(9):547–560.

[Kilpatrick and Bressloff, 2010b] Kilpatrick, Z. P. and Bressloff, P. C. (2010b). Spatially structured oscillations in a two-dimensional excitatory neuronal network with synaptic depression. *Journal of Computational Neuroscience*, 28(2):193–209.

[Kisvárday et al., 1993] Kisvárday, Z. F., Beaulieu, C., and Eysel, U. T. (1993). GABAergic Large Basket Cells in Cat Visual Cortex (Area 18): Implication for Lateral Disinhibition. *Journal of Comparative Neurology*, 327(3):398–415.

[Kohl and Paulsen, 2010] Kohl, M. M. and Paulsen, O. (2010). The roles of GABAB receptors in cortical network activity. *Advances in Pharmacology*, 58(C):205–229.

[Kopell et al., 2010] Kopell, N. J., Börgers, C., Pervouchine, D. D., Malerba, P., and Tort, A. B. L. (2010). *Gamma and Theta Rhythms in Biophysical Models of Hippocampal Circuits*. Springer New York, New York, NY.

[Kronauer, 1982] Kronauer, R. E. (1982). Mathematical model of the human circadian system with two interacting oscillators. *The American Journal of Physiology*, 242(1):R3–R17.

[Krupa and Szmolyan, 2001] Krupa, M. and Szmolyan, P. (2001). Relaxation Oscillation and Canard Explosion. *Journal of Differential Equations*, 174(2):312–368.

[Kumar et al., 2012] Kumar, R., Bose, A., and Mallick, B. N. (2012). A mathematical model towards understanding the mechanism of neuronal regulation of wake-NREMS-REMS states. *PLoS One*, 7(8):1–17.

[Küpper et al., 2011] Küpper, D., Kværnø, A., and Rößler, A. (2011). A Runge-Kutta method for index 1 stochastic differential-algebraic equations with scalar noise. *BIT Numerical Mathematics*, 52(2):437–455.

[Kutta, 1901] Kutta, M. W. (1901). Beitrag zur näherungweisen Integration totaler Differentialgleichungen. *Zeitschrift für Mathematik und Physik*, 46:435–453.

[Kuznetsov, 1998] Kuznetsov, Y. A. (1998). *Elements of Applied Bifurcation Theory*. Springer New York.

[Landsness et al., 2009] Landsness, E. C., Crupi, D., Hulse, B. K., Peterson, M. J., Huber, R., Ansari, H., Coen, M., Cirelli, C., Benca, R. M., Ghilardi, M. F., and Tononi, G. (2009). Sleep-Dependent Improvement in Visuomotor Learning: A Causal Role for Slow Waves. *Sleep*, 32(10):1273–1284.

[Langdon, 2012] Langdon, A. J. (2012). *Neuronal population dynamics in somatosensory processing*. PhD thesis, The University of South Wales.

[Lange et al., 2010] Lange, T., Dimitrov, S., and Born, J. (2010). Effects of sleep and circadian rhythm on the human immune system. *Annals of the New York Academy of Sciences*, 1193:48–59.

[Lazar et al., 2009] Lazar, A., Pipa, G., and Triesch, J. (2009). SORN: a self-organizing recurrent neural network. *Frontiers in Computational Neuroscience*, 3(October):23.

[Lemieux et al., 2014] Lemieux, M., Chen, J.-Y., Lonjers, P., Bazhenov, M., and Timofeev, I. (2014). The impact of cortical deafferentation on the neocortical slow oscillation. *The Journal of Neuroscience*, 34(16):5689–703.

[Léna et al., 2005] Léna, I., Parrot, S., Deschaux, O., Muffat-Joly, S., Sauvinet, V., Renaud, B., Suaud-Chagny, M.-F., and Gottesmann, C.-J. (2005). Variations in extracellular levels of dopamine, noradrenaline, glutamate, and aspartate across the sleep-wake cycle in the medial prefrontal cortex and nucleus accumbens of freely moving rats. *Journal of Neuroscience Research*, 81(6):891–899.

[Liley and Bojak, 2005] Liley, D. T. J. and Bojak, I. (2005). Understanding the transition to seizure by modeling the epileptiform activity of general anesthetic agents. *Journal of Clinical Neurophysiology*, 22(5):300–313.

[Liley et al., 2011] Liley, D. T. J., Bojak, I., and Foster, B. L. (2011). A mesoscopic modelling approach to anaesthetic action on brain electrical activity. In Hutt, A., editor, *Sleep and Anesthesia*, chapter 7, pages 139–166. Springer New York.

[Liley et al., 2002] Liley, D. T. J., Cadusch, P. J., and Dafilis, M. P. (2002). A spatially continuous mean field theory of electrocortical activity. *Network (Bristol, England)*, 13(1):67–113.

[Liley et al., 1999] Liley, D. T. J., Cadusch, P. J., and Wright, J. J. (1999). A continuum theory of electro-cortical activity. *Neurocomputing*, 26-27(May 2000):795–800.

[Liley and Walsh, 2013] Liley, D. T. J. and Walsh, M. (2013). The Mesoscopic Modeling of Burst Suppression during Anesthesia. *Frontiers in Computational Neuroscience*, 7(April):46.

[Liljenström and Hasselmo, 1995] Liljenström, H. and Hasselmo, M. E. (1995). Cholinergic modulation of cortical oscillatory dynamics. *Journal of Neurophysiology*, 74(1):288–297.

[Liu and Gillette, 1996] Liu, C. and Gillette, M. U. (1996). Cholinergic regulation of the suprachiasmatic nucleus circadian rhythm via a muscarinic mechanism at night. *The Journal of Neuroscience*, 16(2):744–751.

[Liu and Jones, 1999] Liu, X.-B. and Jones, E. G. (1999). Predominance of corticothalamic synaptic inputs to thalamic reticular nucleus neurons in the rat. *Journal of Comparative Neurology*, 414(1):67–79.

[Llinás and Steriade, 2006] Llinás, R. R. and Steriade, M. (2006). Bursting of thalamic neurons and states of vigilance. *Journal of Neurophysiology*, 95(6):3297–308.

[Lopes da Silva, 1991] Lopes da Silva, F. H. (1991). Neural mechanisms underlying brain waves: from neural membranes to networks. *Electroencephalography and Clinical Neurophysiology*, 79(2):81–93.

[Lopes da Silva et al., 1974] Lopes da Silva, F. H., Hoeks, A., Smits, H., and Zetterberg, L. H. (1974). Model of brain rhythmic activity. The alpha-rhythm of the thalamus. *Kybernetik*, 15(1):27–37.

[Louvel et al., 2001] Louvel, J., Papatheodoropoulos, C., Siniscalchi, A., Kurcewicz, I., Pumain, R., Devaux, B., Turak, B., Esposito, V., Villemeure, J. G., and Avoli, M. (2001). GABA-mediated synchronization in the human neocortex: Elevations in extracellular potassium and presynaptic mechanisms. *Neuroscience*, 105(4):803–813.

[Loxley and Robinson, 2007] Loxley, P. N. and Robinson, P. A. (2007). Spike-rate adaptation and neuronal bursting in a mean-field model of brain activity. *Biological Cybernetics*, 97(2):113–22.

[Lu et al., 2006] Lu, J., Sherman, D., Devor, M., and Saper, C. B. (2006). A putative flip-flop switch for control of REM sleep. *Nature*, 441(7093):589–594.

[Luppi et al., 2006] Luppi, P. H., Gervasoni, D., Verret, L., Goutagny, R., Peyron, C., Salvert, D., Leger, L., and Fort, P. (2006). Paradoxical (REM) sleep genesis: The switch from an aminergic-cholinergic to a GABAergic-glutamatergic hypothesis. *Journal of Physiology Paris*, 100(5-6):271–283.

[Lüthi and McCormick, 1998] Lüthi, A. and McCormick, D. A. (1998). Periodicity of thalamic synchronized oscillations: the role of Ca2+- mediated upregulation of Ih. *Neuron*, 20(3):553–563.

[Lüthi and McCormick, 1999] Lüthi, A. and McCormick, D. A. (1999). Modulation of a pacemaker current through Ca(2+)-induced stimulation of cAMP production. *Nature Neuroscience*, 2(7):634–641.

[Lyapunov, 1892] Lyapunov, A. M. (1892). *General Problem of Stability of Motion.* PhD thesis, Kharkov.

[Lydic and Baghdoyan, 2015] Lydic, R. and Baghdoyan, H. A. (2015). Sleep, Anesthesiology, and the Neurobiology of Arousal State Control. *Anesthesiology*, 103(6):1268–1295.

[Madden, 2002] Madden, D. R. (2002). Ion Channel Structurethe Structure and Function of Glutamate Receptor Ion Channels. *Nature Reviews. Neuroscience*, 3(2):91–101.

[Madison et al., 1987] Madison, D. V., Lancaster, B., and Nicoll, R. A. (1987). Voltage clamp analysis of cholinergic action in the hippocampus. *The Journal of Neuroscience*, 7(3):733–741.

[Madison and Nicoll, 1982] Madison, D. V. and Nicoll, R. A. (1982). Noradrenaline blocks accommodation of pyramidal cell discharge in the hippocampus. *Nature*, 299:636–638.

[Madison and Nicoll, 1984] Madison, D. V. and Nicoll, R. A. (1984). Controll of the repetitive discharge of rat CA1 pyramidal neurons in vitro. *The Journal of Physiology*, 354:319–331.

[Madison and Nicoll, 1986] Madison, D. V. and Nicoll, R. A. (1986). ACTIONS OF NORADRENALINE RECORDED INTRACELLULARLY IN RAT HIPPOCAMPAL CA1 PYRAMIDAL NEURONES, IN VITRO. *Journal of Physiology*, 372:221–244.

[Maier et al., 2003] Maier, N., Nimmrich, V., and Draguhn, A. (2003). Cellular and network mechanisms underlying spontaneous sharp wave-ripple complexes in mouse hippocampal slices. *The Journal of Physiology*, 550(Pt 3):873–87.

[Malinow and Malenka, 2002] Malinow, R. and Malenka, R. C. (2002). AMPA receptor trafficking and synaptic plasticity. *Annual Review of Neuroscience*, 25(1):103–26.

[Mann et al., 2005] Mann, E. O., Radcliffe, C. A., and Paulsen, O. (2005). Hippocampal gamma-frequency oscillations: from interneurones to pyramidal cells, and back. *The Journal of Physiology*, 562(Pt 1):55–63.

[Maquet, 2001] Maquet, P. (2001). The role of sleep in learning and memory. *Science*, 294(5544):1048–52.

[Maren and Baudry, 1995] Maren, S. and Baudry, M. (1995). Properties and mechanism of long-term synaptic plasticity in the mammalian brain: relationships to learning and memory. *Neurobiology of Learning and Memory*, 63:1–18.

[Marks et al., 1995] Marks, G. A., Shaffery, J. P., Oksenberg, A., Speciale, S. G., and Roffwarg, H. P. (1995). A functional role for REM sleep in brain maturation. *Behavioural Brain Research*, 69(1-2):1–11.

[Marrosu et al., 1995] Marrosu, F., Portas, C., Mascia, M. S., Casu, M. A., Fà, M., Giagheddu, M., Imperato, A., and Gessa, G. L. (1995). Microdialysis Measurement of Cortical and Hippocampal Acetylcholine-Release during Sleep-Wake Cycle in Freely Moving Cats. *Brain Research*, 671(2):329–332.

[Marshall et al., 2006] Marshall, L., Helgadóttir, H., Mölle, M., and Born, J. (2006). Boosting slow oscillations during sleep potentiates memory. *Nature*, 444(7119):610–613.

[Massimini and Amzica, 2001] Massimini, M. and Amzica, F. (2001). Extracellular calcium fluctuations and intracellular potentials in the cortex during the slow sleep oscillation. *Journal of Beurophysiology*, 85(3):1346–1350.

[Massimini et al., 2004] Massimini, M., Huber, R., Ferrarelli, F., Hill, S. L., and Tononi, G. (2004). The sleep slow oscillation as a traveling wave. *The Journal of Neuroscience*, 24(31):6862–70.

[Mayer et al., 2006] Mayer, J., Schuster, H. G., and Claussen, J. C. (2006). Role of inhibitory feedback for information processing in thalamocortical circuits. *Physical Review E*, 73(3).

[McCarley and Hobson, 1975] McCarley, R. W. and Hobson, J. A. (1975). Neuronal Excitability Modulation over the Sleep Cycle: A Structural and Mathematical Model Abstract. *Science*, 189(4196):58–60.

[McCormick, 1989] McCormick, D. A. (1989). Cholinergic and noradrenergic modulation of thalamocortical processing. *Trends in Neurosciences*, 12(6):215–221.

[McCormick and Bal, 1997] McCormick, D. A. and Bal, T. (1997). Sleep and arousal: thalamocortical mechanisms. *Annual Review of Neuroscience*, 20:185–215.

[McCormick and Huguenard, 1992] McCormick, D. A. and Huguenard, J. R. (1992). A model of the electrophysiological properties of thalamocortical relay neurons. *Journal of Neurophysiology*, 68(4):1384–400.

[McCormick and Pape, 1990] McCormick, D. A. and Pape, H.-C. (1990). Properties of a hyperpolarization-activated cation current and its role in rhythmic oscillation in thalamic relay neurons. *The Journal of Physiology*, 431:291–318.

[McCormick and von Krosigk, 1992] McCormick, D. A. and von Krosigk, M. (1992). Corticothalamic activation modulates thalamic firing through glutamate "metabotropic" receptors. *Proceedings of the National Academy of Sciences of the United States of America*, 89(April):2774–2778.

[Menicucci et al., 2013] Menicucci, D., Piarulli, A., Allegrini, P., Laurino, M., Mastorci, F., Sebastiani, L., Bedini, R., and Gemignani, A. (2013). Fragments of wake-like activity frame down-states of sleep slow oscillations in humans: new vistas for studying homeostatic processes during sleep. *International Journal of Psychophysiology*, 89(2):151–7.

[Metherate et al., 1992] Metherate, R., Cox, C. L., and Ashe, J. H. (1992). Cellular bases of neocortical activation: modulation of neural oscillations by the nucleus basalis and endogenous acetylcholine. *The Journal of Neuroscience*, 12(12):4701–4711.

[Miles et al., 1996] Miles, R., Tóth, K., Gulyás, A. I., Hájos, N., and Freund, T. F. (1996). Differences between somatic and dendritic inhibition in the hippocampus. *Neuron*, 16(4):815–823.

[Miller, 2003] Miller, K. D. (2003). Understanding layer 4 of the cortical circuit: a model based on cat V1. *Cerebral Cortex*, 13(1):73–82.

[Miller et al., 2001] Miller, K. D., Pinto, D. J., and Simons, D. J. (2001). Processing in layer 4 of the neocortical circuit: new insights from visual and somatosensory cortex. *Current Opinion in Neurobiology*, 11(4):488–497.

[Miller et al., 2005] Miller, P., Zhabotinsky, A. M., Lisman, J. E., and Wang, X.-J. (2005). The stability of a stochastic CaMKII switch: dependence on the number of enzyme molecules and protein turnover. *PLoS Biology*, 3(4):e107.

[Min et al., 1999] Min, M. Y., Melyan, Z., and Kullmann, D. M. (1999). Synaptically released glutamate reduces gamma-aminobutyric acid (GABA)ergic inhibition in the hippocampus via kainate receptors. *Proceedings of the National Academy of Sciences of the United States of America*, 96(17):9932–9937.

[Mirmiran, 1995] Mirmiran, M. (1995). The function of fetal/neonatal rapid eye movement sleep. *Behavioural Brain Research*, 69(1-2):13–22.

[Mirmiran et al., 1983] Mirmiran, M., Scholtens, J., van de Poll, N. E., Uylings, H. B., van der Gugten, J., and Boer, G. J. (1983). Effects of experimental suppression of active (REM) sleep during early development upon adult brain and behavior in the rat. *Brain Research*, 283(2-3):277–86.

[Molaee-Ardekani et al., 2007] Molaee-Ardekani, B., Senhadji, L., Shamsollahi, M. B., Vosoughi-Vahdat, B., and Wodey, E. (2007). Brain activity modeling in general anesthesia: enhancing local mean-field models using a slow adaptive firing rate. *Physical Review E*, 76(4):1–43.

[Mölle et al., 2011] Mölle, M., Bergmann, T. O., Marshall, L., and Born, J. (2011). Fast and slow spindles during the sleep slow oscillation: disparate coalescence and engagement in memory processing. *Sleep*, 34(10):1411–1421.

[Mölle et al., 2009] Mölle, M., Eschenko, O., Gais, S., Sara, S. J., and Born, J. (2009). The influence of learning on sleep slow oscillations and associated spindles and ripples in humans and rats. *European Journal of Neuroscience*, 29(5):1071–1081.

[Mölle et al., 2002] Mölle, M., Marshall, L., Gais, S., and Born, J. (2002). Grouping of spindle activity during slow oscillations in human non-rapid eye movement sleep. *The Journal of Neuroscience*, 22(24):10941–7.

[Mölle et al., 2006] Mölle, M., Yeshenko, O., Marshall, L., Sara, S. J., and Born, J. (2006). Hippocampal sharp wave-ripples linked to slow oscillations in rat slow-wave sleep. *Journal of Neurophysiology*, 96:62–70.

[Montgomery and Madison, 2004] Montgomery, J. M. and Madison, D. V. (2004). Discrete synaptic states define a major mechanism of synapse plasticity. *Trends in Neurosciences*, 27(12):744–750.

[Moran et al., 2007] Moran, R. J., Kiebel, S. J., Stephan, K. E., Reilly, R. B., Daunizeau, J., and Friston, K. J. (2007). A neural mass model of spectral responses in electrophysiology. *NeuroImage*, 37(3):706–20.

[Moran et al., 2011] Moran, R. J., Mallet, N., Litvak, V., Dolan, R. J., Magill, P. J., Friston, K. J., and Brown, P. (2011). Alterations in brain connectivity underlying beta oscillations in Parkinsonism. *PLoS Computational Biology*, 7(8):e1002124.

[Moran et al., 2009] Moran, R. J., Stephan, K. E., Seidenbecher, T., Pape, H.-C., Dolan, R. J., and Friston, K. J. (2009). Dynamic causal models of steady-state responses. *NeuroImage*, 44(3):796–811.

[Morison and Bassett, 1945] Morison, R. S. and Bassett, D. L. (1945). Electrical activity of the thalamus and basal ganglia in decorticate cats. *Journal of Neurophysiology*, 8(5):309–314.

[Morris and Lecar, 1981] Morris, C. and Lecar, H. (1981). Voltage oscillations in the barnacle giant muscle fiber. *Biophysical Journal*, 35(1):193–213.

[Moruzzi, 1972] Moruzzi, G. (1972). The sleep-waking cycle. *Ergebnisse der Physiologie, biologischen Chemie und experimentellen Pharmakologie*, 64:1–165.

[Munro and Börgers, 2010] Munro, E. and Börgers, C. (2010). Mechanisms of very fast oscillations in networks of axons coupled by gap junctions. *Journal of Computational Neuroscience*, 28(3):539–555.

[Ngo et al., 2013a] Ngo, H.-V. V., Claussen, J. C., Born, J., and Mölle, M. (2013a). Induction of slow oscillations by rhythmic acoustic stimulation. *Journal of Sleep Research*, 22(1):22–31.

[Ngo et al., 2013b] Ngo, H.-V. V., Martinetz, T., Born, J., and Mölle, M. (2013b). Auditory closed-loop stimulation of the sleep slow oscillation enhances memory. *Neuron*, 78(3):545–553.

[Ngo et al., 2015] Ngo, H.-V. V., Miedema, A., Faude, I., Martinetz, T., Mölle, M., and Born, J. (2015). Driving sleep slow oscillations by auditory closed-loop stimulation - a self-limiting process. *The Journal of Neuroscience*, 35(17):6630–8.

[Nicoll et al., 1990] Nicoll, R. A., Malenka, R. C., and Kauer, J. A. (1990). Functional comparison of neurotransmitter receptor subtypes in mammalian central nervous system. *Physiological Reviews*, 70(2):513–565.

[Nishida et al., 2009] Nishida, M., Pearsall, J., Buckner, R. L., and Walker, M. P. (2009). REM sleep, prefrontal theta, and the consolidation of human emotional memory. *Cerebral Cortex*, 19(5):1158–66.

[Nunez, 1974] Nunez, P. L. (1974). The brain wave equation: A model for the EEG. *Mathematical Biosciences*, 21(3-4):279–297.

[Nunez and Srinivasan, 2006] Nunez, P. L. and Srinivasan, R. (2006). A theoretical basis for standing and traveling brain waves measured with human EEG with implications for an integrated consciousness. *Clinical Neurophysiology*, 117(11):2424–35.

[Oswald, 1980] Oswald, I. (1980). Sleep as restorative process: human clues. *Progress in Brain Research*, 53:279–288.

[Patel et al., 1999] Patel, A. J., Honoré, E., Lesage, F., Fink, M., Romey, G., and Lazdunski, M. (1999). Inhalational anesthetics activate two-pore-domain background K+ channels. *Nature Neuroscience*, 2(5):422–426.

[Perez Velazquez and Carlen, 2000] Perez Velazquez, J. L. and Carlen, P. L. (2000). Gap junctions, synchrony and seizures. *Trends in Neurosciences*, 23(2):68–74.

[Peyrache et al., 2012] Peyrache, A., Dehghani, N., Eskandar, E. N., Madsen, J. R., Anderson, W. S., Donoghue, J. A., Hochberg, L. R., Halgren, E., Cash, S. S., and Destexhe, A. (2012). Spatiotemporal dynamics of neocortical excitation and inhibition during human sleep. *Proceedings of the National Academy of Sciences of the United States of America*, 109(5):1731–6.

[Peyron et al., 1998] Peyron, C., Tighe, D. K., van den Pol, A. N., de Lecea, L., Heller, H. C., Sutcliffe, J. G., and Kilduff, T. S. (1998). Neurons containing hypocretin (orexin) project to multiple neuronal systems. *The Journal of Neuroscience*, 18(23):9996–10015.

[Phillips and Robinson, 2007] Phillips, A. J. K. and Robinson, P. A. (2007). A quantitative model of sleep-wake dynamics based on the physiology of the brainstem ascending arousal system. *Journal of Biological Rhythms*, 22(2):167–179.

[Poskanzer and Yuste, 2011] Poskanzer, K. E. and Yuste, R. (2011). Astrocytic regulation of cortical UP states. *Proceedings of the National Academy of Sciences of the United States of America*, 108(45):18453–8.

[Pospischil et al., 2008] Pospischil, M., Toledo-Rodriguez, M., and Monier, C. (2008). Minimal Hodgkin-Huxley type models for different classes of cortical and thalamic neurons. *Biological Cybernetics*, 99(4-5):427–41.

[Raizen et al., 2008] Raizen, D. M., Zimmerman, J. E., Maycock, M. H., Ta, U. D., You, Y.-j., Sundaram, M. V., and Pack, A. I. (2008). Lethargus is a Caenorhabditis elegans sleep-like state. *Nature*, 451(7178):569–572.

[Rasch and Born, 2013] Rasch, B. and Born, J. (2013). About sleep's role in memory. *Physiological Reviews*, 93(2):681–766.

[Rempe et al., 2010] Rempe, M. J., Best, J., and Terman, D. H. (2010). A mathematical model of the sleep/wake cycle. *Journal of Mathematical Biology*, 60(5):615–644.

[Rennie et al., 2002] Rennie, C. J., Robinson, P. a., and Wright, J. J. (2002). Unified neurophysical model of EEG spectra and evoked potentials. *Biological cybernetics*, 86(6):457–471.

[Roberts and Robinson, 2012] Roberts, J. A. and Robinson, P. A. (2012). Corticothalamic dynamics: structure of parameter space, spectra, instabilities, and reduced model. *Physical Review E*, 011910:1–20.

[Robinson et al., 2001] Robinson, P. A., Loxley, P. N., O'Connor, S. C., and Rennie, C. J. (2001). Modal analysis of corticothalamic dynamics, electroencephalographic spectra, and evoked potentials. *Physical Review E*, 63(4):41909.

[Robinson et al., 2011] Robinson, P. A., Phillips, A. J. K., Fulcher, B. D., Puckeridge, M., and Roberts, J. A. (2011). Quantitative modelling of sleep dynamics. *Philosophical Transactions of the Royal Society A: Mathematical, physical, and engineering sciences*, 369(1952):3840–54.

[Robinson et al., 2002] Robinson, P. A., Rennie, C. J., and Rowe, D. L. (2002). Dynamics of large-scale brain activity in normal arousal states and epileptic seizures. *Physical Review E*, 65(4):041924.

[Robinson et al., 2004] Robinson, P. A., Rennie, C. J., Rowe, D. L., and O'Connor, S. C. (2004). Estimation of multiscale neurophysiologic parameters by electroencephalographic means. *Human Brain Mapping*, 23(1):53–72.

[Robinson et al., 2005] Robinson, P. A., Rennie, C. J., Rowe, D. L., O'Connor, S. C., and Gordon, E. (2005). Multiscale brain modelling. *Philosophical Transactions of the Royal Society of London. Series B, Biological sciences*, 360(1457):1043–50.

[Robinson et al., 2003] Robinson, P. A., Rennie, C. J., Rowe, D. L., O'Connor, S. C., Wright, J. J., Gordon, E., and Whitehouse, R. W. (2003). Neurophysical modeling of brain dynamics. *Neuropsychopharmacology*, 28 Suppl 1(February 2016):S74–S79.

[Robinson et al., 1997] Robinson, P. A., Rennie, C. J., and Wright, J. J. (1997). Propagation and stability of waves of electrical activity in the cerebral cortex. *Physical Review E*, 56(1):826–840.

[Rodriguez-Moreno et al., 1997] Rodriguez-Moreno, A., Herreras, O., and Lerma, J. (1997). Kainate receptors presynaptically downregulate GABAergic inhibition in the rat hippocampus. *Neuron*, 19(4):893–901.

[Rodriguez-Moreno and Lerma, 1998] Rodriguez-Moreno, A. and Lerma, J. (1998). Kainate receptor modulation of GABA release involves a metabotropic function. *Neuron*, 20(6):1211–1218.

[Rosanova and Ulrich, 2005] Rosanova, M. and Ulrich, D. (2005). Pattern-specific associative long-term potentiation induced by a sleep spindle-related spike train. *The Journal of Neuroscience*, 25(41):9398–9405.

[Rößler, 2004] Rößler, A. (2004). Runge-Kutta methods for Stratonovich stochastic differential equation systems with commutative noise. *Journal of Computational and Applied Mathematics*, 164(1):613–627.

[Rößler, 2009] Rößler, A. (2009). Second order Runge-Kutta methods for Ito stochastic differential equations. *Society for Industrial and Applied Mathematics*, 47(3):1713–1738.

[Rößler, 2010] Rößler, A. (2010). Runge-Kutta methods for the strong approximation of solutions of stochastic differential equations. *SIAM Journal on Numerical Analysis*, 48(3):922–952.

[Rotstein et al., 2012] Rotstein, H. G., Coombes, S., and Gheorghe, A. M. (2012). Canard-Like Explosion of Limit Cycles in Two-Dimensional Piecewise-Linear Models of FitzHugh–Nagumo Type. *SIAM Journal on Applied Dynamical Systems*, 11(1):135–180.

[Ruiz-Mejias et al., 2011] Ruiz-Mejias, M., Ciria-Suarez, L., Mattia, M., and Sanchez-Vives, M. V. (2011). Slow and fast rhythms generated in the cerebral cortex of the anesthetized mouse. *Journal of Neurophysiology*, 106(6):2910–21.

[Rulkov et al., 2004] Rulkov, N. F., Timofeev, I., and Bazhenov, M. (2004). Oscillations in Large-Scale Cortical Networks: Map-Based Model. *Journal of Computational Neuroscience*, 17(2):203–223.

[Runge, 1895] Runge, C. (1895). Ueber die numerische Auflösung von Differentialgleichungen. *Mathematische Annalen*, 46(2):167–178.

[Saint et al., 1990] Saint, D. A., Thomas, T., and Gage, P. W. (1990). GABAB agonists modulate a transient potassium current in cultured mammalian hippocampal neurons. *Neuroscience Letters*, 118(1):9–13.

[Sanchez-Vives et al., 2010] Sanchez-Vives, M. V., Mattia, M., Compte, A., Perez-Zabalza, M., Winograd, M., Descalzo, V. F., and Reig, R. (2010). Inhibitory modulation of cortical up states. *Journal of Neurophysiology*, 104(3):1314–24.

[Sanchez-Vives and McCormick, 2000] Sanchez-Vives, M. V. and McCormick, D. A. (2000). Cellular and network mechanisms of rhythmic recurrent activity in neocortex. *Nature Neuroscience*, 3(10):1027–1034.

[Saper et al., 2001] Saper, C. B., Chou, T. C., and Scammell, T. E. (2001). The sleep switch: Hypothalamic control of sleep and wakefulness. *Trends in Neurosciences*, 24(12):726–731.

[Saper et al., 2005] Saper, C. B., Scammell, T. E., and Lu, J. (2005). Hypothalamic regulation of sleep and circadian rhythms. *Nature*, 437(7063):1257–1263.

[Sapin et al., 2009] Sapin, E., Lapray, D., Bérod, A., Goutagny, R., Léger, L., Ravassard, P., Clément, O., Hanriot, L., Fort, P., and Luppi, P. H. (2009). Localization of the brainstem GABAergic neurons controlling Paradoxical (REM) sleep. *PLoS ONE*, 4(1).

[Sauer, 2012] Sauer, T. (2012). Numerical solution of stochastic differential equations in finance. In *Handbook of Computational Finance*, volume 23, chapter 4, pages 529–550. Springer, New York.

[Schellenberger Costa et al., 2016a] Schellenberger Costa, M., Born, J., Claussen, J. C., and Martinetz, T. (2016a). Modeling the effect of sleep regulation on a neural mass model. *Journal of Computational Neuroscience*, 41(1):15–28.

[Schellenberger Costa et al., 2016b] Schellenberger Costa, M., Weigenand, A., Ngo, H.-V. V., Marshall, L., Born, J., Martinetz, T., and Claussen, J. C. (2016b). A Thalamocortical Neural Mass Model of the EEG during NREM Sleep and Its Response to Auditory Stimulation. *PLoS Computational Biology*, 12(9):e1005022.

[Sheng and Hyoung Lee, 2003] Sheng, M. and Hyoung Lee, S. (2003). AMPA receptor trafficking and synaptic plasticity: major unanswered questions. *Neuroscience Research*, 46(2):127–134.

[Shi et al., 2001] Shi, S.-H., Hayashi, Y., Esteban, J. A., and Malinow, R. (2001). Subunit-specific rules governing AMPA receptor trafficking to synapses in hippocampal pyramidal neurons. *Cell*, 105(3):331–43.

[Shilnikov and Cymbalyuk, 2005] Shilnikov, A. and Cymbalyuk, G. (2005). Transition between tonic spiking and bursting in a neuron model via the blue-sky catastrophe. *Physical Review Letters*, 94(4):2–5.

[Shouval et al., 2002a] Shouval, H. Z., Bear, M. F., and Cooper, L. N. (2002a). A unified model of NMDA receptor-dependent bidirectional synaptic plasticity. *Proceedings of the National Academy of Sciences of the United States of America*, 99(16):10831–6.

[Shouval et al., 2002b] Shouval, H. Z., Castellani, G. C., Blais, B. S., Yeung, L. C., and Cooper, L. N. (2002b). Converging evidence for a simplified biophysical model of synaptic plasticity. *Biological Cybernetics*, 87(5-6):383–91.

[Shouval et al., 2010] Shouval, H. Z., Wang, S. S.-H., and Wittenberg, G. M. (2010). Spike timing dependent plasticity: a consequence of more fundamental learning rules. *Frontiers in Computational Neuroscience*, 4(July):1–13.

[Siegel, 2005] Siegel, J. M. (2005). Clues to the functions of mammalian sleep. *Nature*, 437(7063):1264–71.

[Siegel, 2009] Siegel, J. M. (2009). Sleep viewed as a state of adaptive inactivity. *Nature Reviews. Neuroscience*, 10(10):747–53.

[Sik et al., 1995] Sik, A., Penttonen, M., Ylinen, A., and Buzsáki, G. (1995). Hippocampal CA1 interneurons: an in vivo intracellular labeling study. *The Journal of Neuroscience*, 15(10):6651–6665.

[Skinner et al., 1999] Skinner, F. K., Zhang, L., Velazquez, J. L., and Carlen, P. L. (1999). Bursting in inhibitory interneuronal networks: A role for gap- junctional coupling. *Journal of Neurophysiology*, 81(3):1274–1283.

[Smith, 1995] Smith, C. (1995). Sleep states and memory processes. *Behavioural Brain Research*, 69(1-2):137–145.

[Smith, 2001] Smith, C. (2001). Sleep states and memory processes in humans: procedural versus declarative memory systems. *Sleep Medicine Reviews*, 5(6):491–506.

[Soma and Shimegi, 2012] Soma, S. and Shimegi, S. (2012). Cholinergic modulation of response gain in the primary visual cortex of the macaque. *Journal of Neurophysiology*, 107:283–291.

[Sotero et al., 2010] Sotero, R. C., Bortel, A., Martínez-Cancino, R., Neupane, S., O'Connor, P., Carbonell, F., and Shmuel, A. (2010). Anatomically-constrained effective connectivity among layers in a cortical column modeled and estimated from local field potentials. *Journal of Integrative Neuroscience*, 9(4):355–79.

[Sotero et al., 2007] Sotero, R. C., Trujillo-Barreto, N. J., Iturria-Medina, Y., Carbonell, F., and Jimenez, J. C. (2007). Realistically coupled neural mass models can generate EEG rhythms. *Neural Computation*, 19(2):478–512.

[Stacey et al., 2009] Stacey, W. C., Lazarewicz, M. T., and Litt, B. (2009). Synaptic noise and physiological coupling generate high-frequency oscillations in a hippocampal computational model. *Journal of Neurophysiology*, 102(4):2342–2357.

[Steriade, 1993] Steriade, M. (1993). Modulation of information processing in thalamocortical systems: Chairman's introductory remarks. *Progress in Brain Research*, 98(Chapter 41):341–343.

[Steriade, 2003] Steriade, M. (2003). The corticothalamic system in sleep. *Frontiers in Bioscience*, 8(4):878–899.

[Steriade, 2004] Steriade, M. (2004). Acetylcholine systems and rhythmic activities during the waking-sleep cycle. *Progress in Brain Research*, 145:179–196.

[Steriade and Amzica, 1998] Steriade, M. and Amzica, F. (1998). Slow sleep oscillation, rhythmic K-complexes, and their paroxysmal developments. *Journal of Sleep Research*, 7 Suppl 1:30–35.

[Steriade et al., 1993a] Steriade, M., Amzica, F., and Nuñez, A. (1993a). Cholinergic and Noradrenergic Modulation of the Slow (˜0.3 Hz) Oscillation in Neocortical Cells. *Journal of Neurophysiology*, 70(4):1385–1400.

[Steriade and Deschênes, 1984] Steriade, M. and Deschênes, M. (1984). The thalamus as a neuronal oscillator. *Brain Research Reviews*, 8(1):1–63.

[Steriade et al., 1985] Steriade, M., Deschênes, M., Domich, L., and Mulle, C. (1985). Abolition of spindle oscillations in thalamic neurons disconnected from nucleus reticularis thalami. *Journal of Neurophysiology*, 54(6):1473–1497.

[Steriade et al., 1990] Steriade, M., Jones, E. G., and Llinás, R. R. (1990). Thalamic oscillations and signaling. *The Neurosciences Institute publications series.*, page 431pp.

[Steriade and Llinás, 1988] Steriade, M. and Llinás, R. R. (1988). The functional states of the thalamus and the associated neuronal interplay. *Physiological Reviews*, 68(3):649–742.

[Steriade et al., 1993b] Steriade, M., Nuñez, A., and Amzica, F. (1993b). Intracellular analysis of relations between the slow (< 1 Hz) neocortical oscillation and other sleep rhythms of the electroencephalogram. *The Journal of Neuroscience*, 13(8):3266–3283.

[Steriade et al., 1987] Steriade, M., Parent, A., Pare, D., and Smith, Y. (1987). Cholinergic and non-cholinergic neurons of cat basal forebrain project to reticular and mediodorsal thalamic nuclei. *Brain Research*, 408(1-2):372–376.

[Steriade et al., 2001] Steriade, M., Timofeev, I., and Grenier, F. (2001). Natural waking and sleep states: a view from inside neocortical neurons. *Journal of Neurophysiology*, 85(5):1969–1985.

[Steyn-Ross et al., 2005] Steyn-Ross, D. A., Steyn-Ross, M. L., Sleigh, J. W., Wilson, M. T., Gillies, I. P., and Wright, J. J. (2005). The sleep cycle modelled as a cortical phase transition. *Journal of Biological Physics*, 31(3-4):547–569.

[Steyn-Ross et al., 2001] Steyn-Ross, D. A., Steyn-Ross, M. L., Wilcocks, L., and Sleigh, J. W. (2001). Toward a theory of the general-anesthetic-induced phase transition of the cerebral cortex. II. Numerical simulations, spectral entropy, and correlation times. *Physical Review E*, 64(1):1–12.

[Steyn-Ross et al., 2004] Steyn-Ross, M. L., Steyn-Ross, D. A., and Sleigh, J. W. (2004). Modelling general anaesthesia as a first-order phase transition in the cortex. *Progress in Biophysics and Molecular Biology*, 85(2-3):369–85.

[Steyn-Ross et al., 2013] Steyn-Ross, M. L., Steyn-Ross, D. A., and Sleigh, J. W. (2013). Interacting Turing-Hopf Instabilities Drive Symmetry-Breaking Transitions in a Mean-Field Model of the Cortex: A Mechanism for the Slow Oscillation. *Physical Review X*, 3(2):021005.

[Steyn-Ross et al., 1999] Steyn-Ross, M. L., Steyn-Ross, D. A., Sleigh, J. W., and Liley, D. T. J. (1999). Theoretical electroencephalogram stationary spectrum for a white-noise-driven cortex: evidence for a general anesthetic-induced phase transition. *Physical Review E*, 60(6 Pt B):7299–311.

[Steyn-Ross et al., 2003] Steyn-Ross, M. L., Steyn-Ross, D. A., Sleigh, J. W., and Whiting, D. (2003). Theoretical predictions for spatial covariance of the electroencephalographic signal during the anesthetic-induced phase transition: Increased correlation length and emergence of spatial self-organization. *Physical Review E*, 68(2):1–18.

[Steyn-Ross et al., 2011] Steyn-Ross, M. L., Steyn-Ross, D. A., Sleigh, J. W., and Wilson, M. T. (2011). A Mechanism for Ultra-Slow Oscillations in the Cortical Default Network. *Bulletin of Mathematical Biology*, 73:398–416.

[Steyn-Ross et al., 2007] Steyn-Ross, M. L., Steyn-Ross, D. A., Wilson, M. T., and Sleigh, J. W. (2007). Gap junctions mediate large-scale Turing structures in a mean-field cortex driven by subcortical noise. *Physical Review E*, 76(1):1–16.

[Steyn-Ross et al., 2009] Steyn-Ross, M. L., Steyn-Ross, D. A., Wilson, M. T., and Sleigh, J. W. (2009). Modeling brain activation patterns for the default and cognitive states. *NeuroImage*, 45(2):298–311.

[Stickgold and Walker, 2007] Stickgold, R. and Walker, M. P. (2007). Sleep-dependent memory consolidation and reconsolidation. *Sleep medicine*, 8(4):331–43.

[Stratonovich, 1966] Stratonovich, R. L. (1966). A New Representation for Stochastic Integrals and Equations. *SIAM Journal on Control*, 4(2):362–371.

[Stratonovich, 1967] Stratonovich, R. L. (1967). *Topics in the theory of random noise*, volume 2. CRC Press.

[Suffczynski et al., 2004] Suffczynski, P., Kalitzin, S., and Lop (2004). Dynamics of non-convulsive epileptic phenomena modeled by a bistable neuronal network. *Neuroscience*, 126(2):467–484.

[Sun et al., 2016] Sun, W., Tan, Z., Mensh, B. D., and Ji, N. (2016). Thalamus provides layer 4 of primary visual cortex with orientation- and direction-tuned inputs. *Nature Neuroscience*, 19(2).

[Szabadics et al., 2001] Szabadics, J., Lorincz, A., and Tamás, G. (2001). Beta and gamma frequency synchronization by dendritic gabaergic synapses and gap junctions in a network of cortical interneurons. *The Journal of Neuroscience*, 21(15):5824–5831.

[Szmolyan and Wechselberger, 2001] Szmolyan, P. and Wechselberger, M. (2001). Canards in 3. *Journal of Differential Equations*, 177(2):35.

[Talley and Bayliss, 2002] Talley, E. M. and Bayliss, D. A. (2002). Modulation of TASK-1 (Kcnk3) and TASK-3 (Kcnk9) potassium channels volatile anesthetics and neurotransmitters share a molecular site of action. *Journal of Biological Chemistry*, 277(20):17733–17742.

[Tamakawa et al., 2006] Tamakawa, Y., Karashima, A., Koyama, Y., Katayama, N., and Nakao, M. (2006). A quartet neural system model orchestrating sleep and wakefulness mechanisms. *Journal of Neurophysiology*, 95(4):2055–2069.

[Tamás et al., 2000] Tamás, G., Buhl, E. H., Lorincz, A., and Somogyi, P. (2000). Proximally targeted GABAergic synapses and gap junctions synchronize cortical interneurons. *Nature Neuroscience*, 3(4):366–371.

[Tiesinga and José, 2000] Tiesinga, P. H. E. and José, J. V. (2000). Robust gamma oscillations in networks of inhibitory hippocampal interneurons. *Network*, 11(1):1–23.

[Tilley and Empson, 1978] Tilley, A. J. and Empson, J. A. C. (1978). REM sleep and memory consolidation. *Biological Psychology*, 6(4):293–300.

[Timmons et al., 2004] Timmons, S. D., Geisert, E., Stewart, A. E., Lorenzon, N. M., and Foehring, R. C. (2004). Alpha 2 -Adrenergic receptor-mediated modulation of calcium current in neocortical pyramidal neurons. *Brain Research*, 1014:184–196.

[Timofeev and Bazhenov, 2005] Timofeev, I. and Bazhenov, M. (2005). Mechanisms and biological role of thalamocortical oscillations. In Columbus, F., editor, *Trends in Chronobiology Research*, number c, chapter 1, pages 1–47. Nova Science Publishers.

[Timofeev et al., 2001a] Timofeev, I., Bazhenov, M., Sejnowski, T. J., and Steriade, M. (2001a). Contribution of intrinsic and synaptic factors in the desynchronization of thalamic oscillatory activity. *Thalamus and Related Systems*, 1(1):53–69.

[Timofeev and Chauvette, 2013] Timofeev, I. and Chauvette, S. (2013). The spindles: are they still thalamic? *Sleep*, 36(6):825–6.

[Timofeev et al., 2000] Timofeev, I., Grenier, F., Bazhenov, M., Sejnowski, T. J., and Steriade, M. (2000). Origin of Slow Cortical Oscillations in Deafferented Cortical Slabs. *Cerebral Cortex*, pages 1185–1199.

[Timofeev et al., 2001b] Timofeev, I., Grenier, F., and Steriade, M. (2001b). Disfacilitation and active inhibition in the neocortex during the natural sleep-wake cycle: an intracellular study. *Proceedings of the National Academy of Sciences of the United States of America*, 98(4):1924–9.

[Timofeev and Steriade, 1996] Timofeev, I. and Steriade, M. (1996). Low-frequency rhythms in the thalamus of intact-cortex and decorticated cats. *Journal of Neurophysiology*, 76(6):4152–4168.

[Touboul et al., 2011] Touboul, J., Wendling, F., Chauvel, P., and Faugeras, O. (2011). Neural mass activity, bifurcations, and epilepsy. *Neural Computation*, 23(12):3232–3286.

[Traub and Bibbig, 2000] Traub, R. D. and Bibbig, A. (2000). A model of high-frequency ripples in the hippocampus based on synaptic coupling plus axon-axon gap junctions between pyramidal neurons. *The Journal of Neuroscience*, 20(6):2086–93.

[Traub et al., 2004] Traub, R. D., Bibbig, A., LeBeau, F. E. N., Buhl, E. H., and Whittington, M. A. (2004). Cellular mechanisms of neuronal population oscillations in the hippocampus in vitro. *Annual Review of Neuroscience*, 27(1):247–78.

[Traub et al., 2005] Traub, R. D., Contreras, D., Cunningham, M. O., Murray, H., LeBeau, F. E. N., Roopun, A., Bibbig, A., Wilent, W. B., Higley, M. J., and Whittington, M. A. (2005). Single-column thalamocortical network model exhibiting gamma oscillations, sleep spindles, and epileptogenic bursts. *Journal of Neurophysiology*, 93(4):2194–2232.

[Traub et al., 1999] Traub, R. D., Schmitz, D., Jefferys, J. G. R., and Draguhn, A. (1999). High-frequency population oscillations are predicted to occur in hippocampal pyramidal neuronal networks interconnected by axoaxonal gap junctions. *Neuroscience*, 92(2):407–426.

[Traub et al., 2012] Traub, R. D., Schmitz, D., Maier, N., Whittington, M. A., and Draguhn, A. (2012). Axonal properties determine somatic firing in a model of in vitro CA1 hippocampal sharp wave/ripples and persistent gamma oscillations. *The European Journal of Neuroscience*, 36(5):2650–60.

[Traub et al., 1991] Traub, R. D., Wong, R. K. S., Miles, R., and Michelson, H. B. (1991). A model of a CA3 hippocampal pyramidal neuron incorporating voltage-clamp data on intrinsic conductances. *Journal of Neurophysiology*, 66(2):635–50.

[Tsumoto et al., 2006] Tsumoto, K., Kitajima, H., Yoshinaga, T., Aihara, K., and Kawakami, H. (2006). Bifurcations in Morris-Lecar neuron model. *Neurocomputing*, 69(4-6):293–316.

[Tuckwell, 1988] Tuckwell, H. C. (1988). *Introduction to Theoretical Neurobiology: Nonlinear and Stochastic Theories*, volume 2. Cambridge University Press.

[Urakubo et al., 2008] Urakubo, H., Honda, M., Froemke, R. C., and Kuroda, S. (2008). Requirement of an allosteric kinetics of NMDA receptors for spike timing-dependent plasticity. *The Journal of Neuroscience*, 28(13):3310–3323.

[Ursino et al., 2010] Ursino, M., Cona, F., and Zavaglia, M. (2010). The generation of rhythms within a cortical region: analysis of a neural mass model. *NeuroImage*, 52(3):1080–94.

[van der Werf et al., 2009] van der Werf, Y. D., Altena, E., Schoonheim, M. M., Sanz-Arigita, E. J., Vis, J. C., De Rijke, W., and van Someren, E. J. W. (2009). Sleep benefits subsequent hippocampal functioning. *Nature Neuroscience*, 12(2):122–123.

[Vanini et al., 2012] Vanini, G., Lydic, R., and Baghdoyan, H. a. (2012). GABA-to-ACh ratio in basal forebrain and cerebral cortex varies significantly during sleep. *Sleep*, 35(10):1325–34.

[Varela, 2014] Varela, C. (2014). Thalamic neuromodulation and its implications for executive networks. *Frontiers in Neural Circuits*, 8(June):1–22.

[Vladimirov et al., 2013] Vladimirov, N., Tu, Y., and Traub, R. D. (2013). Synaptic gating at axonal branches, and sharp-wave ripples with replay: a simulation study. *The European Journal of Neuroscience*, 38(10):3435–47.

[Volgushev et al., 2006] Volgushev, M., Chauvette, S., Mukovski, M., and Timofeev, I. (2006). Precise long-range synchronization of activity and silence in neocortical neurons during slow-wave oscillations [corrected]. *The Journal of Neuroscience*, 26(21):5665–72.

[von Krosigk et al., 1993] von Krosigk, M., Bal, T., and McCormick, D. A. (1993). Cellular mechanisms of a synchronized oscillation in the thalamus. *Science*, 261(5119):361–364.

[Vyazovskiy et al., 2009] Vyazovskiy, V. V., Olcese, U., Lazimy, Y. M., Faraguna, U., Esser, S. K., Williams, J. C., Cirelli, C., and Tononi, G. (2009). Cortical firing and sleep homeostasis. *Neuron*, 63(6):865–878.

[Walker and Stickgold, 2004] Walker, M. P. and Stickgold, R. (2004). Sleep-dependent learning and memory consolidation. *Neuron*, 44(1):121–133.

[Wang, 1998] Wang, X.-J. (1998). Calcium coding and adaptive temporal computation in cortical pyramidal neurons. *Journal of Neurophysiology*, 79(3):1549–66.

[Wang and Buzsáki, 1996] Wang, X.-J. and Buzsáki, G. (1996). Gamma oscillation by synaptic inhibition in a hippocampal interneuronal network model. *The Journal of Neuroscience*, 16(20):6402–6413.

[Wang et al., 2003] Wang, X.-J., Liu, Y., Sanchez-Vives, M. V., and McCormick, D. A. (2003). Adaptation and temporal decorrelation by single neurons in the primary visual cortex. *Journal of Neurophysiology*, 89(6):3279–93.

[Webb, 1988] Webb, W. B. (1988). An objective behavioral model of sleep. *Sleep*, 11(5):488–496.

[Wechselberger, 2005] Wechselberger, M. (2005). Existence and Bifurcation of Canards in R3 in the Case of a Folded Node. *SIAM Journal on Applied Dynamical Systems*, 4(1):101–139.

[Weigenand et al., 2014] Weigenand, A., Schellenberger Costa, M., Ngo, H.-V. V., Claussen, J. C., and Martinetz, T. (2014). Characterization of K-Complexes and Slow Wave Activity in a Neural Mass Model. *PLoS Computational Biology*, 10(11):e1003923.

[Weitzman et al., 1971] Weitzman, E. D., Fukushima, D., Nogeire, C., Roffwarg, H. P., Gallager, T. F., and Leon, H. (1971). Twenty-four Hour Pattern of the Episodic Secretion of Cortisol in Normal Subjects. *The Journal of Clinical Endocrinology & Metabolism*, 33(1):14–22.

[Wendling et al., 2002] Wendling, F., Bartolomei, F., Bellanger, J.-J., and Chauvel, P. (2002). Epileptic fast activity can be explained by a model of impaired GABAergic dendritic inhibition. *European Journal of Neuroscience*, 15(9):1499–1508.

[Wendling et al., 2000] Wendling, F., Bellanger, J.-J., Bartolomei, F., and Chauvel, P. (2000). Relevance of nonlinear lumped-parameter models in the analysis of depth-EEG epileptic signals. *Biological Cybernetics*, 83(4):367–378.

[White et al., 1998] White, J. A., Chow, C. C., Ritt, J., Soto-Trevino, C., and Kopell, N. J. (1998). Synchronization and oscillatory dynamics in heterogeneous, mutually inhibited neurons. *Journal of Computational Neuroscience*, 5(1):5–16.

[Wierzynski et al., 2010] Wierzynski, C. M., Lubenov, E. V., Gu, M., and Siapas, A. G. (2010). State-dependent spike timing relationships between hippocampal and prefrontal circuits during sleep. *Neuron*, 61(4):587–596.

[Wilson, 1999] Wilson, H. R. (1999). Simplified dynamics of human and mammalian neocortical neurons. *Journal of Theoretical Biology*, 200(4):375–88.

[Wilson and Cowan, 1973] Wilson, H. R. and Cowan, J. D. (1973). A mathematical theory of the functional dynamics of cortical and thalamic nervous tissue. *Kybernetik*, 13(2):55–80.

[Wilson et al., 2010] Wilson, M. T., Barry, M., Reynolds, J. N. J., Crump, W. P., Steyn-Ross, D. A., and Steyn-Ross, M. L. (2010). An analysis of the transitions between down and up states of the cortical slow oscillation under urethane anaesthesia. *Journal of Biological Physics*, 36(3):245–59.

[Wilson et al., 2006a] Wilson, M. T., Sleigh, J. W., Steyn-Ross, D. A., and Steyn-Ross, M. L. (2006a). General anesthetic-induced seizures can be explained by a mean-field model of cortical dynamics. *Anesthesiology*, 104(3):588–93.

[Wilson et al., 2006b] Wilson, M. T., Steyn-Ross, D. A., Sleigh, J. W., Steyn-Ross, M. L., Wilcocks, L., and Gillies, I. P. (2006b). The K-complex and slow oscillation in terms of a mean-field cortical model. *Journal of Computational Neuroscience*, 21(3):243–57.

[Wilson et al., 2005] Wilson, M. T., Steyn-Ross, M. L., Steyn-Ross, D. A., and Sleigh, J. W. (2005). Predictions and simulations of cortical dynamics during natural sleep using a continuum approach. *Physical Review E*, 72(5):51910.

[Zhang and Arsenault, 2005] Zhang, Z.-W. and Arsenault, D. (2005). Gain modulation by serotonin in pyramidal neurones of the rat prefrontal cortex. *The Journal of Physiology*, 2:379–394.

[Żygierewicz, 2000] Żygierewicz, J. (2000). *Analysis of sleep spindles and a model of their generation*. PhD thesis.

[Żygierewicz et al., 1999] Żygierewicz, J., Blinowska, K. J., Durka, P. J., Szelenberger, W., Niemcewicz, S., and Androsiuk, W. (1999). High resolution study of sleep spindles. *Clinical Neurophysiology*, 110(12):2136–2147.

[Żygierewicz et al., 2001] Żygierewicz, J., Suffczyński, P., and Blinowska, K. J. (2001). A model of sleep spindles generation. *Neurocomputing*, 38-40:1619–1625.